

University of Alberta

**Fragmentation of Large Coal Particles at High Temperature
in a Drop Tube Furnace**

by

Su Tian

A thesis submitted to the Faculty of Graduate Studies and Research
in partial fulfillment of the requirements for the degree of

**Master of Science
in
Chemical Engineering**

Department of Chemical and Materials Engineering

©Su Tian
Fall 2011
Edmonton, Alberta

Permission is hereby granted to the University of Alberta Libraries to reproduce single copies of this thesis and to lend or sell such copies for private, scholarly or scientific research purposes only. Where the thesis is converted to, or otherwise made available in digital form, the University of Alberta will advise potential users of the thesis of these terms.

The author reserves all other publication and other rights in association with the copyright in the thesis and, except as herein before provided, neither the thesis nor any substantial portion thereof may be printed or otherwise reproduced in any material form whatsoever without the author's prior written permission.

*Dedicated to my parents, Shenghe and Juling
for their love and continuous support for me to
pursue my dream*

Examining Committee

Dr. Rajender Gupta, Chemical and Materials Engineering, University of Alberta

Dr. Zhenghe Xu, Chemical and Materials Engineering, University of Alberta

Dr. Japan Trivedi, Civil and Environmental Engineering, University of Alberta

Abstract

The fragmentation of large coal particles at high temperature is important to the efficient operation of Corex process of steelmaking, which uses raw coal instead of coke. The hypothesis is that the heterogeneity within coal particles affects the fragmentation. The interface of minerals and coal matrix is likely to be the weak areas where fragmentation is most likely to occur. Heterogeneity in organic components might also impact the fragmentation behaviour. Advanced characterisation, such as Computer Controlled Scanning Electron Microscope (CCSEM), and petrographic analysis are applied to study the effects of coal properties on the fragmentation of large coal particles.

A custom designed drop tube furnace is used to conduct drop tests at room temperature and at high temperature to assess the fragmentation behaviour of four coals at different experimental conditions. The coals with higher mineral-coal interface area resulted in higher fragmentation. The results agree well with the hypothesis. The effects of other parameters, such as feed size, temperature, and residence time are also studied.

Acknowledgement

The author would like to express her gratitude to Dr. Rajender Gupta, for his guidance, patience, and encouragement. He introduced me into the field of energy research, inspired me through discussions on academic topics and different opinions, and always supported me when confronting difficult problems.

The funding of this work from Baoshan Iron and Steel, Co., Ltd., China, and from Shanghai Municipal Government is greatly appreciated. The author is also grateful to Dr. Qun Zhang and Dr. Zhenghe Xu, who initiated this work, and gave valuable comments and suggestions throughout this project.

Special thanks to Dr. Ambrose Itika, whose contribution to the equipment design, assembly, and calibration is very much appreciated. Thanks to Dr. Arunkumar Samanta for his assistance during the experiments, and valuable suggestions of academic writing.

Thanks to Dr. Moshfiqur Rahman who is very supportive in assisting sample analysis. Also thanks to Mr. Walter Boddez, Mr. Clark Bicknell, who helped to custom design the equipment in the present work.

Table of Contents

| | | |
|-------|---------------------------------------------------------------|----|
| 1 | Introduction..... | 1 |
| 1.1 | Introduction to Corex Process | 3 |
| 1.2 | Research Problem..... | 4 |
| 2 | Literature Review..... | 6 |
| 2.1 | Fragmentation Mechanism..... | 6 |
| 2.1.1 | Primary fragmentation and the influencing factors | 7 |
| 2.1.2 | Devolatilization time and rate | 14 |
| 2.1.3 | Secondary fragmentation | 15 |
| 2.2 | Primary Fragmentation Model | 16 |
| 2.2.1 | VM-driven model..... | 16 |
| 2.2.2 | Thermal stress model | 17 |
| 2.3 | Methods of Investigation..... | 18 |
| 3 | Methodology and Hypothesis | 21 |
| 3.1 | The Characteristics of the Present Study..... | 21 |
| 3.2 | Hypothesis of the Present Study..... | 22 |
| 4 | Experiment..... | 25 |
| 4.1 | Proximate, Ultimate Analysis and Thermal Characteristics..... | 25 |
| 4.2 | SEM Analysis..... | 27 |
| 4.3 | CCSEM and Petrographic Analysis | 27 |
| 4.4 | Fragmentation Drop Test..... | 30 |
| 4.4.1 | Equipment..... | 30 |

| | | |
|-------|-------------------------------------------------------------|-----|
| 4.4.2 | Experiment design | 35 |
| 4.4.3 | Experiment operation procedure..... | 44 |
| 5 | Results and Discussion | 46 |
| 5.1 | Advanced Characterisation Results..... | 46 |
| 5.1.1 | SEM analysis results | 46 |
| 5.1.2 | CCSEM analysis results..... | 49 |
| 5.1.3 | Petrographic analysis results..... | 50 |
| 5.2 | The Effect of Different Coal Types | 53 |
| 5.2.1 | Fragmentation results from room temperature drop test..... | 53 |
| 5.2.2 | Fragmentation results from high temperature drop test | 58 |
| 5.3 | The Effect of Feed size..... | 62 |
| 5.4 | The Effect of Temperature..... | 66 |
| 5.5 | The Effect of Residence Time | 70 |
| 5.6 | Discussion on the Effect of Coal Types | 76 |
| 5.6.1 | The effect of minerals based on CCSEM analysis..... | 76 |
| 5.6.2 | The effect of macerals based on petrographic analysis..... | 82 |
| 6 | Conclusions and Future Recommendations..... | 86 |
| | Bibliography | 89 |
| | Appendix I: Heating time calculation | 92 |
| | Appendix II: CCSEM analysis | 96 |
| | Appendix III: Automated reflectogram | 104 |

List of Tables

| | |
|------------------------------------------------------------------------------------------------------------------------|----|
| Table 4-1 Proximate and ultimate analysis of the four coals | 26 |
| Table 4-2 Thermal characteristics of the Chinese coals [<i>Source: Baosteel</i>] | 26 |
| Table 4-3. Room temperature drop tests matrix..... | 36 |
| Table 4-4 High temperature drop tests matrix | 37 |
| Table 4-5 Size ranges determined by standard sieves..... | 38 |
| Table 5-1 Typical CCSEM data showing detailed information of minerals of coal A..... | 50 |
| Table 5-2 Maceral composition determined by petrographic analysis for coal A, B, C, and D | 52 |
| Table 5-3 Particle numbers of the product in various size ranges at various temperatures for coal A and D | 61 |
| Table 5-4 Interface area of minerals within various size ranges in 1 cm ³ coal of coal A, B, C, and D | 81 |

List of Figures

| | |
|-------------------------------------------------------------------------------------------------------------------------------------------------------------------------|----|
| Figure 1-1 Coking coal price per short ton by US dollars from year 1996 to year 2010, quarterly base. ¹ | 2 |
| Figure 1-2 Corex process flow diagram. ⁶ | 4 |
| Figure 3-1 Mineral distribution in coal matrix. ²⁷ | 23 |
| Figure 3-2 Heterogeneity of coal matrix..... | 23 |
| Figure 4-1 Scheme of the drop tube furnace for thermal fragmentation test..... | 31 |
| Figure 4-2 Drop tube furnace for drop test at high temperature. | 32 |
| Figure 4-3 Impact plate at the bottom of the drop tube furnace. | 33 |
| Figure 4-4 New impact plate (left) and modified impact plate assembly (right).. | 33 |
| Figure 4-5 Tube reactor inside a partly opened split vertical tube furnace..... | 34 |
| Figure 4-6 Locations of thermocouples inside the tube furnace..... | 34 |
| Figure 4-7 Fragmentation Index FI (a) and corresponding deviation (b) in variance with feed weight. Feed: Coal A; Size: 16-8 mm and No. of Balls: 8. | 40 |
| Figure 4-8 Fragmentation Index FI (a) and deviation (b) in variance with ball numbers. Feed: Coal B, Size: 22-11mm and Feed Weight = 50g. | 41 |
| Figure 4-9 T3 (temperature right above the plate) in variance with residence time at (a) different feed sizes, (b) different temperatures, and (c) and different coals. | 44 |
| Figure 5-1 SEM images of coal A. Magnification of Images 1, 2, 3: $\times 50$; Image 4: $\times 360$ | 47 |
| Figure 5-2 SEM images of coal B. Magnification of Images 1, 2, 3: $\times 50$; Image 4: $\times 180$ | 47 |
| Figure 5-3 SEM images of coal C. Magnification of Images 1, 2, 3: $\times 50$; Image 3: $\times 250$; Image 4: $\times 300$ | 48 |
| Figure 5-4 SEM images of coal D. Magnification of Images 1, 2: $\times 50$; Image 3: $\times 250$; Image 4: $\times 350$ | 48 |

| | |
|-----------------------------------------------------------------------------------------------------------------------------------------------------|----|
| Figure 5-5 Cumulative reflectance distribution showing the determination of macerals groups of coal A..... | 51 |
| Figure 5-6 Fragmentation of coal A at room temperature..... | 54 |
| Figure 5-7 Fragmentation of coal B at room temperature. | 54 |
| Figure 5-8 Cumulative size distribution of the fine product from | 55 |
| Figure 5-9 Fragmentation of coal A at room temperature..... | 55 |
| Figure 5-10 Fragmentation of coal B at room temperature. | 56 |
| Figure 5-11 Cumulative size distribution of the fine product from drop tests..... | 56 |
| Figure 5-12 Fragmentation of coal A at room temperature..... | 57 |
| Figure 5-13 Fragmentation of coal B at room temperature. | 57 |
| Figure 5-14 Cumulative size distribution of the fine product from drop tests at room temperature. | 58 |
| Figure 5-15 Fragmentation Index, FI in variance of temperature of coal A, B, C, and D..... | 59 |
| Figure 5-16 Fines Percentatge in variance of temperature of coal A, B, C, and D. | 59 |
| Figure 5-17 Product Particle Number in variance of temperature of coal A, B, C, and D..... | 60 |
| Figure 5-18 Particle number distribution of the product of coal A and D. | 61 |
| Figure 5-19 Fragmentation Index, FI in variance with feed size for coal A, B, and C, at temperatures (a) 800 °C, (b) 900 °C and (c) 1000 °C. | 64 |
| Figure 5-20 Fragmentation Number Index, S in variance with feed size for coal A, B, and C, at various temperatures. | 64 |
| Figure 5-21 Big particle formed by agglomeration of small particles of coal B (left) and coal C (right). Feed Size: -11mm, Temperature: 900 °C..... | 65 |
| Figure 5-22 Fragmentation Index, FI in variance with temperature at various feed sizes: (a) 22-32 mm, (b) 11-22 mm and (c) 5-11 mm..... | 67 |

| | |
|-----------------------------------------------------------------------------------------------------------------------------------------|----|
| Figure 5-23 Product Particle Number in variance with temperature for coal A, B, and C, with various feed sizes..... | 68 |
| Figure 5-24 Comparison of Fragmentation Index, FI at room temperature and high temperature. | 69 |
| Figure 5-25 Fragmentation Index, FI in Variance with Residence Time. Feed sample: coal B, Size: 32-22 mm. | 71 |
| Figure 5-26 Product Particle Number in variance with residence time. Feed sample: coal B, Feed size: 32-22 mm. | 72 |
| Figure 5-27 Particle number distribution in each size range, in variance with residence time. Feed sample: coal B, Size: 32-22 mm. | 73 |
| Figure 5-28 Fines Percentage after fragmentation, in variance with residence time. Feed sample: coal B, Size: 32-22mm. | 74 |
| Figure 5-29 Comparison of the product of residence time: (above) 2 min and (below) 10 min. Feed: coal B, Size: 32-22 mm. | 75 |
| Figure 5-30 Weight loss percentage at various residence time. Feed: coal B, Size: 32-22 mm. | 76 |
| Figure 5-31 Mineral weight percentage of the four coals, determined by CCSEM analysis and proximate analysis..... | 77 |
| Figure 5-32 Mineral particle size distribution of coal A, B, C, and D..... | 79 |
| Figure 5-33 Particle number distribution of coal A, B, C, and D. | 79 |
| Figure 5-34 Coke strength prediction based on petrographic data of coal C..... | 85 |

1 INTRODUCTION

Metallurgical coke, produced from coking coal, is conventionally used in blast furnaces for steel making. As coking coal resources and production become less, their price increases. As shown in Figure 1-1, coking coal price is increasing during the last 15 years.¹ The current price is about four times than that in year 1996. The price of coke is even higher.² As a result, the production cost of iron making in conventional blast furnace increases. Furthermore, coke-ovens that are used to produce metallurgical coke cause a lot of environmental issues. During charging and quenching process, coke oven gas consisting of SO_x, NO_x, volatile organic compounds, and particulate matter are emitted through the oven door. The carcinogenicity of coke oven emission in humans as well as in experimental animal are already established by Environmental Protection Agency (EPA) of United States. International Agency for Research on Cancer classifies coke oven emissions as category I, meaning that they are carcinogenic.³

Because of the increased cost and environmental issues associated with conventional blast furnaces, alternative methods for iron making have been investigated. Among them Corex is the only commercial alternative smelting process. The most important feature of Corex is that the raw coal is used instead of coke. The coal can even be thermal coal that is much cheaper than coking coal. As a result, the cost of production of ironmaking is significantly reduced, and the environmental problems associated with coke oven are also eliminated. Moreover, the export gas of Corex consists mostly of carbon monoxide (44.9%), carbon

dioxide (27.5%), hydrogen (16.2%), and water vapour (10.0%), which can be easily cleaned and used for downstream utilization. ⁴

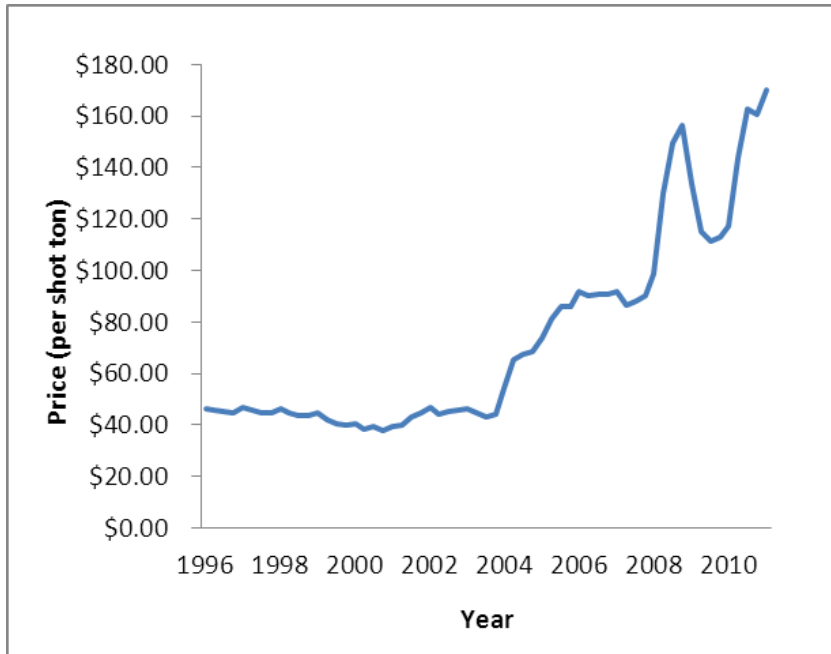


Figure 1-1 Coking coal price per short ton by US dollars from year 1996 to year 2010, quarterly base. ¹

The performance of the Corex operation has also been found sensitive to the quality of raw coal. One of the most important issues is the degradation of large coal particles at high temperature. This will reduce the productivity and reduce the quality of the hot metal. Another problem is the excessive fines resulting from fragmentation that are responsible for the blocking of the gas generation duct and therefore the increase of downtime of the plant. Baoshan Iron and Steel, Co., Ltd. (Baosteel), China, using the Corex process for steelmaking, is facing similar problems due to fragmentation of some coals in their Shanghai steel plant. As a result, Baosteel and University of Alberta agreed to collaborate on study of the fragmentation behaviour of large coal particles at high temperature to understand the fragmentation of different coals under different conditions.

1.1 Introduction to Corex Process

Corex process has been developed by Siemens VAI (VOEST-ALPINE Industrieanlagenbau) based in Austria. Development began in the 1970s and by 1977 a pilot plant was built in Germany. The commercial Corex plants are now available in three modules according to their capacities⁵, namely C-1000, C-2000, and C-3000, with an annual hot metal capacity of 0.3-0.4Mt/y, 1Mt/y, and 1.5Mt/y, respectively. Corex plants are now operated in South Africa, South Korea, India, and recently China.

The Corex plant, shown as Figure 1-2, consists of two major reactors namely the reduction shaft and the melter gasifier. Reduction shaft is where ores are directly reduced by the gas. Lump ore, sinter, pellets, and additives such as limestone and dolomite are charged into the reduction shaft via a lock-hopper system at the top. Reduction gas that consists mostly of carbon monoxide and hydrogen enters the shaft through the bottom at a temperature of 850 °C. By counter flow, the iron ore are reduced up to a metallization degree of over 90%. Spongy iron, or alternatively called direct reduced iron (DRI) is therefore produced, and then fed into the melter gasifier. On the other hand, in melter gasifier, reduction gas is generated by coal gasification and decomposition; DRI is further reduced and then melts in the melter gasifier; finally, hot metal and slag is discharged separately from the bottom of the melter gasifier.^{4,6}

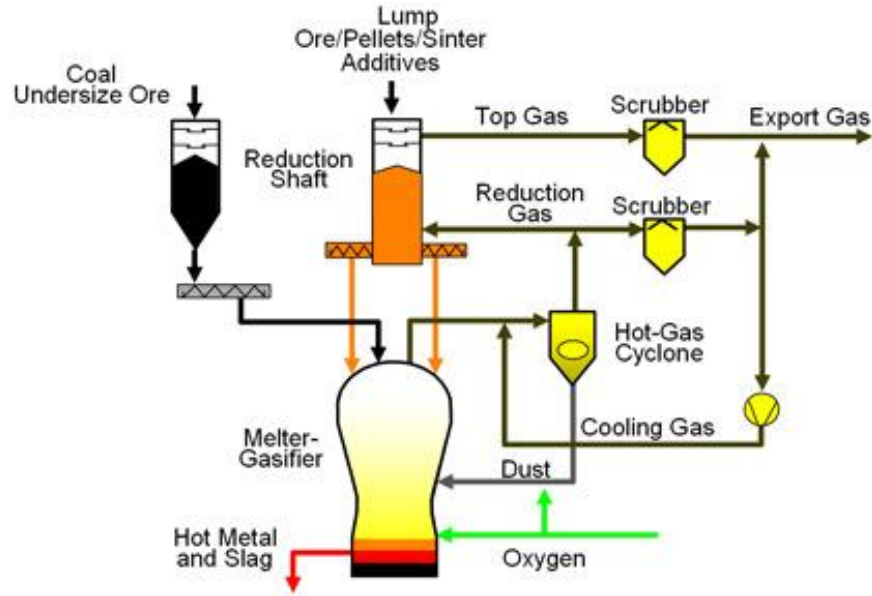


Figure 1-2 Corex process flow diagram. ⁶

1.2 Research Problem

Thermal lumpy coal fed into the melter gasifier serves three major roles:

- Provide reduction gas to reduce iron ore
- Provide heat for the endothermic reaction as well as smelting of iron ore
- Provide a stable char bed in the melter gasifier

A stable char bed is required to have a good permeability, in order to allow reduction gas to flow upwards, and melted metal to flow downwards through the voids. The char particle size is also required to maintain a certain value, and distributes evenly, to reduce gas channelling that will result in instability of operation and deterioration of the metal quality. Furthermore, Baosteel experiences blocking of the gas generation duct above the melter gasifier, which is believed to be related to the excessive fines entering the duct. Most of the fines are the result of coal fragmentation at high temperature.

Kumar et al. ⁷ also concluded that the mean particle size and the fines have a great impact on the operation of the Corex plant of JSW Steel Ltd.. A mean

particle size of 19 - 22 mm is suggested for stable operation, and an upper limitation of 15% is put for fines below 6.3 mm. Based on the statistical analysis of the plant operation data, it is confirmed that with an optimum mean particle size of 19 - 22 mm, the fuel rate and slag rate are the lowest, whereas melting rate is the highest. In addition, as -6.3 mm fines increases, fuel rate and slag rate increase, while melting rate decreases.

Therefore, coal fragmentation under Corex operational conditions need to be studied. In particular, the fragmentation mechanism, factors that might have an impact on the fragmentation behaviour are included in the scope of study. In view of the above, the objectives of this study are as follows:

1. To develop a bench-scale methodology to assess coal performance in Corex melter gasifier.
2. To investigate the effect of coal properties on fragmentation behaviour at high temperature. Coal properties include mineral effect (mineral-coal interface) and quality of organic component (rank – mean vitrinite reflectivity).
3. To investigate the effect of operational parameters, such as coal particle size, temperature and residence time.

2 LITERATURE REVIEW

2.1 Fragmentation Mechanism

The fragmentation mechanisms of large coal particles have been studied by various researchers.⁸⁻¹⁰ Most of the studies are concerned with the particle size reduction in a hot fluidized bed, either in inert atmosphere or oxygen atmosphere, as the particle size is an important parameter for fluidized bed combustor. Particles studied are usually of mm size. Although in Corex, only the surface layer of the char bed is fluidized, the fragmentation mechanism of coal particles remains the same.

Regarding the process of fragmentation of large coal particles, four phenomena are suggested.^{8, 10, 11} When large coal particles are fed into hot fluidized bed, primary fragmentation firstly occurs, turning large coal particles into several smaller fragments. Combustion reduces the size of the char particles furthermore, which is named secondary fragmentation. Attrition is described as the generation of fine particles by abrasion from the char surface. This type of size reduction phenomenon is characterised by generation of lots of fines, while the original char particle size changes little. Another phenomenon is percolation, by which unburned char residue is broken into a number of fines. Among the four phenomena, primary and secondary fragmentation is of the most important as they account for most of the size reduction.

2.1.1 Primary fragmentation and the influencing factors

Primary fragmentation occurs during the devolatilization stage when coal particles are fed into the hot chamber, either a fluidized bed, a drop tube furnace, a TGA chamber, or any other hot environment. When a coal particle is heated, it undergoes a series of reaction. When it is heated above 100 °C, moisture is released. When the temperature goes up to 400 °C, volatile matter starts to get released from the coal particle. The devolatilization proceeds until around 700 °C and after that the coal particle turns into char particle. During the devolatilization process, coal particles tend to break and produce smaller fragments even without external mechanical force, and this phenomenon is called primary fragmentation.¹¹

Two main mechanisms are proposed. One of them regards the fragmentation as the result of the pressure within coal particles produced by rapid volatile matter release during the devolatilization.^{12, 13} As coal particles get heated, volatile matter is released from the coal matrix. The volatile matters transport through pores within the coal particle, arrive at the surface before they finally leave the surface and escape into the environment. In this process, volatile matter releases from the coal matrix much faster than they transport through the coal matrix, especially for coal particles with low porosity. As a result, pressure builds up, and coal particles break when the pressure exceeds the coal strength. The other mechanism of the primary fragmentation of large coal particles is the thermal shock mechanism.^{14, 15} When a coal particle is fed into a hot environment, particle surface is heated first. The inner part of the coal particle is then heated through conduction inwards. As a result, temperature gradient exists within the coal particle, and stress develops accordingly. If the stress exceeds the coal strength, there will be tendency that the coal particle fragments.

A number of researchers^{9, 11, 14} have studied the primary fragmentation and especially factors that influence the fragmentation behaviour during devolatilization. Several factors are concerned. However, the effect of these factors is not restricted to primary fragmentation.

2.1.1.1 Volatile matter

Effect of volatile matter (VM) content on fragmentation of coal is investigated experimentally. Zhang et al.¹¹ studied ten different ranked Chinese coals and found that as VM increased from 15% to 45%, the fragmentation increased continuously. In addition, by visual observation, the product of higher VM coal is found to have a shape of hemispherical and inner cenosphere, which is believed to be caused by devolatilization. This can serve as evidence that VM is one of the important reasons for primary fragmentation. As VM content increases, more VM is released during heating, causing higher pressure within the coal particle, therefore leads to increased fragmentation. However, there are other experiment results against this simple correlation. Dacombe et al.¹⁵ indicated that there existed a peak value of volatile matter content (VM) which produced highest extent of breakage, while low VM and high VM produced less breakage. This value was about 20% for the tested samples which were anthracites and bituminous coal particles with 1-4 mm size. Another observation by Stanmore et al.¹⁴ also implied that the fragmentation behaviour was similar between high and low VM coals with 1.5 mm size. These observations suggest that fragmentation is also greatly influenced by factors other than VM.

2.1.1.2 Porosity

Porosity is believed to have an impact on primary fragmentation as well. As mentioned above, VM has to transport through pores within coal matrix before

they can escape from the coal surface. If the porosity is high, VM has more pathways to travel to the surface and get released, therefore the pressure is reduced, and a lower fragmentation level is expected. On the contrary, if the porosity is low, VM has less pathway to travel, and is more prone to stay longer within coal matrix. As a result, the pressure increases, which increases fragmentation eventually. For instance, Monika et al.⁹ concluded from their study that as porosity increased from 6% to 52%, the average fragments generated by one single particle decreased from around seven to one.

The effect of porosity is also expressed as the effect of Pore Resistance Number (PRN).^{13,16} PRN is defined as the ratio of VM to equilibrium moisture content, while the latter parameter is the water content of air dried coal and is believed to have a correlation with the porosity of the parent coal particle. The experiment result indicates that when PRN is 15, the fragmentation is the most intensive. Considering the fact that the definition of PRN involves VM, the trend is similar to that illustrated by Dacombe et al.¹⁵ that a peak value of VM exist at which fragmentation would be the most intensive.

2.1.1.3 Particle size

The effect of particle size on fragmentation has also been studied. Monika et al.⁹ suggested that for three bituminous coals, the fragments produced by a single particle increased exponentially from 2 to 11 in association with the increase of particle diameter from 2 mm to 11 mm. Zhang et al.¹¹ also observed that for two low VM bituminous coals, the fragmentation increased as the particle size increased from 1 mm to 6 mm. Moreover, it was observed that 4 mm was a critical value. When the particle is smaller than 4 mm, the effect of particle size is less important. Furthermore, Damcombe et al.¹⁵ proposed an empirical

exponential correlation between fragment count and particle diameter, while the correlation parameters varied with different coals. The experiment results of Chirone et al. ¹², Milijana et al. ¹⁶ also reported similar trend.

The effect of particle size can be illustrated from several aspects. Firstly, as particle size increases, volatile matter content increases, while the surface-volume ratio decreases. Therefore, the more volatile matter released during heating has relatively less pathway to escape, leading to a higher pressure within the coal particle. Accordingly, the chance that the pressure exceeds the coal strength increases and fragmentation is likely to happen more frequently. Secondly, as particle size increases, the temperature gradient increases as well. As a consequence, the fragmentation resulted from thermal shock is likely to increase. Moreover, larger particles tend to have a decreased strength. Coal is a highly heterogeneous matter, consisting of minerals, and different types of macerals. As a coal particle becomes bigger, the heterogeneity of a single particle intensifies. As a result, there are more boundaries between different compositions, leading to a lower value of strength. Therefore, the chance of fragmentation increases accordingly.

2.1.1.4 Carbon content

Carbon content is also tried to be linked to the fragmentation behaviour of large coal particles. For example, Monika et al. ⁹ observed that as carbon content increased from 50% to above 80%, the general trend was that primary fragmentation increased accordingly. The effect of carbon content is supposed to be a result of porosity. The brown coals were found no primary fragmentation, because they have much higher porosity, which reduces the pressure thus reduces the fragmentation. However, for hard coals, the primary fragmentation data are

scattered, which means that carbon content effect for hard coals is not obvious. In addition, Dacombe et al.¹⁵ also suggested that higher carbon content resulted in the increase of fragmentation. This might be due to combined effect of primary fragmentation and combustion.

2.1.1.5 Ash content

Ash content reflects the effect of minerals in coal particles. Minerals do not directly lead to fragmentation, but it might affect the coal/char strength therefore affect fragmentation. According to Dacombe et al.¹⁵, there is a tendency that fragmentation increases with increasing ash content. Based on the SEM images of coal particles after devolatilization at 1000 °C, Kim et al.¹⁷ reported more crack in coal with higher inorganic content. However, no further analysis was given.

2.1.1.6 Swelling

Swelling property of coal also might influence the fragmentation behaviour of large coal particles. Kim et al.¹⁷ investigated the SEM images of five char samples obtained through devolatilization in a hot chamber. They suggested that highly swelled char samples have a rough and fluffy surface with fewer cracks. The reason is that as a coal sample has good plasticity, when VM is released during devolatilization, the particle will swell instead of break to reduce the pressure inside the coal particle. In contrast, if the coal sample is resistant to swelling, it is likely that breakage occurs to create more travel route for the VM. However, opposite opinion is raised by Arina et al.⁸, who tested the fragmentation of two coals with almost the same proximate and ultimate analysis, but different values of Free Swelling Index (FSI). The fragments generated per feed particle of the higher FSI sample are about 5 times than that of the lower FSI sample. However, they used a Circulating Fluidized Bed Combustor (CFBC) for

their test. In this case, the strength of the char particle affects the fragmentation. Highly swelled char particle might have a lower strength, thus less resistant to external mechanical forces in a CFBC.

2.1.1.7 Moisture

The effect of moisture content is reported by Dacombe et al.¹⁵ For 12 coal samples with moisture ranging from 0.7% to 5.5%, no specific trend is observed between fragmentation and moisture content. This indicates that moisture, at least at a lower percentage, does not significantly affect fragmentation behaviour.

2.1.1.8 Strength

Also suggested by Dacombe et al.¹⁵, as compressive strength increases, fragmentation decreases, following an exponential trend. It is further emphasized that the particle size effect is essentially the effect of strength, as the exponential correlation is similar to the variation of fragmentation with particle size. This conclusion is in agreement with the earlier explanation regarding the particle size effect, which assumes that as particle size increases, particle strength decreases, leading to more fragmentation.

2.1.1.9 Temperature

Besides these coal properties discussed above, experiment parameters also impact the fragmentation behaviour. These factors include temperature, residence time, as well as experiment conditions. The various experiment apparatus will be explained later.

Experiment temperature might affect the fragmentation, as higher temperature results in higher heating rate and higher temperature gradient, which is likely to cause more fragmentation. Kim et al.¹⁷ concluded that the

devolatilization rate constant increased at higher temperature. The devolatilization time was also found to reduce. Zhang et al.¹¹ also suggested that fragmentation increased with increasing bed temperature. Furthermore, Monika et al.⁹ observed that as bed temperature increased from 700 °C to 900 °C, the fragments generated per feed particle increased from 1 to 8, and 1 to 3 for two different coal samples.

2.1.1.10 Residence time

Regarding residence time effect, Zhang et al.¹¹ observed that as residence time increased, fragmentation increased accordingly, until a peak value; after that, fragmentation decreased with longer residence time. This can be explained by devolatilization process. Before the peak value, the pressure resulted from devolatilization is increasing with residence time, therefore fragmentation as a result of the inner pressure also increases with residence time. After the peak value, the devolatilization approaches the end, therefore the pressure decreases; the thermal shock also reduces at this time. As a result, the fragmentation does not increase anymore. In the meantime, some fine particles burn out with longer residence time, which reduces the fragmentation count. Similar trend was also observed by Dacombe et al.¹⁵, who further suggested that as particle size increases, more time is required to reach the fragmentation peak value.

Since there are many coal properties and other parameters that might affect coal fragmentation, it is difficult to predict coal fragmentation based on a single factor. Instead, some of the abnormal fragmentation behaviour whose prediction is based on a single factor can be explained if several factors are taken into consideration. For example, samples of high and low VM produce the same level of fragmentation, while coal sample with 20% VM generates the most fragments.

¹⁵ The result might be explained from two aspects. As VM increases, the inner

pressure during devolatilization increases. On the other hand, the increase of VM usually associates with lower coal rank and higher porosity. Combining these two factors, it is possible that sample of low VM releases less VM thus less pressure; sample of high VM has a high porosity, which allows more travel route for VM, thus reduces the pressure inside the coal particle. Both of these cases lead to reduced fragmentation.

2.1.2 Devolatilization time and rate

Primary fragmentation is largely determined by the devolatilization process. An empirical exponential correlation between devolatilization time and particle size is suggested and approved by various researchers.¹⁸⁻²⁰ A typical exponential correlation is as follows:

$$t = A \times d_p^n$$

where, t is devolatilization time, d_p is particle diameter, and A and n are the parameters varying with different conditions. The dominant role of particle size in determining devolatilization time of large coal particles is illustrated by Stubington et al.²¹ For small particles, the pyrolysis rate is controlled by chemical kinetics. As particle becomes bigger, the limiting factor changes to heat and/or mass transfer that is largely determined by particle size. A critical value, 2 mm, is suggested for heating rates $< 100 \text{ }^\circ\text{C s}^{-1}$. For the purpose of this study, the heat and/or mass limiting mechanism is applicable. Furthermore, the author observed that the measured devolatilization time was close to the calculated time for the centre of the particle to reach the bed temperature. Therefore, the heat transfer controlling hypothesis is verified.

As far as the devolatilization time of large coal particle concerns, coal type is not a significant factor. Stubington et al.²² showed that for three bituminous coals,

the difference of devolatilization time for the same sized coal was limited. The same value of n could be used for all the three samples, while the values of A varied from 2.35 to 2.99. Similar conclusion can be drawn from the experiment result of Stubington et al.²¹. These observations are in agreement with the hypothesis that for large coal particles, the controlling factor of devolatilization time is heat and/or mass transfer instead of chemical kinetics.

On the other hand, temperature has a great impact on devolatilization rate and therefore reaction time. It has been noticed by Kim et al.¹⁷ that devolatilization rate constant increases with increase of temperature. Stubington et al.²⁰ also investigated the effect of temperature with 7 varying temperatures from 600 °C to 1000 °C. Assuming the same value of n as 1.5, the values of A vary from 1.76 for 1000 °C to 4.82 for 600 °C for the same sample, which means that the devolatilization time increases as the increase of temperature.

2.1.3 Secondary fragmentation

Secondary fragmentation refers to char fragmentation as combustion weakens the bridges and network within the char particles. Before secondary fragmentation experiment, char particle is firstly prepared by devolatilizing a coal particle in inert gas. Then char particles are gently sieved to get a narrow sized batch.

As secondary fragmentation is closely related to combustion, the combustion progress affects the fragmentation extent. In particular, carbon conversion is used as an indication of combustion degree. Arena et al.⁸ measured carbon conversion degree for different char particles and found that no secondary fragmentation occurred until the degree of conversion reached 40%; as the conversion degree further increased, fragments generated by a single char particle increased as well. In addition, Dacombe et al.²³ showed the SEM images of char particles at different stages of combustion. As residence time increases, char conversion

degree increases, resulting more deteriorated char structure.

Initial char size is also found to have an impact on secondary fragmentation. As observed by Arena et al. ⁸, the number of fragments generated per feed char particle increased with the increase of initial char size at the same conversion degree. It is further suggested by the author that the reason might be the increase of heterogeneity in larger particles. However, Arena ⁸ and Chirone et al. ¹⁰ both noticed that very large particles had less fragmentation. The phenomenon is supposed to be a result of carbon conversion degree. Since the time interval is set a certain value, for example, 30 s in the work by Chirone et al. [9], it is possible that the conversion degree is much less for larger particle, especially the inner region. Therefore, the strength of the large particles remains high, which is responsible for the less secondary fragmentation. In addition, both of these works show that the size distribution of the fragments is not necessarily related to the initial char size.

2.2 Primary Fragmentation Model

2.2.1 VM-driven model

Chirone et al. ¹² used a base model to predict primary fragmentation. It is assumed that thermal stress is neglected in this circumstance, for particles with size up to 18 mm. Pressure profile resulted from devolatilization is estimated by combination of coal pyrolysis kinetics and heat and mass transport. Voidage evolution is also considered. Firstly, the repulsive force resulted from pressure is calculated. The result indicates that the repulsive force increases and then decreases with the increase of residence time. When it comes to calculation of resistant force, two submodels are described. One assumes a critical stress in variance with temperature, and the other is based on Weibull theory, a probability

distribution theory. The prediction based on critical strength indicates that no fragmentation will occur for particles smaller than 12 mm. In contrast, the prediction based on Weibull probability theory matches well with experiment results.

2.2.2 Thermal stress model

Based on the assumption that primary fragmentation is mainly a result of thermal shock, thermal stress model is developed. No and Syred²⁴ determined the thermal stress distribution of small particles whose size is suitable for an internal quasi-static temperature distribution. Stanmore et al.¹⁴ applied this model to predict the thermal stress of particles with a size of 2.5 mm. The calculation predicts maximum tensile stress at the centre and maximum compressive stress at the surface after only 1-2 s when the coal is fed into the fluidized bed. Therefore, it is suggested that fragmentation resulted from thermal shock occurs at the first few seconds. Moreover, fissure is likely to happen at the centre, while the outer part is likely to be delaminated. Dacombe et al.¹⁵ further improved the model by considering the transient problem for particles with larger size in which case the quasi-static assumption is not appropriate. The calculation result indicates that the tensile stress at the centre far exceeds the tensile strength within a short time of entering the furnace; therefore, crack is expected at this region. For the outer part, the stress is compressive, and the value is lower than the compressive strength at the beginning. As particles get heated, the compressive stress increases. Fragmentation occurs when the compressive stress finally exceeds the compressive strength. Moreover, the initiation of fragmentation is very soon at the experiment condition, calculated as 131 ms for the 1633 μm , 78 ms for the 2433 μm , 67 ms for the 2868 μm , and 35 ms for the 3390 μm .

These two primary fragmentation models predict fragmentation based on two

mechanisms, but they are not contradictory. As suggested by Stanmore et al.¹⁴, for relatively small particles, thermal stress might be the main reason of fragmentation, because small particles have less VM, and more relative surface for the VM to escape. This statement agrees with the result of VM-driven model based on critical strength theory by Chirone et al.¹² that particles smaller than 12 mm never fragment. On the other hand, with larger particles, VM tends to build up higher pressure within the coal particles, thus the effect of VM becomes more important.

2.3 Methods of Investigation

The fragmentation behaviour of large particles has been investigated using various types of experiments. Fluidized bed is the most common apparatus.^{8, 13, 25} Inert gas, usually nitrogen, or nitrogen with different concentration of oxygen, is used as the fluidizing gas for different study purposes. The particle size is commonly several millimetres, while the largest one is mentioned to be in the range of 9-10 mm. According to Stubington et al.²¹, fluidized bed has a high heat transfer coefficient, ranging from $460 \text{ Wm}^{-2}\text{K}^{-1}$ at $750 \text{ }^\circ\text{C}$ to $500 \text{ Wm}^{-2}\text{K}^{-1}$ at $950 \text{ }^\circ\text{C}$. As stated previously, the heating rate affects the devolatilization rate that will exert an impact on the fragmentation behaviour. CFBC works with the same principle, but it involves more mechanical force compared to a fluidized bed.

Drop tube furnace was used by Dacombe et al.^{15, 23} for their study on combustion induced fragmentation. Test in a drop tube furnace is believed to better represent the condition in an entrained flow environment. The furnace itself has a height of around 2 m, and a diameter of 40 mm. It also has a hot chamber at the top to heat the particles as soon as they enter the furnace. A series of sampling points are arranged at different distance from the feed point, allowing variance of

residence time. For example, for a particle with a size of 3390 μm , the residence time varies from less than 100 ms to 2 s. In this case, inert gas is not provided, which means the particles will devolatilize and combust in the air.

TGA and similar gravimetric rig are utilized in some work.^{17, 20, 22} This kind of apparatus is able to record the weight change with time, therefore determines the devolatilization status easily. Moreover, the fragmentation of coal particles in these rigs is exclusively primary fragmentation, if inert gas is provided. Only thermal shock and devolatilization cause fragmentation, and the effect of external mechanical force is eliminated. Camera can also be installed in the rig to record the change during devolatilization, therefore the analysis of VM release, swelling behaviour, crack, and agglomeration can be done.

Drop test is another test method to investigate the fragmentation behaviour. A drop tower is designed for the drop test by Sahoo and Roach.⁵ A maximum height of 10 m is available from the drop tower. Different drop heights, drop surfaces, sample mass, coal types, handling conditions can be tested by the rig. The fragmentation by volume breakage and surface breakage can be determined by different drop heights. However, the drop tower is only suitable to test fragmentation under cold conditions.

Apart from these experiment apparatus, some standard tests also give information about the fragmentation behaviour of coal particles at high temperatures. A number of ways have been developed to assess the strength of coal and/or its char giving an indication of their susceptibility to fragmentation. Char Reactivity Index (CRI), Char Strength after Reaction (CSR) and the Thermal Decrepitation Index (TDI) are among the analytical methods that have been standardised to assess the expected stability of char and char beds. These characteristics are directly or indirectly linked to the organic nature of coal. The

CRI and CSR of coal char are carried as per IS4023:1991 standard.

$$\text{CRI} = \frac{\text{Initial weight of sample} - \text{weight after reaction with CO}_2}{\text{Initial weight of sample}} \times 100$$

$$\text{CSR} = \frac{\text{Weight of +10mm sample}}{\text{Weight of sample after reaction with CO}_2} \times 100$$

Kumar et al.²⁶ recommended CRI below 30%., and CSR above 45%.

The test procedure to determine thermal decrepitation index is explained by Kumar et al.²⁶ The coal sample is kept at 1000 °C in N₂ atmosphere for 1h. The sample is then performed tumbler test. Calculation is based on the sieving analysis as follows:

$$\%_{+10\text{mm}} = \frac{\text{weight of +10mm sample}}{\text{initial weight of sample}} \times 100$$

$$\%_{-2\text{mm}} = \frac{\text{weight of -2mm sample}}{\text{initial weight of sample}} \times 100$$

In summary, besides VM and porosity, ash content and swelling index are two dominant coal properties that influence the fragmentation behaviour. Ash content is a reflection of mineral and swelling index is related to organic character of coal. These are studied in more fundamental manner by using advanced characterization of coal such as Computer Controlled Scanning Electron Microscope (CCSEM) and automated reflectogram.

3 METHODOLOGY AND HYPOTHESIS

3.1 The Characteristics of the Present Method

Based on the above review of the literature, all the fragmentation test methods are considered for the present study purpose. Most of the fragmentation of large coal particles at high temperature is studied in a fluidized bed condition, which is not the condition in a Corex plant. Gravimetric rig is only suitable for pure primary fragmentation test, while in a Corex plant, coal particles are impacted by their own momentum onto the char bed, as well as the drop momentum of the newer fed coal particles on them. In a Corex melter gasifier, coal particles fall onto the char bed from a height of about 10 – 15m. The temperature in the gasifier is of the order of about 800 – 1000 °C and the bed at about 600 °C. The drop test in the drop tower is only at room temperature, which fails to represent the more complex behaviour of lumpy coal at high temperature. The drop tube furnace therefore is a better choice, since it can provide a high temperature environment. As a result, a drop tube furnace for drop test at high temperature is custom designed, as explained later in the next section. Higher impact resulting from a 15m height is simulated in the drop tube furnace (height of about 1m) by dropping some steel balls.

The interested coal particle size of this study is larger than that in most studies in the literature review part, except for the drop test of large coal particles

at room temperature in a drop tower. In the present study, the size ranges from 5 mm to 38 mm, covering the optimum size ranges suggested for Corex plant.

From the view point of fragmentation mechanism, the fragmentation produced by drop test in a drop tube furnace is the combined results of primary fragmentation and those resulted from impact momentum. In order to simulate the condition in a meter gasifier, 8 steel balls are dropped on top of the fed coal particles to facilitate fragmentation after thermal treatment for certain time. In this case, the underlying mechanism is further complicated. The char strength after devolatilization, that implies the resistance to external mechanical force, probably becomes more important to determine the final fragmentation result.

Finally, the effect of mineral in coal on fragmentation behaviour at high temperature has not been fully investigated in earlier studies. As indicated in the literature review part, there are experimental results showing that mineral/ash has an impact on the fragmentation,^{15, 17} but detailed analysis is not done. Furthermore, as char strength is a greater concern for Corex process, mineral might have an increased importance because of the possible relationship of mineral coal interface with char strength. Therefore, the effect of minerals on fragmentation of large coal particles is investigated in the present study.

3.2 Hypothesis of the Present Study

Coal is a highly heterogeneous material as shown in Figure 3-1. The black part is coal matrix, while the coloured part represents minerals. There are different types of coal particles. A few particles are almost pure coal or pure mineral, but the majority consists of both coal and minerals. The mineral percentage within a single particle, represented by the area percentage of the coloured part, varies a lot. It also shows that the mineral size distribution varies for different particles. Some

minerals are of large particle size, while some smaller particles disperse within the coal matrix. Besides the mineral-coal interface, heterogeneity also exists within coal matrix. Different grey shades, as shown in Figure 3-2, represent different maceral compositions. The brightest part is probable bright minerals, while darker part represents different types of macerals.

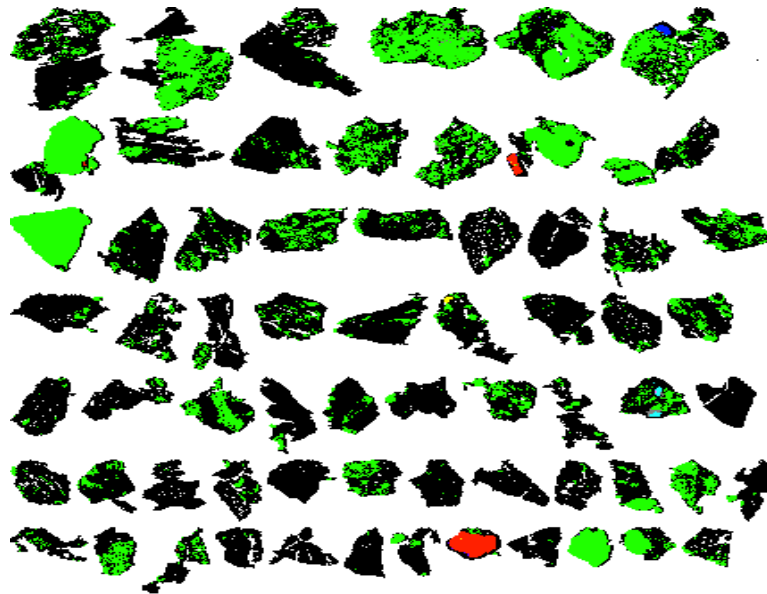


Figure 3-1 Mineral distribution in coal matrix.²⁷

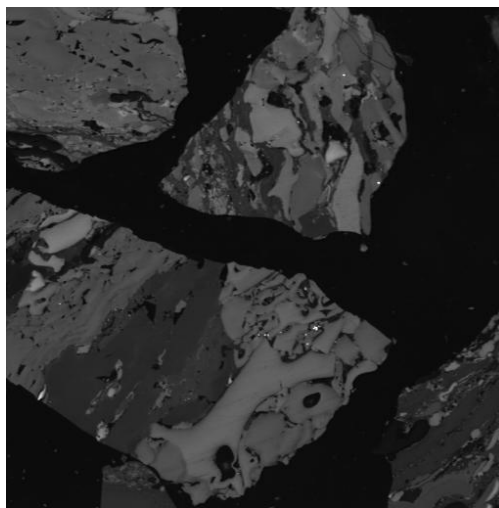


Figure 3-2 Heterogeneity of coal matrix.

The hypothesis of this work lies in the heterogeneity of coal particles, especially the heterogeneity caused by mineral particles. The interface between mineral and coal matrix as well as between different macerals are supposed to be the weak area where fragmentation is most likely to occur. Therefore, CCSEM analysis is applied to give detailed information about mineral in order to assess the fragmentation probability. The heterogeneity of macerals can be assessed by grain data report from petrographic analysis.

In addition, at the dome of Corex plant, the temperature is around 1050 °C, therefore coal particles are devolatilized and form char particles. During this process, factors that affect devolatilization and primary fragmentation need to be investigated. VM content and the organic component are therefore studied as well. Petrographic analysis is applied to characterise the organic components in detail.

4 EXPERIMENT

4.1 Proximate, Ultimate Analysis and Thermal Characteristics

Two Chinese coals, labelled A, and B, supplied by Baosteel and two Canadian coals, labelled C, and D were used for fragmentation experiments of this work. Table 4-1 shows the results of proximate and ultimate analysis of the four coals. Table 4-2 shows coal decrepitation test and char reactivity test of the two Chinese coals.

From the analysis, it shows that all the four coals are bituminous coal, with dry, ash-free VM ranging from 27% to 40%. The ash content ranges from 9% to more than 14%. The thermal decrepitation index provided by Baosteel shows that coal A and B have close values of TS + 10, while coal B has much higher value of TMS + 10 than that of coal A. This indicates that coal B has higher char strength than coal A. However, tumble drum test is criticized by Teo et al.²⁸ because it cannot differentiate surface breakage and volume breakage, and it is also affected by a number of drum and materials parameters. In contrast, drop test is verified from theoretical aspect and experimental work as a better method to test volume breakage that plays a more important role to determine size reduction.

Table 4-1 Proximate and ultimate analysis of the four coals

| Sample | Proximate analysis (wt. %) | | | | |
|--------|--------------------------------------|----------|----------|---------|------|
| | Moisture (ad) | Ash (ad) | VM (daf) | FC (ad) | |
| A | 5.01 | 10.39 | 31.0 | 58.39 | |
| B | 2.39 | 9.74 | 38.0 | 54.51 | |
| C | 1.26 | 14.07 | 27.0 | 61.85 | |
| D | 9.46 | 12.30 | 40.0 | 46.94 | |
| | | | | | |
| | Ultimate analysis (wt. %; dry basis) | | | | |
| | S | C | H | N | O |
| A | 0.56 | 66.8 | 3.86 | 0.78 | 8.99 |
| B | 1.87 | 73.41 | 4.57 | 9.28 | 8.96 |
| C | 0.61 | 79.4 | 4.48 | 1.46 | 3.83 |
| D | 0.33 | 56.06 | 4.13 | 1.03 | NA |

Table 4-2 Thermal characteristics of the Chinese coals [Source: Baosteel]

| | Coal decrepitation | | | | Reactivity of char | |
|-----------|--------------------|-------------------|---------------------|--------------------|--------------------|-----------|
| | TS+10 [*] | TS-2 [*] | TMS+10 [#] | TMS-2 [#] | CRI | CSR |
| Average A | 90.2 | 1.6 | 27.7 | 15.1 | 39.1 | 74.5 |
| Range A | 85.7-93.3 | 1.3-2.1 | 20.7-37.6 | 10.3-17.7 | 33.7-49.5 | 68.6-78.4 |
| Average B | 90.59 | 1.65 | 45.12 | 14.37 | 40.77 | 69.02 |
| Range B | 86-93.8 | 1.3-2.1 | 30.1-52.9 | 13.4-15.64 | 30.8-47.9 | 62.2-77.5 |

^{*}TS+10/-2: Percentage of particles larger than 10 mm/smaller than 2 mm after devolatilization; [#]TMS+10/-2: Percentage of particles larger than 10 mm/smaller than 2 mm after tumbler test of char.

4.2 SEM Analysis

A portion of the lump coal was crushed manually to -10 mm size, after which the sample was dried in an oven for 1 hr at 105 °C. It was cooled in a desiccators and then ground in a ball mill. The product was classified by sieving into a size fraction + 150 - 250 µm. This size fraction was used to make pellets using epoxy resin as the carrier medium. The pellets were polished ready for microscopic analysis on the SEM. The remaining samples were kept in sealed polyethylene bags and stored in the freezer.

Scanning Electron Microscope (SEM) analyses were done at University of Alberta laboratories on the pellets of the two Chinese coals. Energy Dispersive X-Ray Spectroscopy (EDX) technique was used to determine the elemental composition of the minerals found in the coal samples.

4.3 CCSEM and Petrographic Analysis

In order to characterise minerals in detail, CCSEM analysis was applied. It is capable to analyse mineral based on individual mineral particle, instead of bulk composition. In particular, it provides information about individual particle size, shape, composition, and its association with coal particles. This information is helpful to assess the fragmentation behaviour of coal particles at high temperature, as mineral distribution is closely related to char strength.

CCSEM analysis involves a scanning electron microscope and an energy-dispersive X-ray spectrometer. A computer program was developed for the SEM to automatically scan preselected area of a polished sample. Over 1500 points were scanned and recorded for each sample. For each point, a recognition program was designed followed by chemical composition detection. Three magnifications were usually applied, × 50 for 22.0 - 400 µm particle, × 250 for

4.6 - 200 μm particle, and $\times 800$ for 1- 4.6 μm particle. The area for each particle was measured, and assumed to represent the volume from a statistical point of view. Weight percentage was then calculated by multiplying the area by the density of the particular minerals.²⁹⁻³¹

Petrographic analysis of coal has been a standard method widely used. Geologists use petrographic analysis to obtain information about coal deposition, while coal researchers use petrographic analysis to evaluate coal performance from many aspects, such as coal tar and pitch quality, and in particular, coking performance. The volume change and coke oven pressure can be predicted by petrographic data. Petrographic analysis can also suggest the optimum blending ratio of different coals for coke making. For example, best coking quality requires an appropriate ratio of reactive to inert component. Petrographic analysis is able to determine the reactive and inert components in a certain coal. In fact, a system of evaluating coking performance is developed based on petrographic analysis, and this system has been widely used since 1950.³²⁻³⁶

Petrographic analysis is based on optical distinctness of different components. To be specific, the reflectance of a coal sample is measured point by point, either manually using an optometer, or using an image analysis program automatically. A reflectogram is then generated, either in the form of reflectance frequency or full maceral reflectogram.^{37,38} Schapiro et al.³⁹ investigated the relationship between reflectance and a series of coal physical and chemical properties. It was found that the VM, maximum Gieseler fluidity, volume change, and coking pressure are all related to the reflectance value. In addition, besides mean vitrinite reflectance value, which is believed to be an indication of coal rank, Full Maceral Reflectance (FMR) is also used by some researchers. Defined as the summarization of each reflectance value multiplied by its frequency, FMR gives information of the whole

coal instead of just vitrinite information.³⁷

The petrographic analysis in the present work was done by automated reflectogram. 250 images were taken for each sample by a camera. Each image had a resolution of 512×512 pixels. The grey scale was 256, and calibrated so that each grey scale corresponded to a certain reflectance value. By detecting the reflectance value of each pixel in all the images, a reflectance distribution was obtained. Typically around 30 million reflectance values were involved for analysis.

For the case of CCSEM and petrographic analysis, a small portion (200 - 300 g) was manually crushed to -10 mm size. The crushed sample was then dried in a standard oven for 1 h at 105 °C. It was allowed to cool in desiccators before being ground batch-wise in a planetary ball mill. The product was sieved at +150-212 μm and the oversize material was recycled into the mill. The finer fraction (-150 μm) was kept in different containers and stored in the freezer for possible future use. The + 150 - 212 μm fraction was properly labelled and placed in sealed polyethylene bags and stored in the freezer. The sample was later divided into 20 - 30 g portions that were put in small sealed glass bottles, labelled and packed ready for shipping to the analysing laboratory. The same procedure was followed for all the coals that were to be tested by the two methods.

CCSEM analysis was conducted at Microbeam Technologies Inc., a specialised laboratory in North Dakota, USA. Representative samples in the size fraction + 150 – 212 μm were used in the analysis. Petrographic analysis was done by CSIRO at Brisbane in Australia for coal A and B, and at Pearson Coal Petrography in British Columbia for coal C and D. The same size fraction as for CCSEM analysis was used for the petrographic studies.

4.4 Fragmentation Drop Test

4.4.1 Equipment

A special test rig was designed and fabricated to simulate the conditions in the melter gasifier, shown in Figure 4-1. The reactor consisted of a vertical split furnace with three heated zones that was capable to deliver high temperatures up to 1200 °C. A perforated impact plate was provided at the bottom. The coal particles were dropped onto the impact plate to get heated. The top of the reactor tube was a sealing system of double valves to ensure no emissions and loss of heat. A cooling water jacket was provided to protect the valves from damage by the heat. Thermocouples were installed at various points to record the internal temperature inside the reactor tube. The readings were automatically transferred to a computer dedicated for the tests. A gas inlet was provided at the top of the reactor to allow nitrogen gas during the tests. The gas exited at the bottom of the reactor. A practical view of the experiment rig is shown in Figure 4-2.

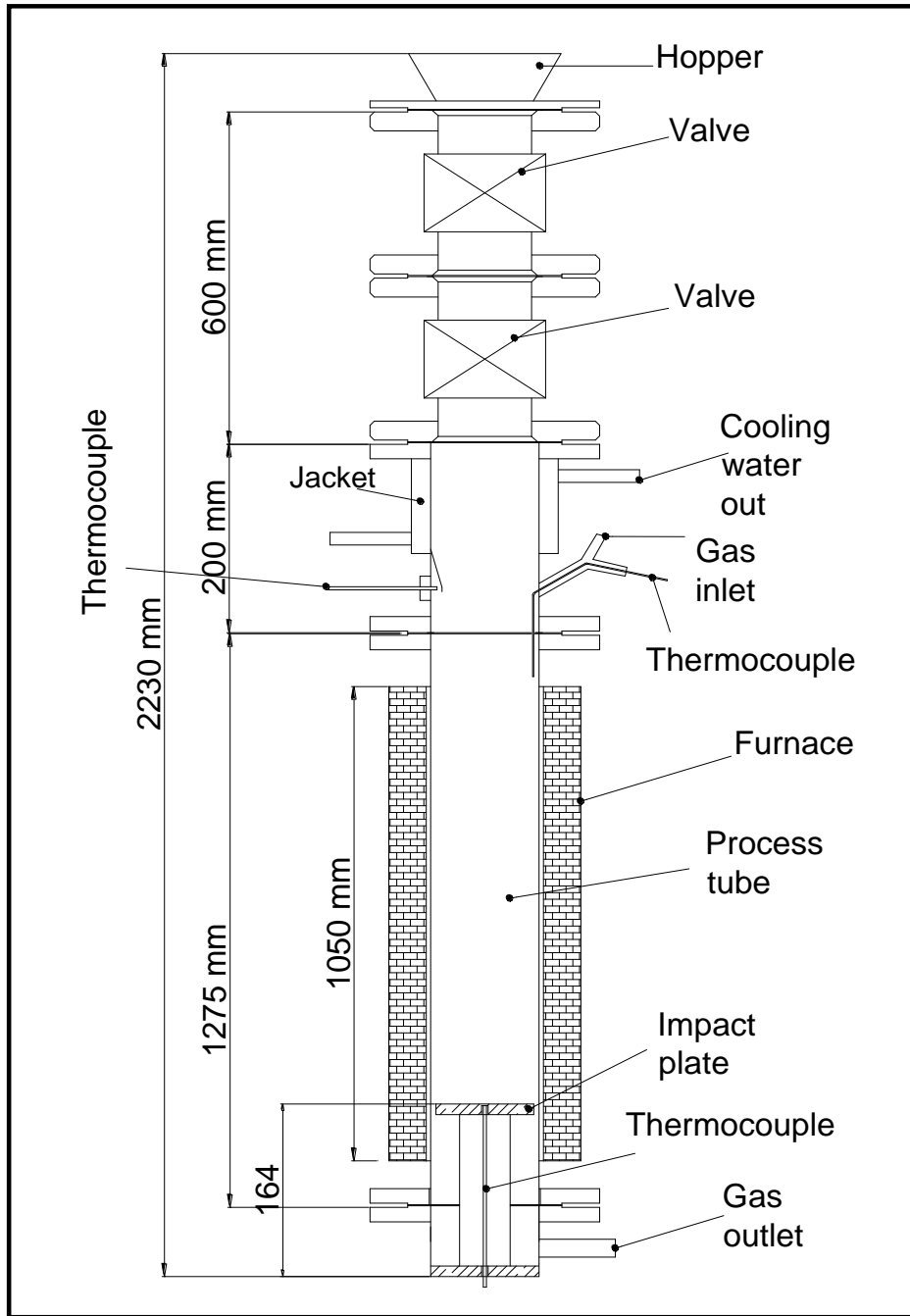


Figure 4-1 Scheme of the drop tube furnace for thermal fragmentation test.



Figure 4-2 Drop tube furnace for drop test at high temperature.

The impact plate (Figure 4-3) was perforated to allow gas to pass through. One of the thermocouples was positioned just below the surface of the impact plate to give an indication of the temperature in that region during experiments. Initially the height of the perforated plate from the bottom was designed as 164 mm. However, heat loss from the bottom made it hard to achieve the target temperature, even though proper insulation had been placed. To raise the temperature of the plate where coal particles rest on to get heated, a new perforated plate was custom made, with a height of 85 mm, and was designed to be easily installed on top of the original one, shown in Figure 4-4.



Figure 4-3 Impact plate at the bottom of the drop tube furnace.



Figure 4-4 New impact plate (left) and modified impact plate assembly (right).



Figure 4-5 Tube reactor inside a partly opened split vertical tube furnace.

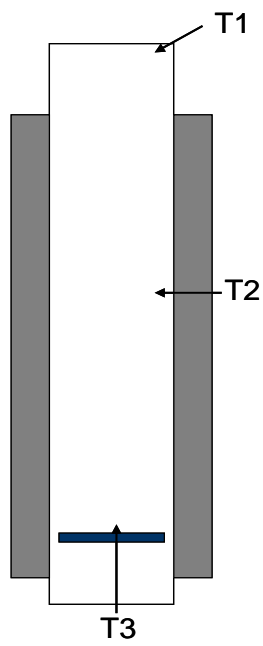


Figure 4-6 Locations of thermocouples inside the tube furnace.

Figure 4-5 shows the position of the tube relative to the furnace. Ceramic fibre insulation was placed at the top and the bottom of the furnace to minimize heat loss at the gap between the furnace and the tube reactor. Nitrogen gas was provided to maintain an inert atmosphere.

Thermocouples were installed to detect the temperatures at different locations inside the tube, shown in Figure 4-6. T1 implied the temperature near the valve to ensure that the temperature was below the maximum temperature that the valve could withstand. T2 detected the temperature in the middle zone of the tube, and it was the target temperature as well. T3 detected the temperature slightly above the plate surface. After coal particles were dropped, T3 indicated the temperature around the coal particles. The recording from experiments showed that T3 was about 150 °C lower than the target temperature because of the heat loss. The same T3 at the same target temperature was maintained by adjusting the temperature setting of the bottom zone.

4.4.2 Experiment design

Experimental matrix was prepared to include a good number of variables. Besides coal type, parameters such as feed size, reactor temperature, and residence time were also included in the experiment plan. Drop tests were designed both at room temperature as well as at high temperatures comparable to those in the melter gasifier.

4.4.2.1 Cold tests

Table 4-3 shows the experimental design for the drop tests conducted at room temperature. Coal A and B were tested, as tests at room temperature were preliminary tests. Three different fractions of the two coal samples were used in these experiments. 8 steel balls were used as mechanical force to facilitate

fragmentation. Each test was repeated three times to obtain a statistically acceptable level of repeatability.

Table 4-3 Room temperature drop tests matrix

| Coal type | Size fraction [mm] | Reactor temperature (°C) | Stress | Numbers of drop tests | No. of experiments |
|-----------|--------------------|--------------------------|------------|-----------------------|--------------------|
| A B | 26.7-38 | 23 | No balls | 3 | 12 |
| | | | With balls | 3 | 12 |
| | 16-26.7 | 23 | With balls | 3 | 12 |
| | | | No balls | 3 | 12 |
| | 8-16 | 23 | With balls | 3 | 12 |
| | | | No balls | 3 | 12 |
| | | | Total | 72 | |

4.4.2.2 High temperature drop tests

Table 4-4 shows the planned experiments at different temperatures that approximated those found in the Corex melter gasifier. The experiment matrix included four coals, labelled A, B, C, and D, whose proximate and ultimate analysis was already given in Table 4-1. During the industrial process, coal experienced various mechanical impacts, such as drop momentum from the particle itself as well as from newer fed particles, collision between coal particles, as well as between coal particles and feed ore, etc. Therefore, stress was applied in the experiment to facilitate the fragmentation by dropping steel balls after coal particles were adequately heated. Moreover, replication was applied for each test. Two replications were minimal. If the deviation exceeded the accepted range,

additional experiment was required. In the experiment, < 7% deviation from the average was seemed acceptable. In addition, in order to compare the effect of thermal treatment, the same drop test was conducted at room temperature for coal A, B, and C, with feed size 22-11 mm.

Table 4-4 High temperature drop tests matrix

| Coal type | Size fraction [mm] | Reactor temperature (°C) | Stress | Replication | No. of experiments |
|------------------|--------------------|---------------------------|------------|-------------|--------------------|
| A B C D | 32-22 | 800 | With balls | 2 | 72 |
| | | 900 | With balls | | |
| | | 1000 | With balls | | |
| | 22-11 | 800 | With balls | | |
| | | 900 | With balls | | |
| | | 1000 | With balls | | |
| | 11-5 | 800 | With balls | | |
| | | 900 | With balls | | |
| | | 1000 | With balls | | |

In this work, the drop test of coal D was done only with the size range of 32-22 mm, because the effect of other parameters such as feed size on fragmentation degree was already clearly shown by the results of the test of other three coals. Therefore, only the effect of different coal types needed to be further investigated.

Besides the above parameters, residence time was tested as well. Coal B, in

the size fraction of 32 - 22 mm, was used in this set of experiment. The target temperature was maintained as 900 °C, and steel balls were applied in all the tests. The residence time variables included 2 min, 5 min, 10 min, 20 min, and 40 min.

4.4.2.3 Fragmentation criteria

Sieving analysis was done to determine particle size distribution. Standard sieves were selected to perform sieving analysis, so that the included size ranges were as follows:

Table 4-5 Size ranges determined by standard sieves

| | | | | | | |
|--------------------|--------------|----------------|----------------|----------------|-------------|----|
| Size range (mm) | 32 ~ 22.6 | 22.6 ~ 11.2 | 11.2 ~ 5.66 | 5.66 ~ 3.35 | 3.35 ~ 1 | <1 |
|--------------------|--------------|----------------|----------------|----------------|-------------|----|

To indicate the degree of fragmentation, several indexes were defined. Similar indexes were also defined by other researchers.^{11, 16}

Fragmentation Index, FI:

$$FI = (\sum f_i \times \bar{d}_i) / \bar{d}_f \quad (1)$$

where f_i and \bar{d}_i are the mass fraction and mean diameter, respectively, within the i^{th} size range, $i=1\sim6$. \bar{d}_f is the mean diameter of the feed particles. This serves as the main criterion of fragmentation. The definition of FI involves the feed size, so that it can be used to compare the degree of fragmentation with different feed sizes. The smaller the F value, the more fragmentation is.

Product Particle Number:

The number of particles that are retained above the sieve with an opening of 3.35 mm in sieving analysis. As each experiment is repeated once, the Product Particle Number is the sum of the particle numbers of the two experiments at the same condition.

Fragmentation Number Index, S:

$$S = N_{\text{out}} / N_{\text{in}} \quad (2)$$

where, N_{out} is the Product Particle Number and N_{in} is the number of feed particles. S can be interpreted as the number of particles each feed particle breaks into. Since the feed particle number is not the same for different feed sizes, S is used instead of Product Particle Number to compare the fragmentation behaviour of samples with different feed sizes. A bigger S implies more fragmentation.

Fines Percentage:

Particles that are smaller than 3.35 mm are difficult to count. However, they are an important indicator of the fragmentation behaviour, and can exert great impact on COREX operation. Therefore, the fines are characterized by Fines Percentage, which is defined as:

$$\text{Fines Percentage} = \frac{\text{Weight} - 3.35\text{mm}}{\text{Total Weight}} \times 100\% \quad (3)$$

4.4.2.4 Standardization

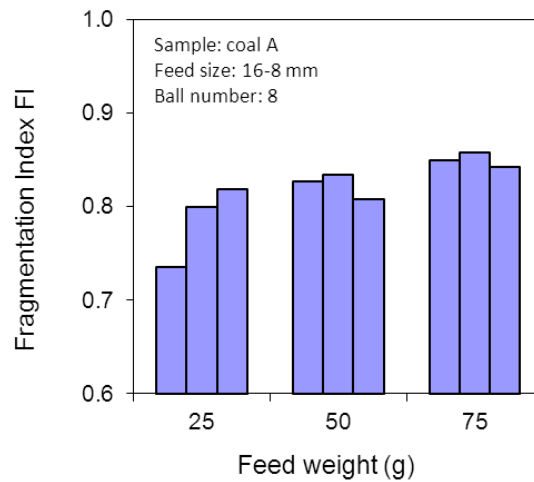
In order to improve repeatability, proper weight and ball numbers were determined. Tested weights included 25g, 50g, and 75g, while tested ball numbers included 4 and 8. Fragmentation Index, FI was applied as a major criterion for comparison. All the tests were done at room temperature.

From Figure 4-7, it is clear that as feed weight increases, the deviation of each test decreases, indicating a better repeatability. To be specific, when the feed weight is 25g, the deviation can be as high as over 6%, while for feed weight 50g and 75g, the deviation is below 2%. As a result, to produce a better repeatability, 50g is selected as the standard weight in the experiment.

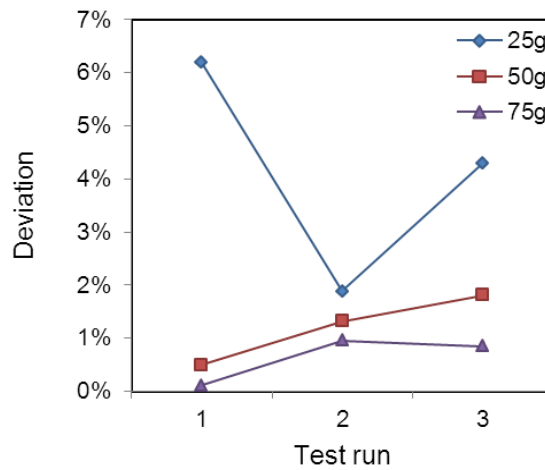
In practice, the weight was controlled as close as possible to 50g. In addition,

the numbers of feed particles were controlled the same, 3 particles for 32- 22 mm category, 20 particles for 22- 11 mm category, and 80 particles for 11- 5 mm category. This enabled more than one index to indicate fragmentation behavior.

On the other hand, the effect of ball number on the test result is not as big as that of feed weight (Figure 4-8). The deviation of the mean diameter of 4 balls and 8 balls test is close to each other, and within a reasonable range. In order to cover the whole area of the impact plate, 8 balls were used in the “with balls” test.

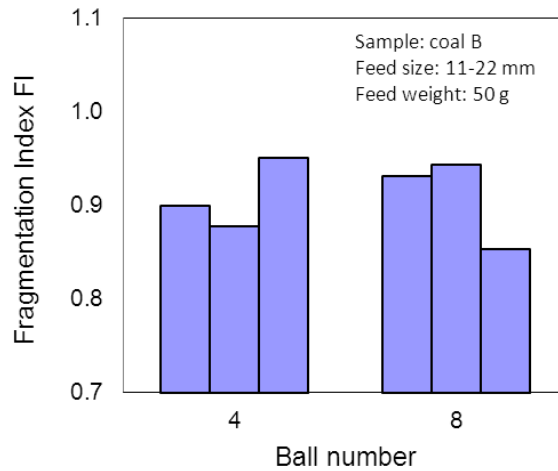


(a)

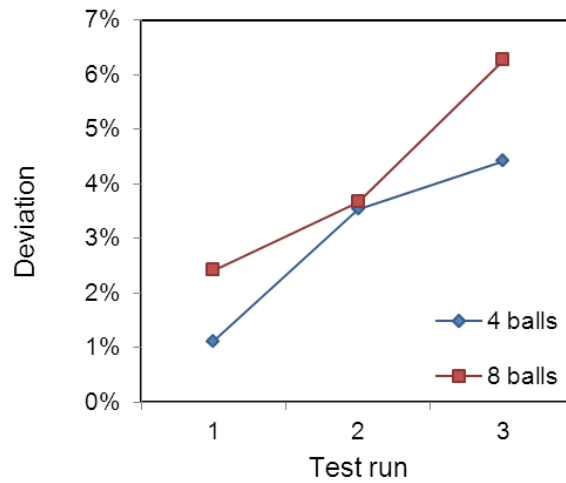


(b)

Figure 4-7 Fragmentation Index FI (a) and corresponding deviation (b) in variance with feed weight. Feed: Coal A; Size: 16-8 mm and No. of Balls: 8.



(a)



(b)

Figure 4-8 Fragmentation Index FI (a) and deviation (b) in variance with ball numbers. Feed: Coal B, Size: 22-11mm and Feed Weight = 50g.

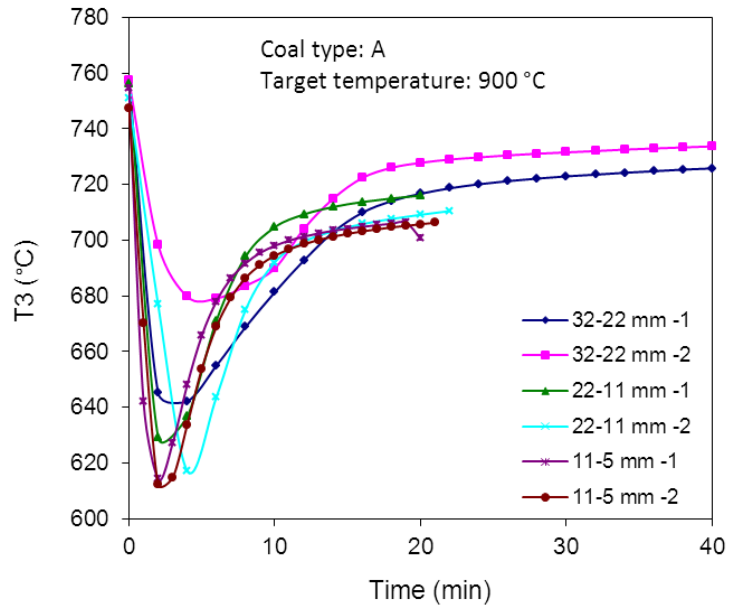
Although proper ball numbers and feed weight were selected to produce as good repeatability as possible, the deviation of some test can be as high as above 10% in the experiment. This is because of the nature of the randomness of the drop test. In the experiment, the deviation was controlled as maximum 7%. Those tests with a deviation beyond 7% were regarded as experiment error and excluded from the analysis.

4.4.2.5 Heating time calculation

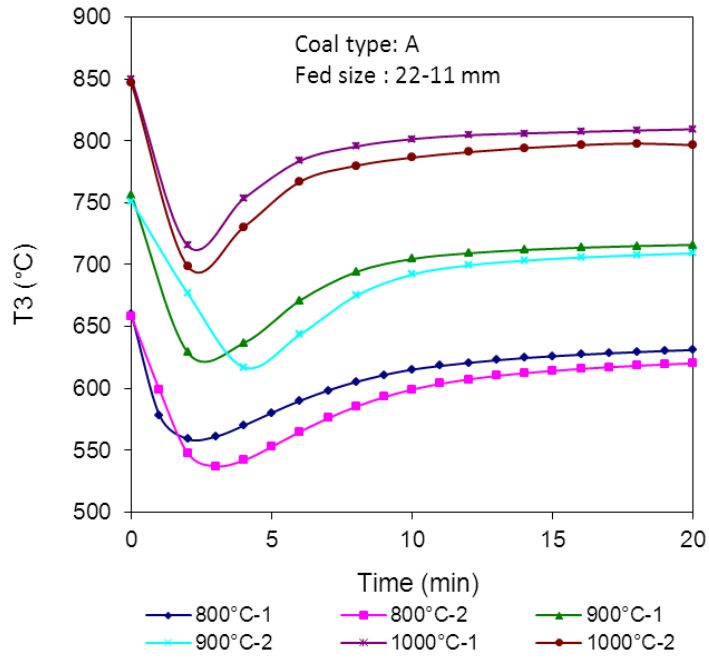
Coal particles were allowed to get heated on the plate. Calculation was performed to determine the adequate time to ensure complete heating. Another indication of complete heating was the stabilization of T3 after coal particles drop. Detailed calculation of the adequate heating time for the feed particle to reach 95% of the target temperature at the centre was shown in Appendix I. 40 min, 20 min, and 10 min was specified to heat coal particles within 32-22 mm, 22-11 mm, 11-5 mm, respectively.

As the calculation was based on a single particle, it might not be suitable in practical operation. In addition, simulation of the particle temperature in the experiment condition was complicated and its accuracy was difficult to verify. On the other hand, T3 directly measured the temperature right above the plate where coal particles rested on. Therefore, T3 was used as an indication of the particle surface temperature and the stabilization of T3 was viewed as an indication of adequate heating.

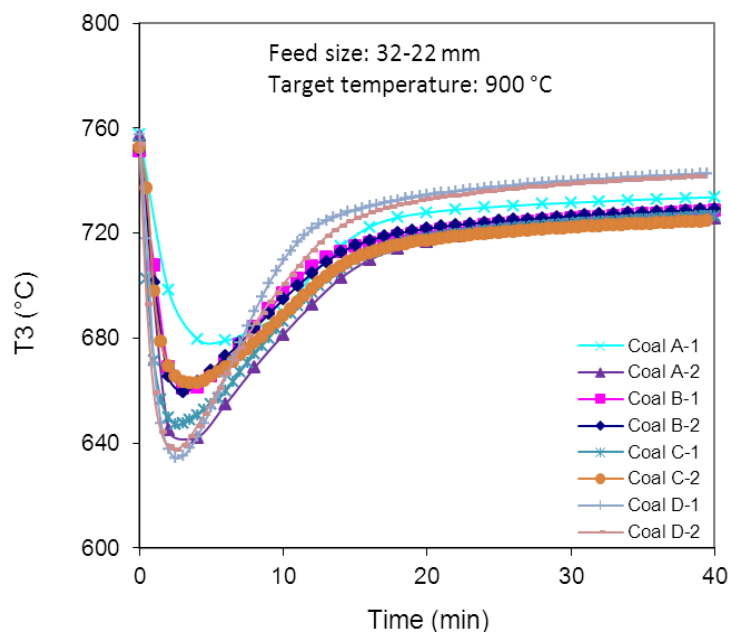
Figure 4-9 shows the practical measurement of T3. It suggests that for feed sample within 11-5 mm, 10 min is insufficient and it takes 20 min for T3 to stabilize. Therefore, the heating time for 11-5 mm was revised as 20 min. Furthermore, it is shown that different coals have similar T3 profiles, meaning their heating process is similar. Moreover, it is noticed that the effect of feed size on T3 is less important as the temperature profiles of various feed sizes are similar to each other. This is because T3 measures the surface temperature instead of that at the centre. The similarities of T3 of different feed sizes implies that T3 cannot be used as an indication of adequate heating of the centre, and the effect of residence time therefore needs to be investigated.



(a)



(b)



(c)

Figure 4-9 T3 (temperature right above the plate) in variance with residence time at (a) different feed sizes, (b) different temperatures, and (c) and different coals.

4.4.3 Experiment operation procedure

4.4.3.1 Materials preparation

For each coal, the three size fractions as indicated in the experiment design were obtained by sieving the bulk coal. Particles bigger than the top designed size were crushed and then sieved. All samples were kept in sealed bags and stored in airtight containers.

4.4.3.2 Room temperature test procedure

Before and after each test, the weight of the feed particles and that of the product was recorded. Pictures were also taken showing the comparison of the feed particles and the product. For the room temperature test, the two valves on top of the reactor were opened for dropping the particles. The bottom was then opened and the samples were collected in a tray. The products were eventually

sieved to determine the size distribution of the breakage. Each test was repeated three times maintaining the same conditions. Another set of three experiments were done with 8 steel balls of 20 mm diameter each dropping on the particles. Thereafter the mixture of particles and balls were collected from the bottom, the balls were separated, and then sieving analysis was done for the product.

4.4.3.3 High temperature test procedure

For each run, the furnace was preheated to the target temperature. The temperature of the furnace was set 10 °C higher than the designed temperature to compensate possible heat loss. From the finished experiments, when the temperature inside the tube stabilized, T2 was within - 10 °C to the target temperature. T3 was approximately - 150 °C to the target temperature. After coal particles were dropped and rested on the plate, T3 dropped dramatically, more than 100 °C, and then started to rise, until about - 40 °C to the original T3.

Nitrogen gas was purged during the experiment to maintain an inert atmosphere and help heat the plate at the bottom. 5 L/min purge rate was found to be optimum for the heating purpose.

When T3 reached - 150 °C to the target temperature, coal particles were fed from the top. The dual-valve feed system insured that limited air entered the tube. Coal samples were kept on the plate for specified time to allow thorough heating. Then steel balls were fed into the tube the same way as coal particles, and heating was turned off immediately.

Nitrogen gas was kept on until T3 dropped below 200 °C. After the coal particles were cooled to room temperature, the bottom plate was uninstalled and experiment product was obtained from the bottom. Steel balls were easily separated. Sample weight was recorded. Sieving analysis was then done to determine the particle size distribution.

5 RESULTS AND DISCUSSION

5.1 Advanced Characterisation Results

5.1.1 SEM analysis results

SEM images obtained from SEM analysis are shown in Figure 5-(1-4). They show the heterogeneous nature of the coals that have been analysed. The bright parts represent minerals, while the dark parts are mostly coal, sometimes dark minerals. Elemental compositions of some representative particles are determined by EDX.

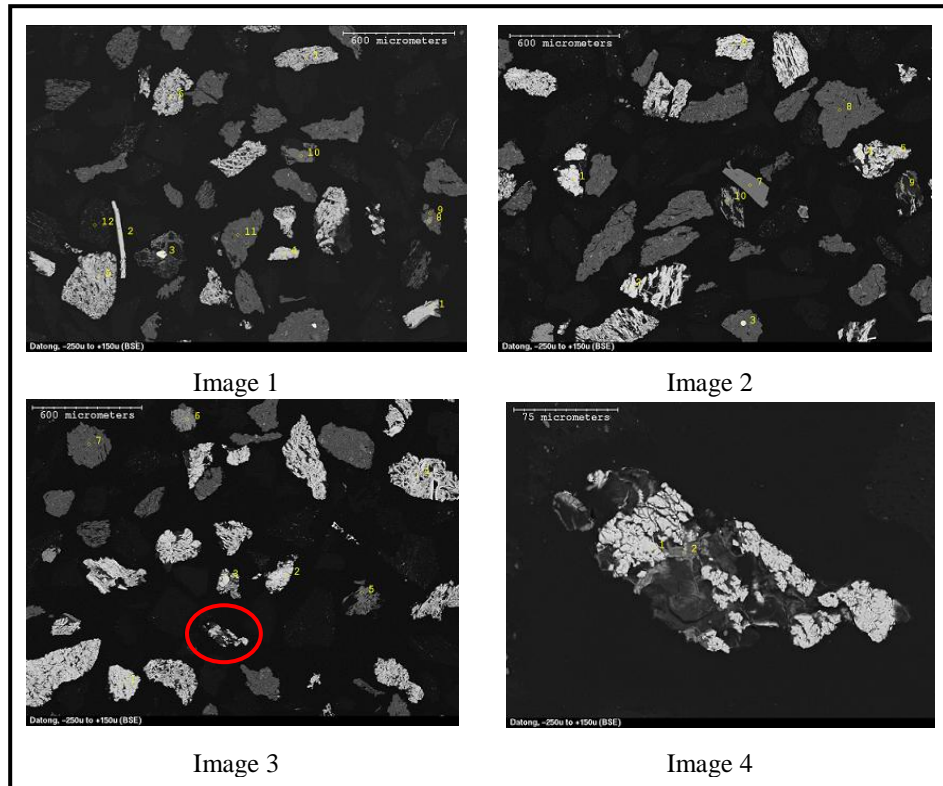


Figure 5-1 SEM images of coal A. Magnification of Images 1, 2, 3: $\times 50$; Image 4: $\times 360$.

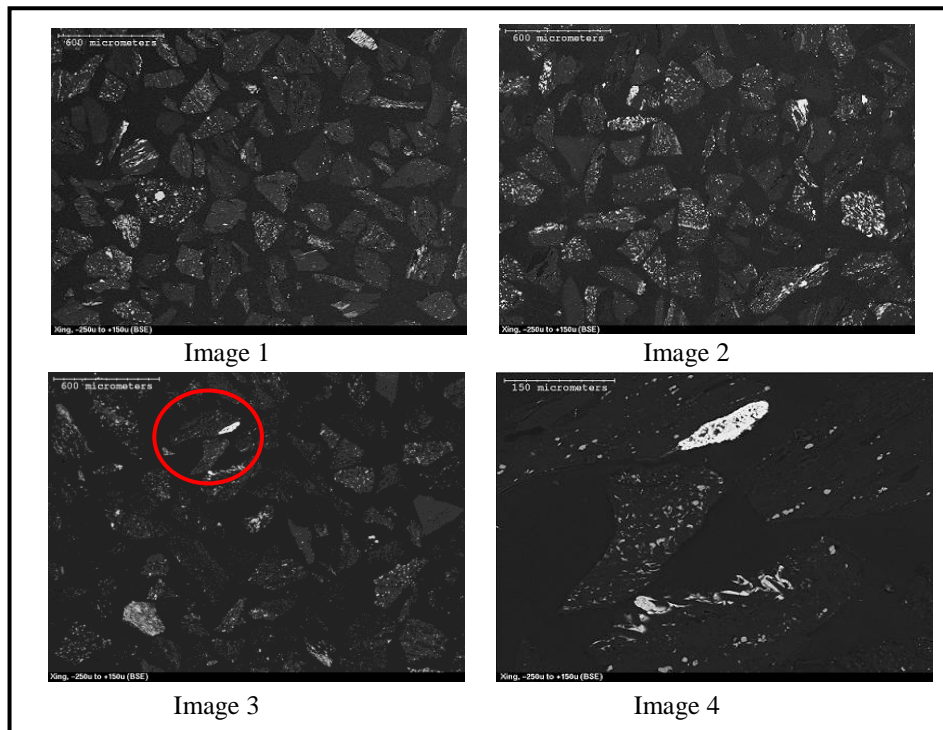


Figure 5-2 SEM images of coal B. Magnification of Images 1, 2, 3: $\times 50$; Image 4: $\times 180$.

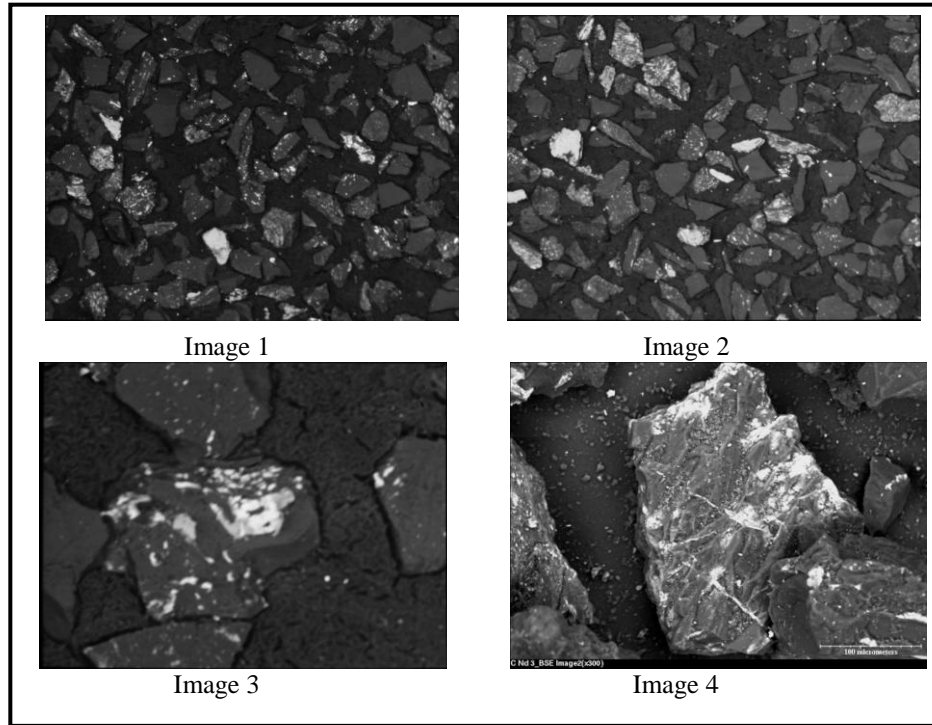


Figure 5-3 SEM images of coal C. Magnification of Images 1, 2, 3: $\times 50$; Image 3: $\times 250$; Image 4: $\times 300$.

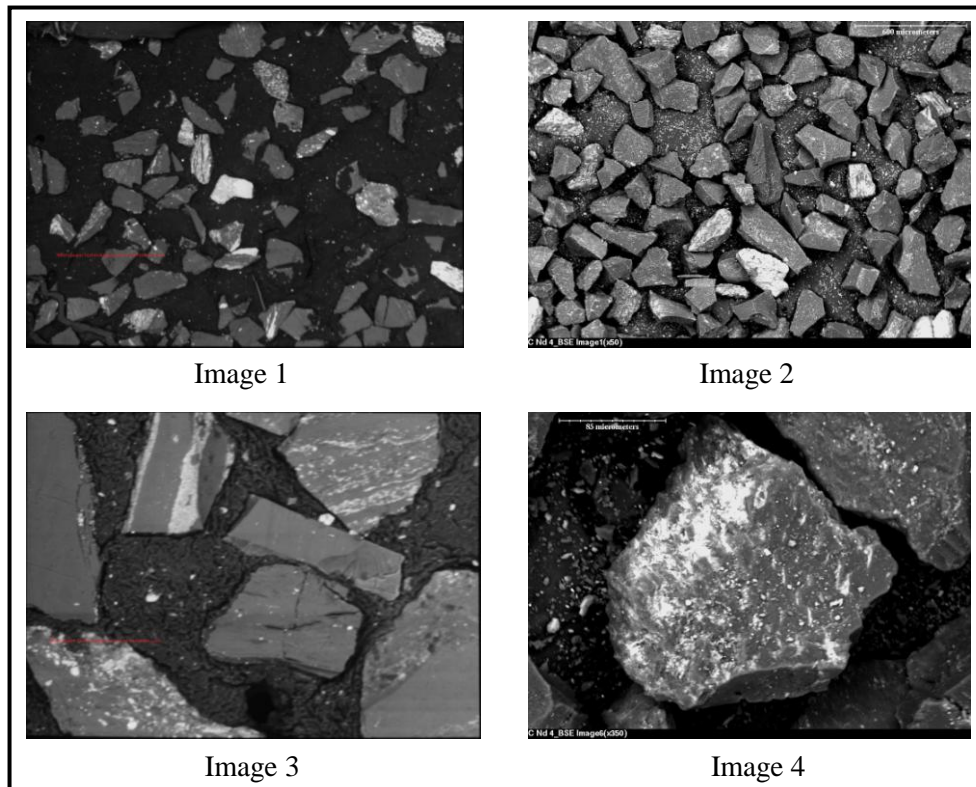


Figure 5-4 SEM images of coal D. Magnification of Images 1, 2: $\times 50$; Image 3: $\times 250$; Image 4: $\times 350$.

Image 4 of Figure 5-1, Image 3 and 4 of Figure 5-3, as well as Image 3 and 4 of Figure 5-4, clearly show the presence of heterogeneity within a single particle. Take Image 4 of Figure 5-1 as an example. According to EDX analysis, the bright portions are composed of Fe and S, while the dark parts are mainly composed of phosphor, S, and calcium. Thus it is a single particle with different types of minerals. Another example is the particle shown in Image 4 of Figure 5-3. The bright parts are mainly composed of Al, Si, and Ti, while the darker parts are coal matrix. Thus it shows minerals within coal matrix.

A visual comparison between the SEM images of the four coals suggests that coal B is significantly different from the other three. The minerals, shown as bright parts, are generally of much smaller size, and disperse within coal matrix evenly. In contrast, the mineral particles in the other three coals are mostly larger particles, and compose a higher portion of coal. However, visual comparison cannot easily tell the difference between coal A, C, and coal D. Therefore, quantitative analysis is needed to further characterise the effect of minerals.

5.1.2 CCSEM analysis results

Various data has been generated from the CCSEM analysis. Among the data available includes weight percentage of each phase in each size range on mineral basis and on coal basis, area percentage of each phase in each size range on mineral basis and on coal basis, size distribution of each phase, the number of particles of each phase in each size range, and the included/excluded distribution, etc. There are six categories of size ranges in total. The analysis in the present study focuses on the physical properties of minerals, such as size, distribution, etc.

Table 5-1 shows a summary of the main data from CCSEM results of coal A. Detailed information of each phase is not provided here. The weight percentage of minerals on mineral basis, and the area percentage of minerals on coal basis of the

four coals are listed in Appendix II.

Table 5-1 Typical CCSEM data showing detailed information of minerals of coal A

| Size range (μm) | 1-2.2 | 2.2-4.6 | 4.6-10 | 10-22 | 22-46 | 46-400 | Total |
|---------------------------------|-------|---------|--------|-------|-------|--------|--------|
| Wt. % (minerals basis) | 2.9 | 10.5 | 7.0 | 23.9 | 15.2 | 40.5 | 100 |
| Wt. % (coal basis) | 0.475 | 1.713 | 1.136 | 3.899 | 2.469 | 6.600 | 16.292 |
| Area % (minerals basis) | 3.3 | 10.2 | 6.4 | 20.7 | 14.2 | 45.2 | 100 |
| Area % (coal basis) | 0.243 | 0.738 | 0.463 | 1.502 | 1.029 | 3.279 | 7.254 |
| Number of particles | 261 | 194 | 250 | 186 | 391 | 228 | 1510 |

5.1.3 Petrographic analysis results

The reflectograms of the four coal samples are shown Appendix II. According to the reflectogram, the components within a coal sample are characterised by their reflectance based on an interval of either 0.1 (for coal A and B) or 0.05 (for coal C and D), and the volume frequency is obtained. The distribution of vitrinite is known to follow a normal distribution. To determine maceral composition, a cumulative reflectance distribution is obtained. The probability scale is specially designed so that the cumulative distribution of a normal distribution appears as a straight line.^{32, 40} An example of the cumulative reflectance distribution of coal A is shown in Figure 5-5. The straight line represents vitrinite distribution, while the inflection points of the straight line are used to determine other maceral

compositions. Mean vitrinite reflectance (MVR) can also be determined as the value corresponding to the middle point of the vitrinite distribution line. Moreover, a full comparison of the maceral components of the four coals is shown in Table 5-2.

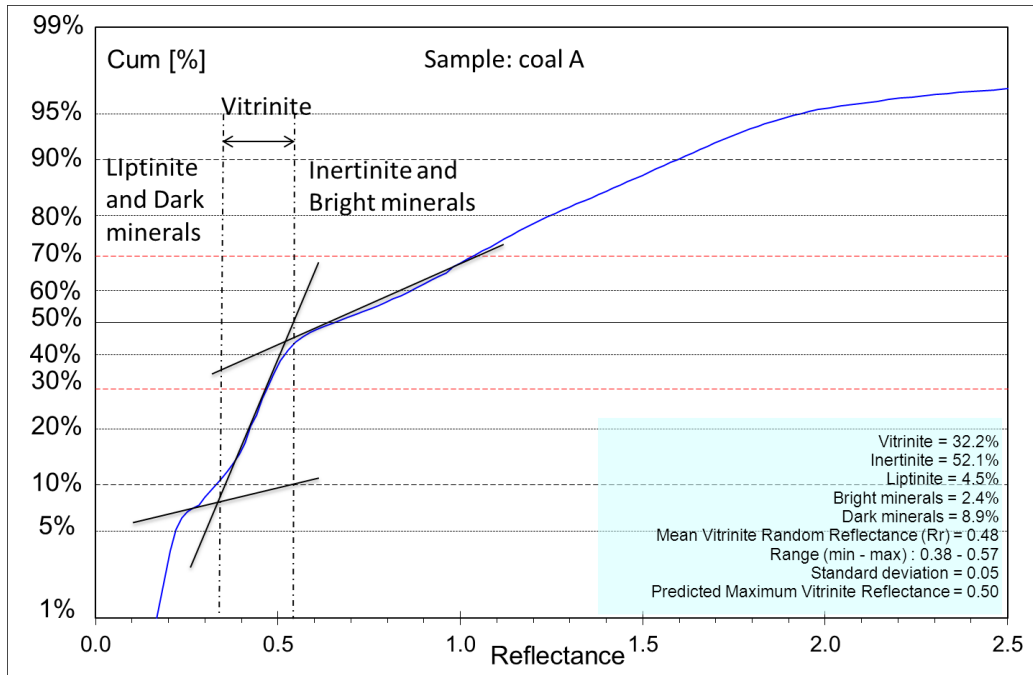


Figure 5-5 Cumulative reflectance distribution showing the determination of macerals groups of coal A.

The most important information from Table 5-2 is that coal C has a much higher MVR than the other three coals. As the measurement of coal rank, MVR indicates the overall quality of macerals. As MVR increases, coal rank increases, meaning a series of change of composition and structure. In addition, the comparison of maceral compositions suggests that coal A has the highest percentage of inertinite, while coal D has the highest percentage of vitrinite. These macerals are expected to have different impact on the fragmentation behaviour of large coal particles.

Table 5-2 Maceral composition determined by petrographic analysis for coal A, B, C, and D

| | | A | B | C | D |
|----------------------------------------------------|--------------------|-------------|-------------|----------------|----------------|
| Maceral Abundance (includes minerals) | Vitrinite | 32.2% | 44.6% | 44.8% | 65.1% |
| | Inertinite | 52.1% | 39.5% | 44.9% | 22.1% |
| | Liptinite | 4.5% | 12.5% | 5.1% | 2.1% |
| | Bright minerals | 2.4% | 0.0% | 0.0% | 0.0% |
| | Dark minerals | 8.9% | 3.4% | 5.2% | 10.6% |
| Mean Vitrinite Random Reflectance | | 0.48 | 0.69 | 1.15 | 0.56 |
| Range (min - max) | | 0.38 - 0.57 | 0.54 - 0.82 | 1.02 – 1.24 | 0.45 – 0.65 |
| Proximate Ash | | 18.40% | 6.00% | 9% | 19% |
| Predicted Maximum Vitrinite Reflectance | | 0.50 | 0.73 | 1.22 | NA |

5.2 The Effect of Different Coal Types

5.2.1 Fragmentation results from room temperature drop test

The drop test result at room temperature as shown in Figure 5-6 to Figure 5-13 provides the information of the two different coals under cold conditions. In the product bigger particles come from the breakage of the feed particles, and the fines are probably resulted from the surface shelling. It is obvious that the tests with balls produce much more fragmentation than those without balls for both coals. Moreover, the pictures of the tests of coal B show that under the conditions without balls, the number of big particles remains the same as the feed, indicating that coal B hardly breaks without balls. But there are still some fines in the product, implying the flaking of the surface. In contrast, coal A breaks into several smaller particles even without balls.

Cumulative weight distribution of the product is obtained after sieving test, shown in Figures 5-8, 5-11 and 5-14. For all three feed sizes, coal A under the condition of with balls has the most fragmentation, followed by coal B with balls. Under the condition without balls, the fragmentation is much lower, especially for coal B whose product almost remain the same size with its feed with a feed size of 8-16 mm, and 26.7 - 38 mm.

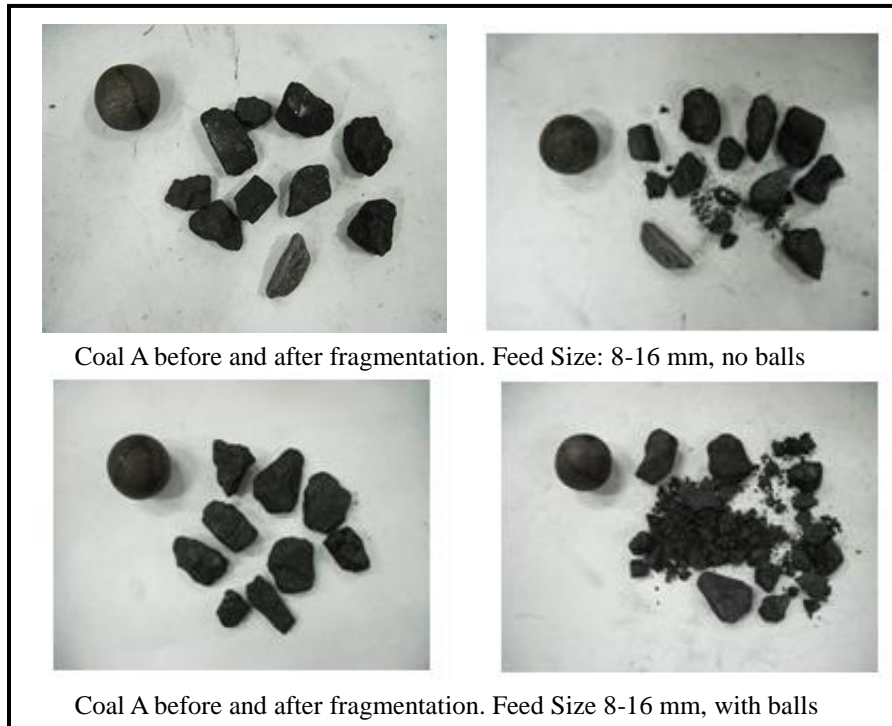


Figure 5-6 Fragmentation of coal A at room temperature.

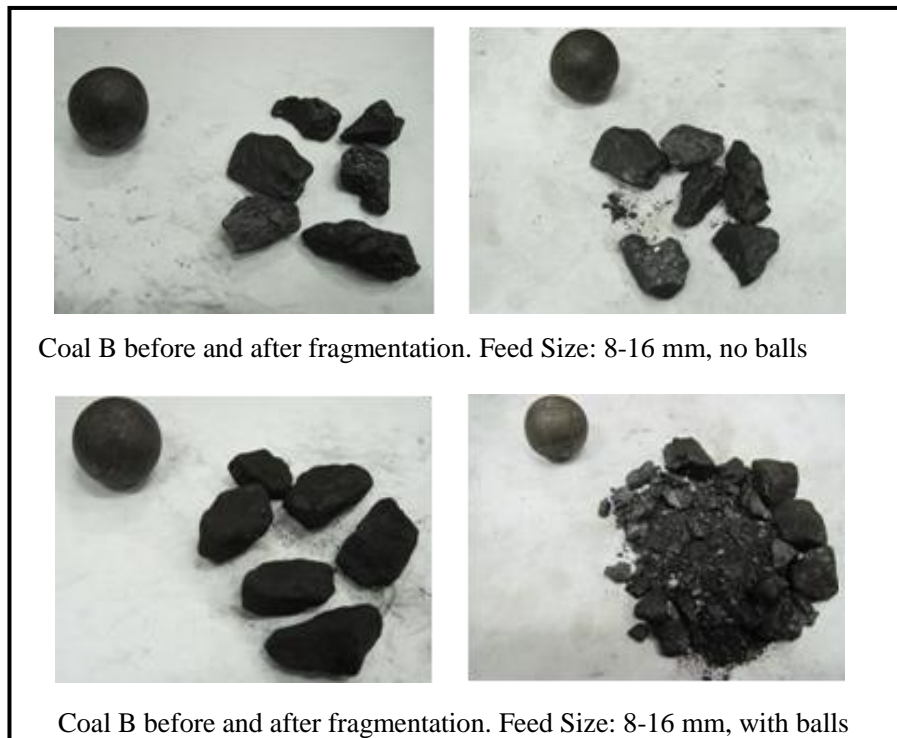


Figure 5-7 Fragmentation of coal B at room temperature.

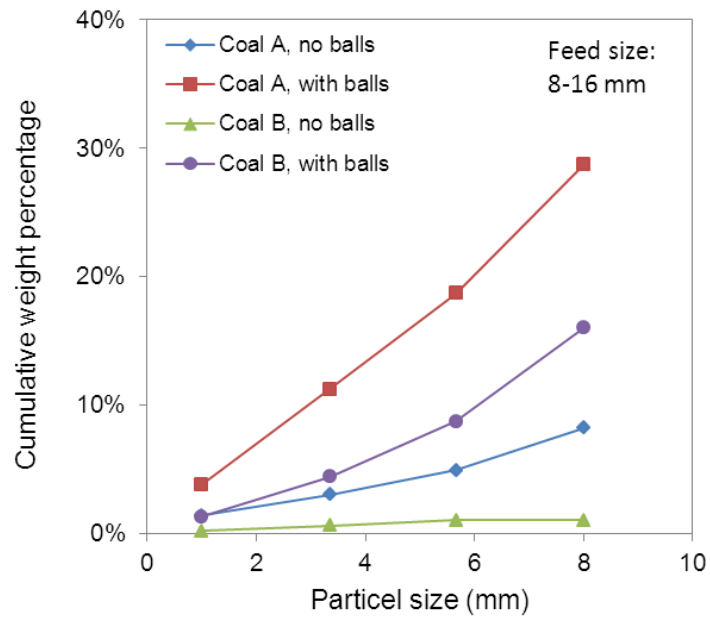


Figure 5-8 Cumulative size distribution of the fine product from drop tests at room temperature.

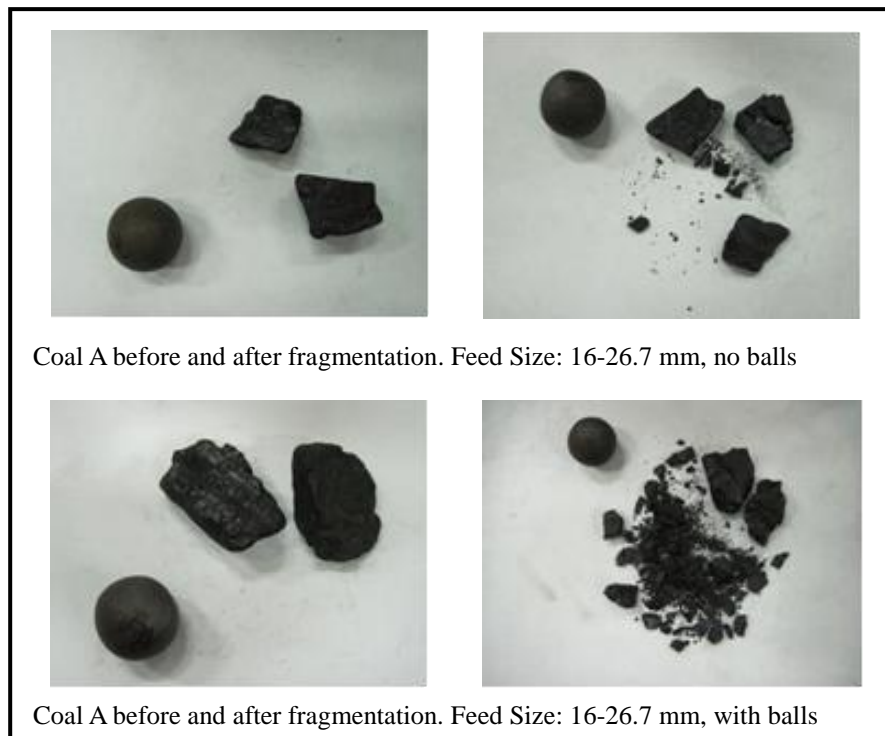


Figure 5-9 Fragmentation of coal A at room temperature.

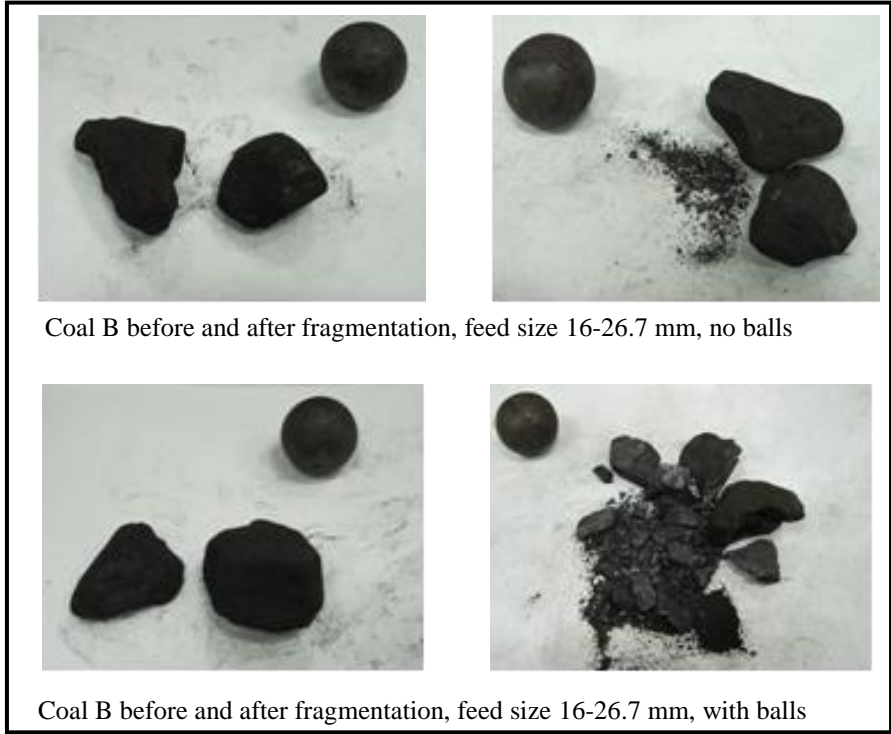


Figure 5-10 Fragmentation of coal B at room temperature.

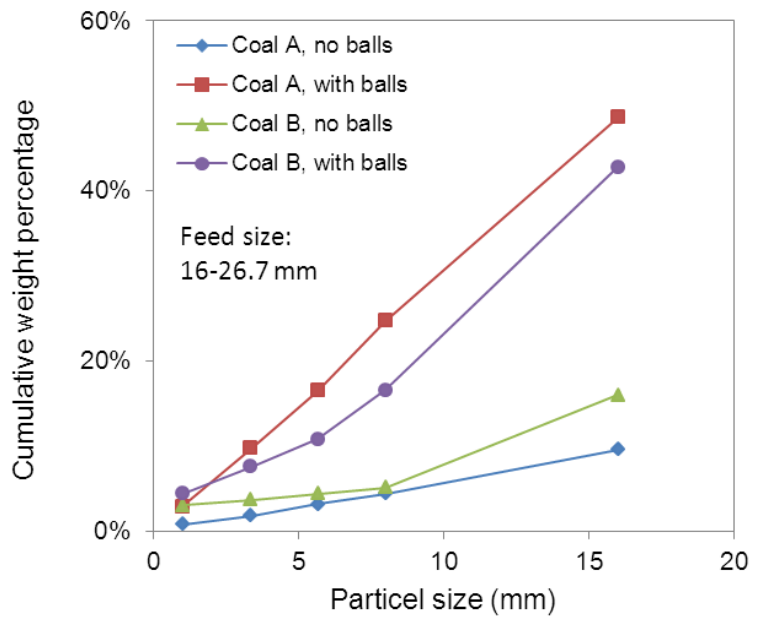


Figure 5-11 Cumulative size distribution of the fine product from drop tests at room temperature.

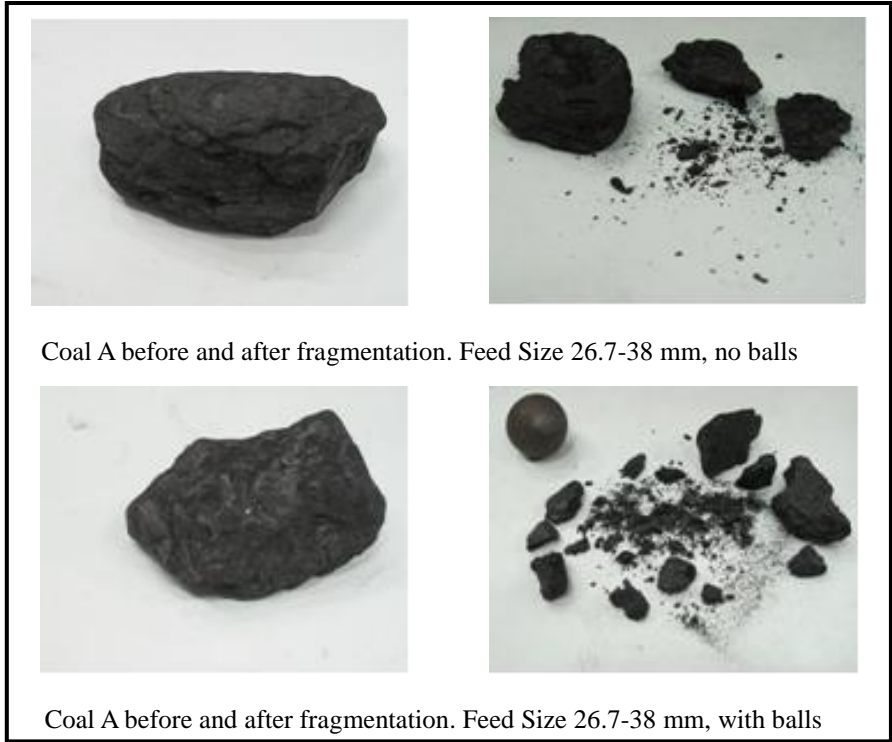


Figure 5-12 Fragmentation of coal A at room temperature.

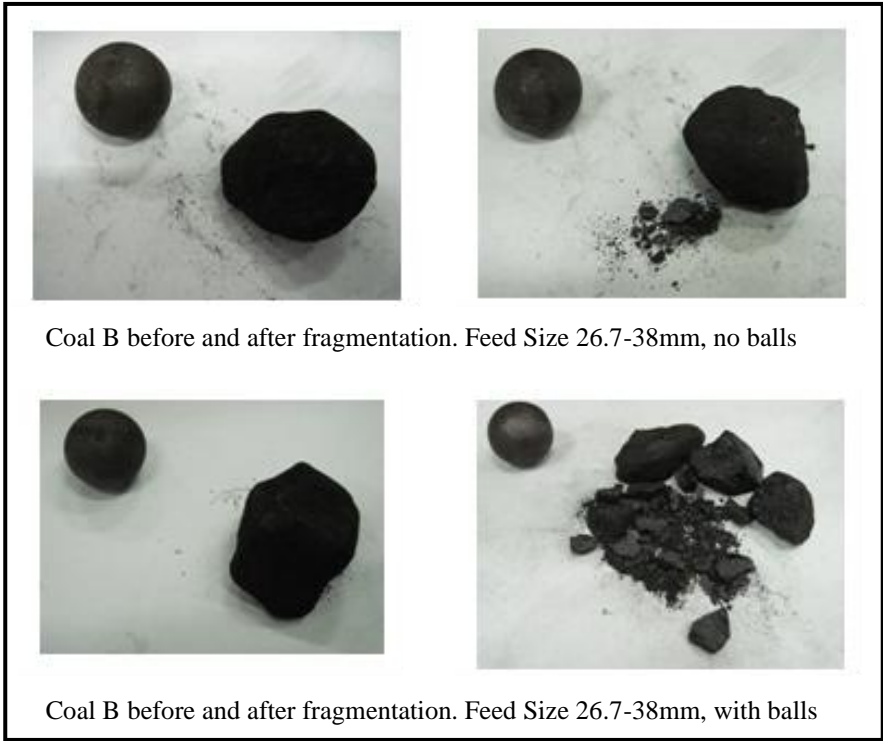


Figure 5-13 Fragmentation of coal B at room temperature.

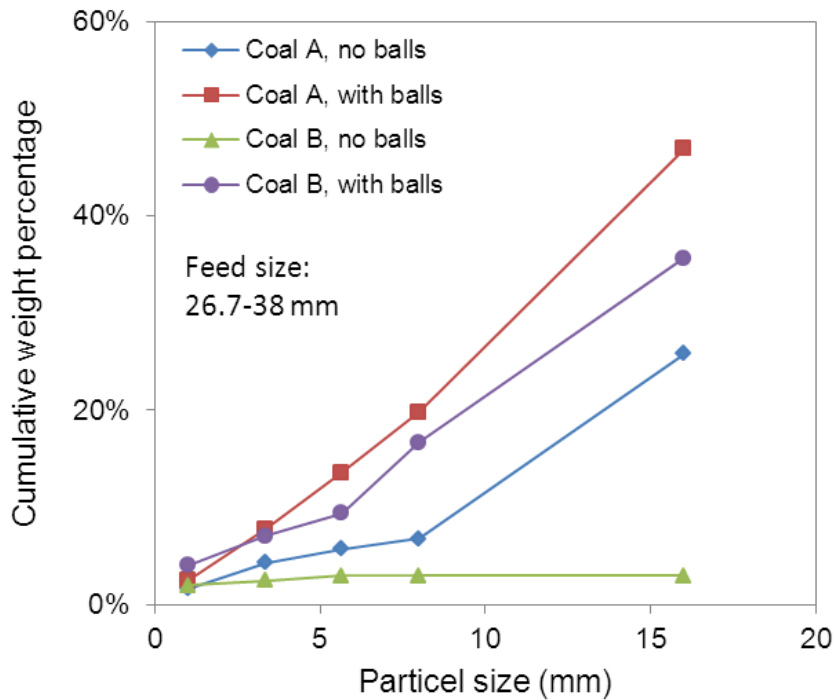


Figure 5-14 Cumulative size distribution of the fine product from drop tests at room temperature.

5.2.2 Fragmentation results from high temperature drop test

The values of the FI of the four coals at various temperatures are shown in Figure 5-15. It is apparent that at all the three temperatures, coal D has the lowest values of FI, ranging from 0.16 to 0.2. In contrast, coal B and C both have higher values of FI, ranging from 0.49 to 0.58, almost three times as that of coal D. The values of FI at various temperatures for coal A range from 0.28 to 0.35, lying between the values of coal D and that of coal B and C. These comparisons suggest that coal D has the highest level of fragmentation, while coal B and C have much less fragmentation. The fragmentation of coal A is more intense than that of coal B and C, but less than coal D. In addition, this trend is valid at all the three testing temperatures.

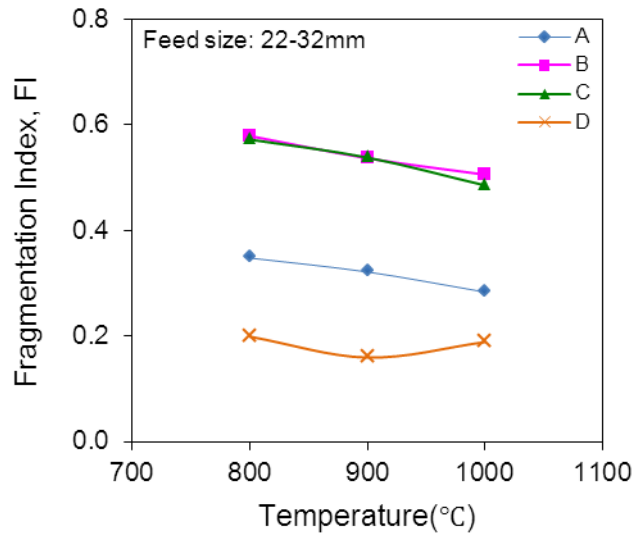


Figure 5-15 Fragmentation Index, FI in variance of temperature of coal A, B, C, and D.

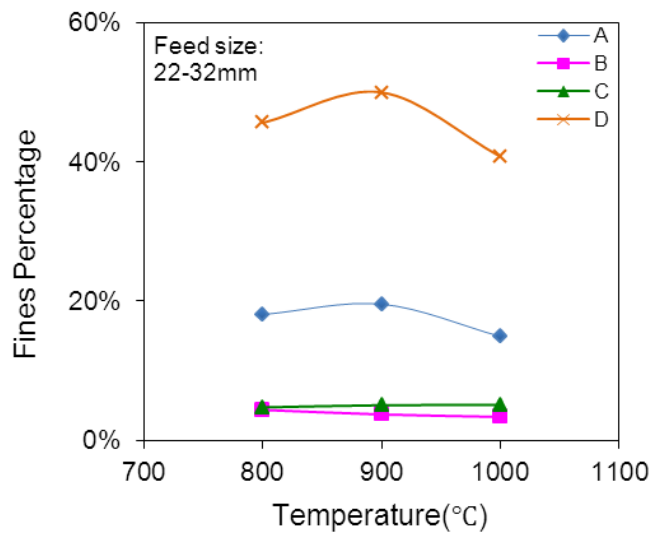


Figure 5-16 Fines Percentage in variance of temperature of coal A, B, C, and D.

Comparing the Fines Percentage shown in Figure 5-16, coal D has much higher value of Fines Percentage than the other three. The highest Fines Percentage of coal D can go up to 50%, while others are all above 40%. In contrast, the values of Fines Percentage of coal B and C are close to each other, and all below 5%. Moreover, similar to the trend in the value of FI, Fines Percentage of coal A lies in the middle, ranging from 15% to 18%. The result

implies that Fines Percentage is related to the level of fragmentation in the present study. As fragmentation increases, the fraction of fines that are smaller than 3.35 mm increases as well.

The values of Product Particle Number of the four coals are also compared in Figure 5-17. In agreement with the comparison of the value of FI, coal B and C have relatively fewer particles after the drop test, implying less fragmentation. On the other hand, the values of Product Particle Number of coal A and D fall into the range of 294 to 364, and 309 to 343, respectively. Unlike the conclusion drawn from the comparison of the value of FI, and Fines Percentage, little difference is observed between the behaviour of coal A and D.

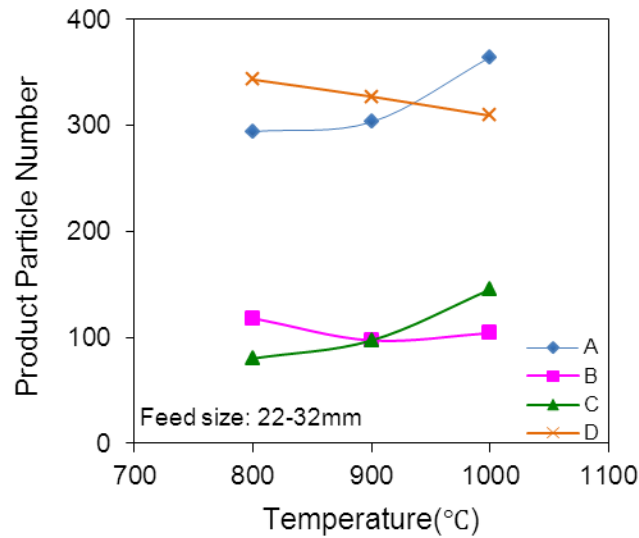


Figure 5-17 Product Particle Number in variance of temperature of coal A, B, C, and D.

However, the size distribution of the product gives another opinion. Table 5-3 gives the particle numbers of coal A and D in each size range at various temperatures. The values of total particle number are close to each other as stated previously. But the size distribution indicates that coal D generally has more particles within 3.35 ~ 5.66 mm, while fewer particles larger than 5.66 mm. An

example is shown in Figure 5-18 for results at 900 °C. Therefore, it is obvious that coal D has more fragmentation than coal A.

Table 5-3 Particle numbers of the product in various size ranges at various temperatures for coal A and D

| T (°C) \ Size range (mm) | A | | | D | | |
|--------------------------|-----|-----|------|-----|-----|------|
| | 800 | 900 | 1000 | 800 | 900 | 1000 |
| 22.6 ~ 32 | 0 | 0 | 0 | 0 | 0 | 0 |
| 11.2 ~ 22.6 | 15 | 11 | 8 | 5 | 0 | 1 |
| 5.66 ~ 11.2 | 86 | 100 | 116 | 78 | 73 | 86 |
| 3.35 ~ 5.66 | 193 | 192 | 240 | 260 | 254 | 222 |
| Total | 294 | 303 | 364 | 343 | 327 | 309 |

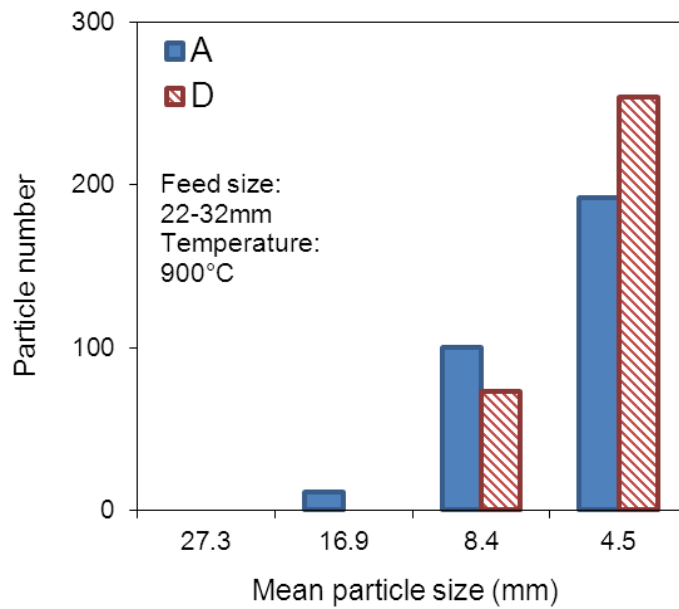


Figure 5-18 Particle number distribution of the product of coal A and D.

In summary, coal D has the highest level of fragmentation as suggested by both the value of FI and product particle size distribution. Coal D also has the highest value of Fines Percentage that is closely related to fragmentation level. In contrast, coal B and C both have much less fragmentation and lower value of Fines Percentage. The behaviour of coal A lies in the middle of coal D and that of coal B or C.

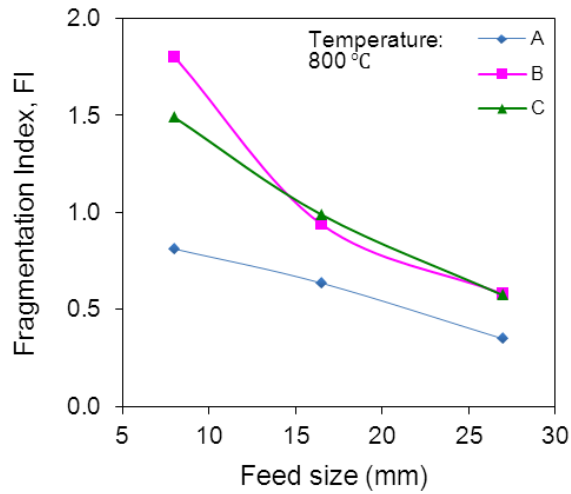
5.3 The Effect of Feed Size

The effect of feed size is illustrated by FI and Fragmentation Number Index, S. The values of FI in variance with feed size for coal A, B, and C are shown in Figure 5-19. The results of all the three coals, at various temperatures suggest the same trend. It is evident that as feed size increases, the value of FI decreases, meaning more fragmentation. In addition, the value of S in variance with feed size, shown in Figure 5-20, implies that increased feed size leads to increased value of S, also suggesting that more fragmentation occurs with increased feed size.

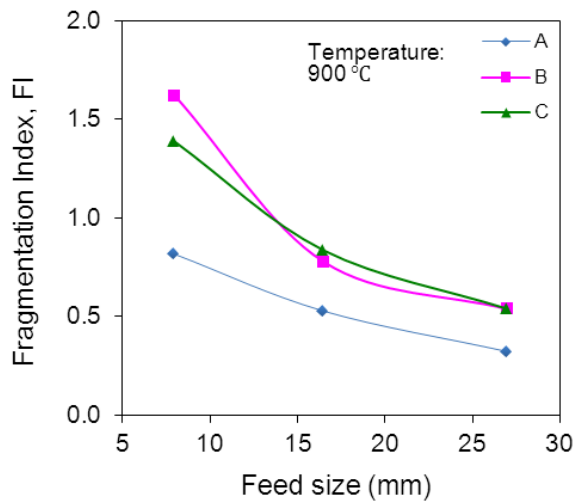
This trend agrees well with literature.^{9, 11, 15} It has been suggested that bigger particles are more likely to experience fragmentation. The most important reason is that there are more imperfections in bigger particles. Since coal is a highly heterogeneous material and composed of different types of macerals and minerals, imperfections exist in the complex coal matrix. The boundaries between minerals are likely to be weaker than other parts within the coal particles. In bigger particles, the heterogeneity increases and therefore, there are more weak boundaries as well. In addition, at high temperature, bigger particles are likely to experience greater pressure from volatile matter release, and increased temperature gradient, both leading to increased fragmentation.

Despite the general trend that fragmentation increases with increasing feed

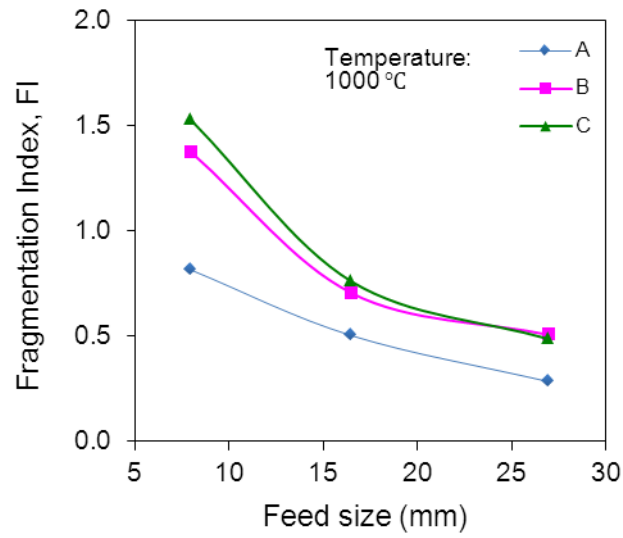
size, the effect of feed size differs for different coals. The variance of FI for coal B is more than 0.8, and can be as high as 1.2 at 800 °C. While for coal A, the variance of FI is smaller, around 0.5 between the value of the largest feed size and that of the smallest feed size. Taking a closer look at the behaviour of coal B and C, it is found that most of the increase of the value of FI occurs when feed size is decreased from 22 – 11 mm to 11 -5 mm. Moreover, the values of FI are above 1.0, which implies that the mean diameter of the product is larger than that of the feed sample.



(a)



(b)



(c)

Figure 5-19 Fragmentation Index, FI in variance with feed size for coal A, B, and C, at temperatures (a) 800 °C, (b) 900 °C and (c) 1000 °C.

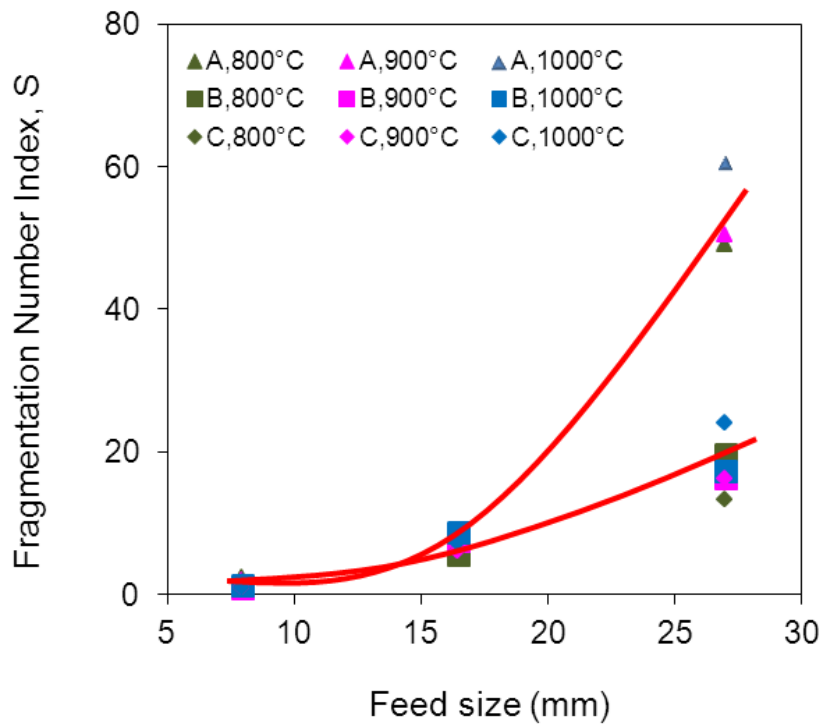


Figure 5-20 Fragmentation Number Index, S in variance with feed size for coal A, B, and C, at various temperatures.

Pictures were taken to explain the phenomenon that the mean particle size increases after drop test. As shown in Figure 5-21, some of the small particles agglomerate and form a bigger particle whose diameter is even bigger than the feed. The figure also suggests that the bonding of individual particles is strong. As a matter of fact, these agglomerated particles are able to withstand the mechanical force of both the dropping of 8 steel balls and the shaking during sieving analysis. Therefore, the agglomeration might be responsible for the reduction of fragmentation, and thus properties that determine agglomeration behaviour also affect the fragmentation behaviour.

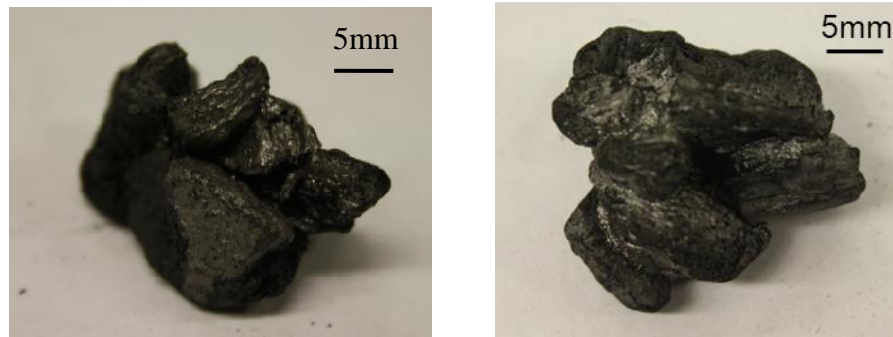


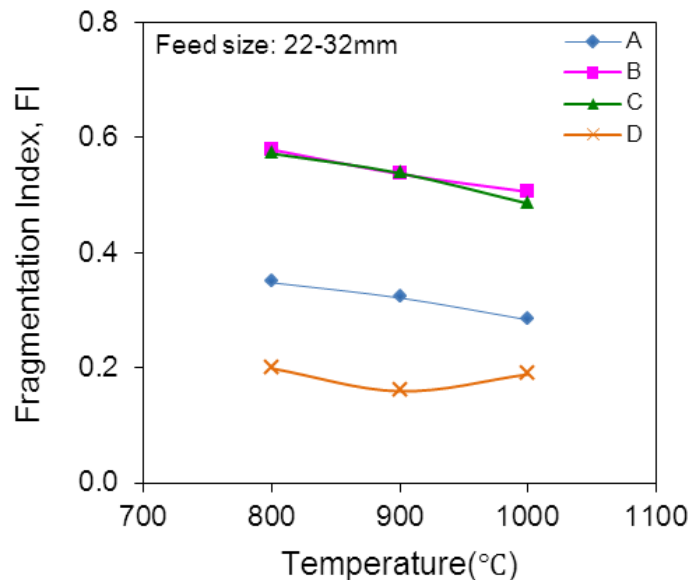
Figure 5-21 Big particle formed by agglomeration of small particles of coal B (left) and coal C (right). Feed Size: -11mm, Temperature: 900 °C.

No agglomeration is observed for coal A or D. Although there is agglomeration of small particles, it is not common that larger particles agglomerate. According to Kim et al. ¹⁷, small particles (0.8 – 1.0 mm) agglomerate after heating, while large particles are more likely to swell and crack, as there are less contact surface areas for large particle to agglomerate.

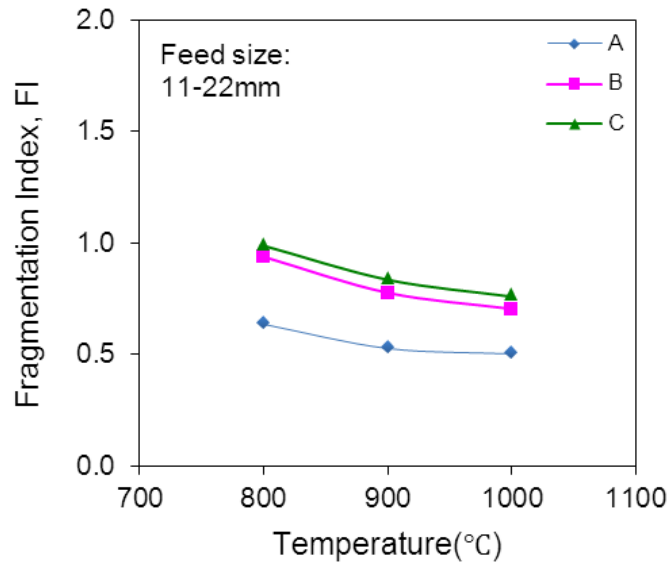
In summary, as feed size increases, fragmentation increases. Agglomeration tends to reduce fragmentation, therefore properties that facilitates agglomeration are likely to reduce fragmentation as well.

5.4 The Effect of Temperature

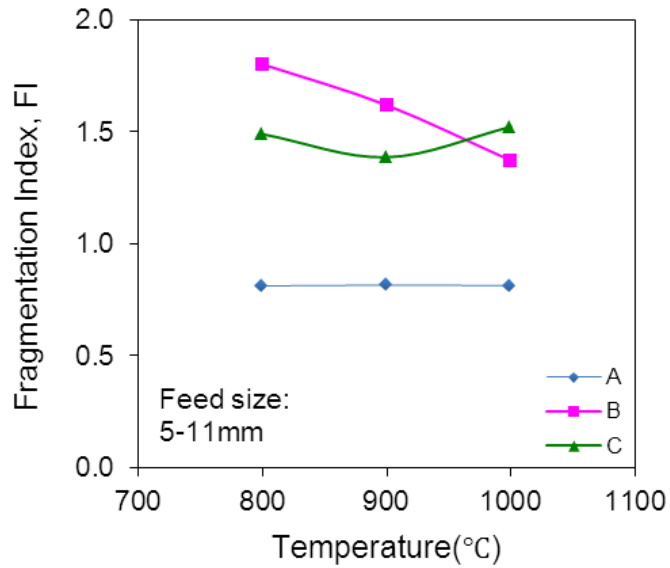
As shown in Figure 5-22, in most cases with the same feed size, the value of FI decreases as temperature increases but only to a limited extent. The variance with temperature is smaller than 0.2, except that of coal B with feed size of 11-5 mm at 1000 °C, which has a variance of 0.4. Considering the fact that fragmentation drop test is by its nature random,¹⁵ it is reasonable to conclude from the above observation that the effect of temperature is insignificant to fragmentation under the current conditions, especially in comparison with other factors investigated in this study, such as coal types and feed size. In addition, as shown in Figure 5-23, Product Particle Number does not show a clear tendency with temperature, either. Instead, for the same coal, the value of Product Particle Number falls into a range indicated by the circle. This further confirms the conclusion that the effect of temperature is not important.



(a)



(b)



(c)

Figure 5-22 Fragmentation Index, FI in variance with temperature at various feed sizes: (a) 22-32 mm, (b) 11-22 mm and (c) 5-11 mm.

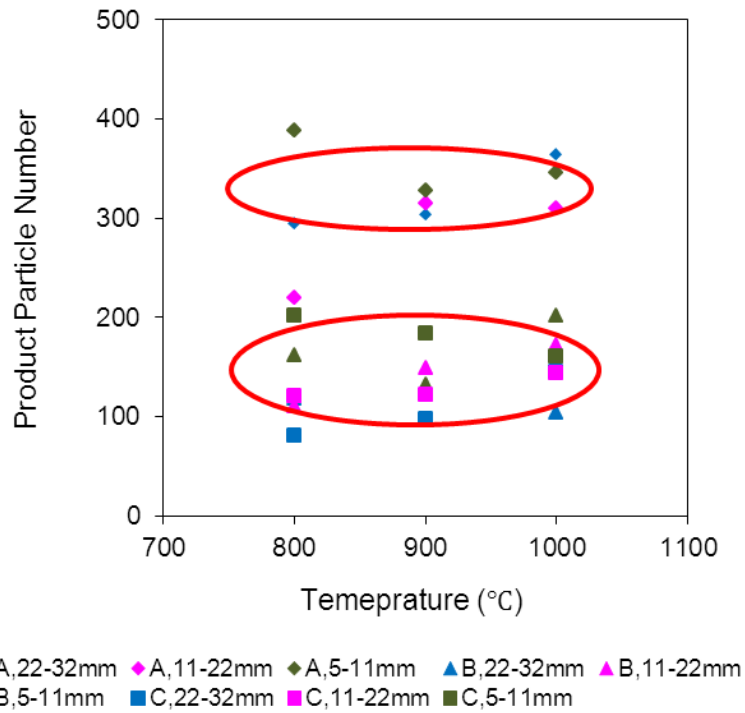


Figure 5-23 Product Particle Number in variance with temperature for coal A, B, and C, with various feed sizes.

As stated in the literature review part, it is suggested by some researchers ^{9, 11, 17} that higher temperature favours more fragmentation because of higher heating rate and greater temperature gradient. However, the experiment results in the present study do not agree with this statement. The possible reason is that the heating condition in the present study is different from those in the literature. All the experiment work ^{9, 11, 17} was conducted in a fluidized bed that was characterised by rapid heat transfer, while the present study used a drop tube furnace, with much lower heating rate. According to Stubington et al. ²², in the fluidized bed used in the experiment, the time required for a particle with 7 – 8 mm to reach 800 °C at the centre is around 80 s. The average heating rate is 10 °Cs⁻¹. In contrast, the T3 profile shown in Figure 4-9 suggests that the heating rate of the particle surface is barely 2.5 °Cs⁻¹ for a particle within 22-11 mm, when

the target temperature is 1000 °C; the heating rate of the particle centre is even lower than that of the surface. In addition, T3 profile also implies that the heating rate of the particle surface does not vary much with furnace temperature. In this case, it is reasonable that the effect of temperature on fragmentation in the current experiment condition is not important.

Nevertheless, the fragmentation behaviour at high temperatures and that at room temperature is greatly different. The values of FI at 900 °C are lower than that at room temperature, as shown in Figure 5-24. Other conditions the same, the increase of the fragmentation at 900 °C is due to thermal treatment, which deteriorates coal particles because of devolatilization. In addition, thermal treatment has varied degree of impact on the tested three coals. Coal A is the most sensitive. Coal C has a ratio of almost 1.0, meaning that the fragmentation does not increase significantly at high temperature. This phenomenon can be understood in the later section of the effect of coal types.

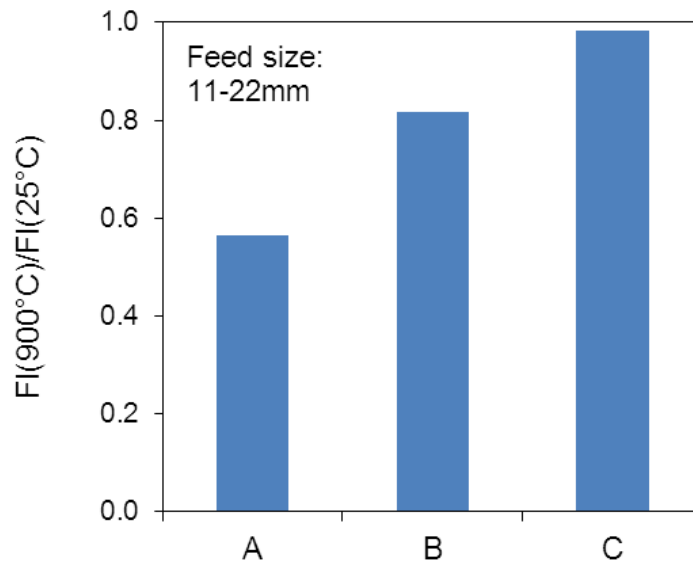


Figure 5-24 Comparison of Fragmentation Index, FI at room temperature and high temperature.

5.5 The Effect of Residence Time

Residence time is defined as the time from the point when the sample is fed into the preheated drop tube furnace until the time when the steel balls are dropped and heating is turned off. As residence time is longer, the sample is heated more thoroughly, and is allowed more time to devolatilize. Figure 5-25 suggests that as residence time increases, the value of FI decreases, indicating that more fragmentation happens. Moreover, when residence time is longer than 5 min, the value of FI does not decrease any more, suggesting that fragmentation does not increase significantly.

The decrease of the value of FI along with residence time in the first few minutes is likely to be the result of the release of moisture and volatile matter, which weakens the coal structure. As residence time increases, more moisture and volatile matter is released, resulting in more fragmentation, as well as a weaker coal structure that is much more vulnerable to the mechanical force of the drop of the steel balls. On the other hand, as residence time further increases, the release of moisture and volatile matter is less intense; therefore the fragmentation caused by inner pressure does not increase any more.

The observed trend generally agrees with that reported by Zhang et al.¹¹, that for a coal particle with a size of 5-7 mm in a fluidized bed, with the increase of residence time, fragmentation first increases, then decreases after a maximum value. The decrease of fragmentation after a maximum value is supposed to be the result of the burn out of fine coal particles during the combustion. Furthermore, the residence time at which coal particles have the maximum fragmentation is around 6 s, while the devolatilization time of coal particles with 7 mm in a fluidized bed can be estimated according to the equation suggested by Stubington and his group^{21, 22} to be around 55 s ($n = 1.5$, $A = 3$ for estimation). Therefore, the

maximum fragmentation occurs at the initial stage of devolatilization; the decrease of fragmentation after the peak value implies that devolatilization rate decreases rather than that devolatilization is over.

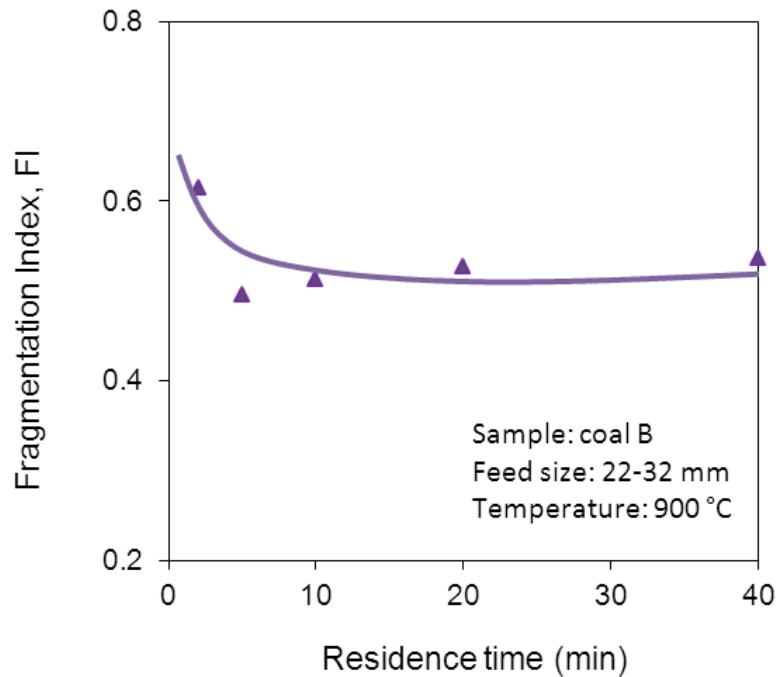
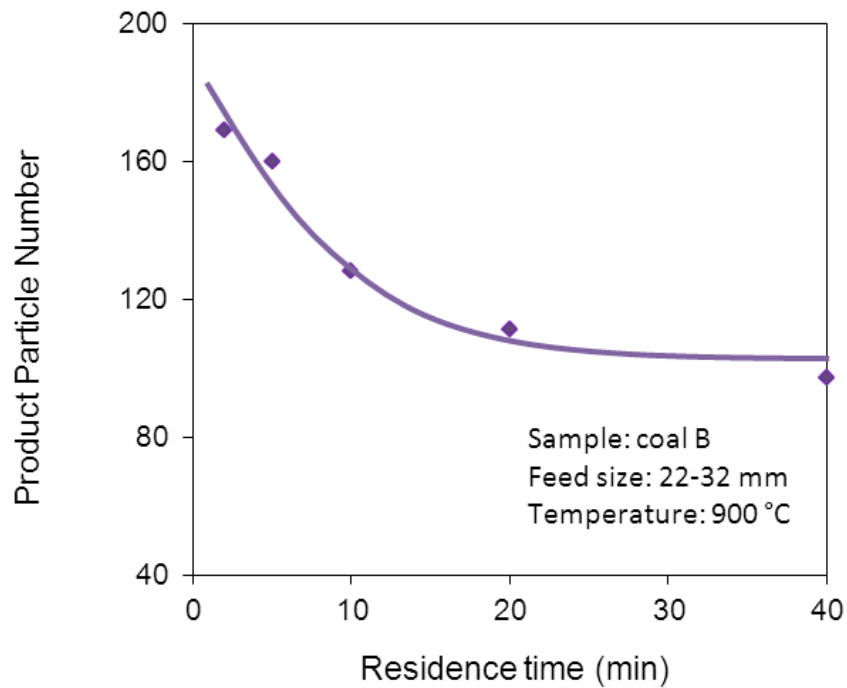


Figure 5-25 Fragmentation Index, FI in Variance with Residence Time.
Feed sample: coal B, Size: 32-22 mm.

Since it is assumed that more fragmentation is associated with lower value of FI, higher value of Product Particle Number, and higher Fines Percentage, the trend that more fragmentation occurs as residence time increases as suggested by Figure 5-25, predicts that as residence time increases, the value of Product Particle Number increases as well. However, the result shown in Figure 5-26 does not match the expectation. Right oppositely, increasing residence time leads to lower value of Product Particle Number. The decrease is most significant in the initial 10 min, and the same with the trend of FI, the effect of residence time is less important after 10 min.



**Figure 5-26 Product Particle Number in variance with residence time.
Feed sample: coal B, Feed size: 32-22 mm.**

To investigate the reason why the value of Product Particle Number decreases with increase of residence time, the product particle size distribution is shown in Figure 5-27. It is clear that as residence time increases, particle number in the category of 5-3 mm decreases steadily. In addition, after 10 min, the number of particles larger than 5 mm does not vary much with residence time, which means that the increased residence time does not cause large particles to fragment. Therefore, the superficial contradiction between the trend of FI and that of Product Particle Number can be explained. Based on the definition, the value of FI is predominantly determined by particles with larger size, while the effect of particles within 5-3 mm is not as important, especially for coal B that overall has a low mass percentage within 5-3 mm. As a result, as larger particles fragment with the increase of residence time, the value of FI decreases; as larger particles

do not fragment significantly with longer residence time, the value of FI does not change significantly, either. On the other hand, particles within 5-3 mm affect the value of Product Particle Number greatly. For example, the value of Product Particle Number is high at 2 min, because there are 98 particles within 5-3 mm out of a total number of 169. The value of Product Particle Number at 40 min is much lower because the number of particles within 5-3 mm decreases to 30, despite that the number of particles larger than 5 mm is only 10 less than that at 2 min.

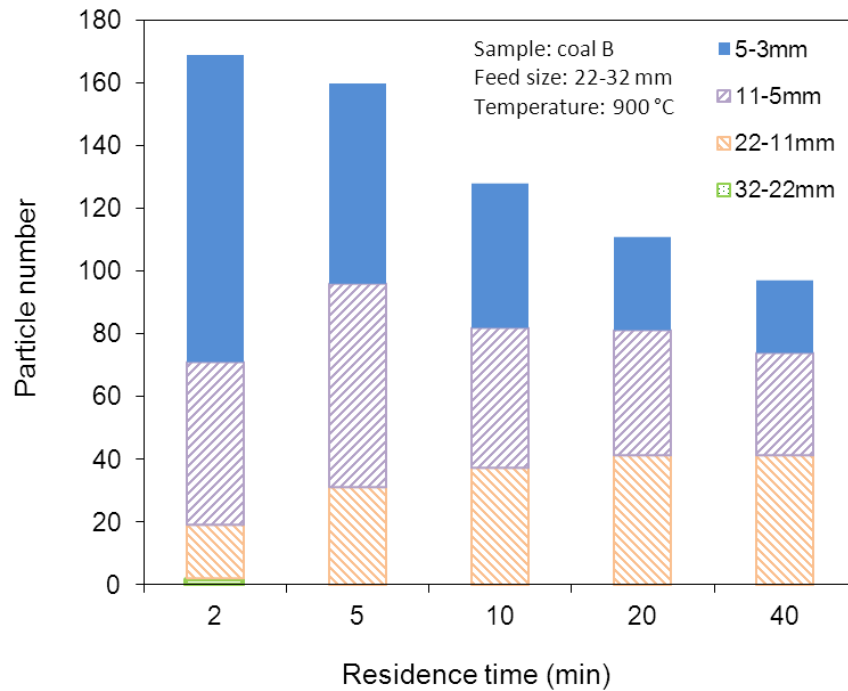


Figure 5-27 Particle number distribution in each size range, in variance with residence time. Feed sample: coal B, Size: 32-22 mm.

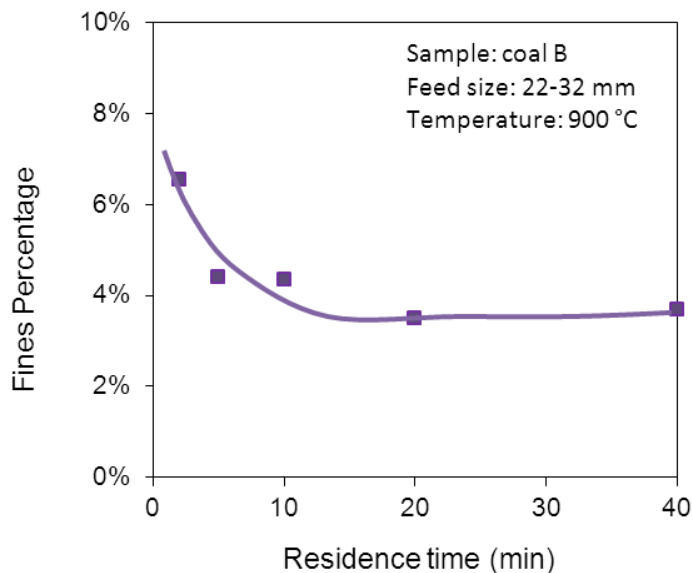


Figure 5-28 Fines Percentage after fragmentation, in variance with residence time. Feed sample: coal B, Size: 32-22mm.

Similar to the trend of particle number, Fines Percentage in variance with residence time shown in Figure 5-28 also demonstrates that as residence time increases, Fines Percentage decreases. This is in agreement with the fact that the number of smaller particles decreases with longer residence time. It is also verified that after 5-10 min, Fines Percentage does not decrease significantly with further increase of residence time.

One phenomenon might be helpful to explain the fact that the number of smaller particle decreases as residence time increases. After the drop test, some deposition is found at the bottom of the tube reactor. The deposition adheres to the bottom and the side walls and is difficult to remove. It is probable that the deposition comes from tar that is released during heating. At high temperatures, tar is semifluid and able to trap fine particles; as the furnace is cooled down to room temperature, the tar solidifies and forms the deposition together with trapped fine particles. As residence time increases, there is more tar released. Therefore, it is expected that more fine particles get trapped and disappear from

the final product. As residence time is further increased, most of the tar has been released, thus the effect of residence time is not as important.

This hypothesis can be verified by comparing the product from 2 min residence time experiment and that of 10 min residence time test, shown as Figure 5-29. The product of 2 min residence time test is almost black, as the feed sample; while the product of 10 min residence time test is grey, with a shiny metallic lustre. The big particles from the product of 2 min residence time test is more porous than that of 10 min residence time test. Moreover, comparing the weight loss percentage, shown in Figure 5-30, at 10min residence time, the loss is 6% more than that at 2 min. All these observations suggest that as residence time increases, the devolatilization allows more tar released. As a result, smaller particles get trapped and their number decreases.

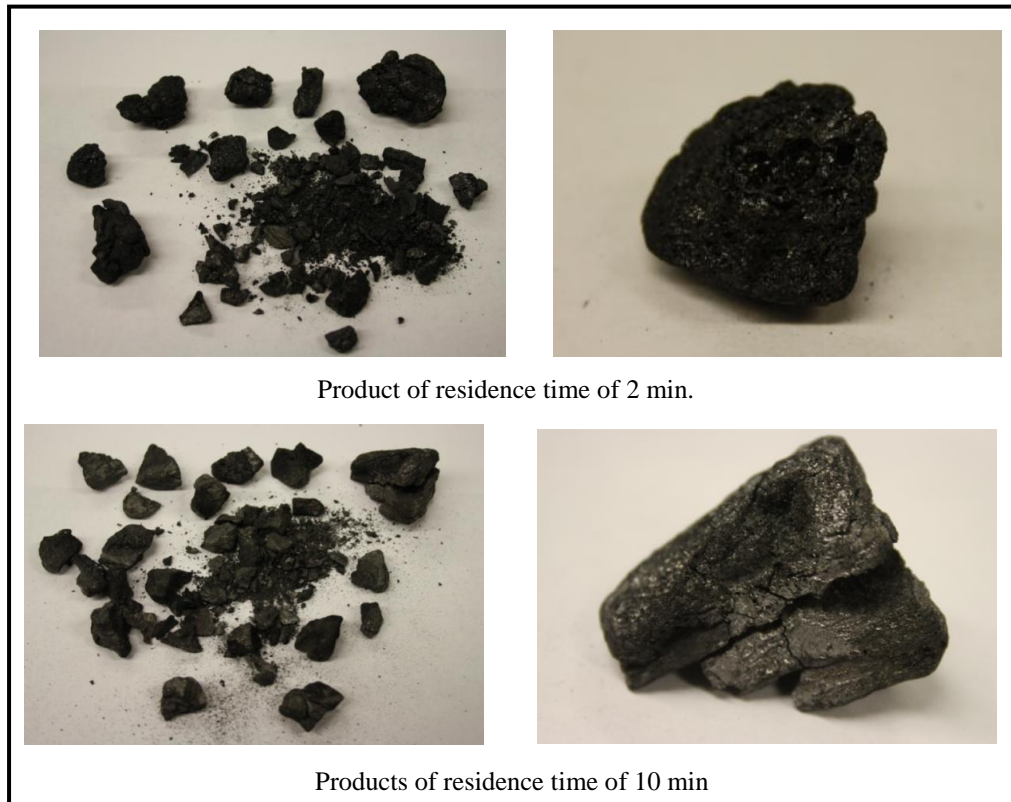


Figure 5-29 Comparison of the product of residence time: (above) 2 min and (below) 10 min. Feed: coal B, Size: 32-22 mm.

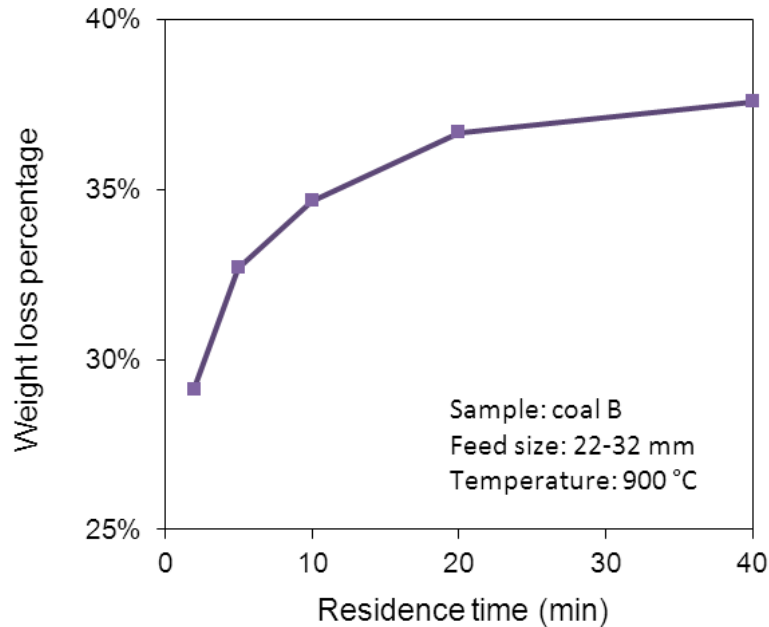


Figure 5-30 Weight loss percentage at various residence time. Feed: coal B, Size: 32-22 mm.

5.6 Discussion on the Effect of Coal Types

5.6.1 The effect of minerals based on CCSEM analysis

5.6.1.1 Mineral weight percentage and size distribution

Figure 5-31 shows the mineral weight percentage determined by CCSEM analysis and by proximate analysis for the four coals. From the comparison, CCSEM underestimates the mineral weight percentage of coal B to a great extent. While CCSEM is able to detect both crystalline species and complex nonstoichiometric, and provides detailed information in terms of mineral size, shape, distribution, it also has limitations. The smallest particle that is detectable by CCSEM is 0.5 μm . As a result, submicrometer particles cannot be detected by CCSEM analysis. Moreover, organically bound materials and dissolved salts are not detectable by CCSEM as well. Therefore, the underestimation of the mineral weight percentage of coal B indicates the existence of large amount of

submicrometer particles. The behaviour of these fine mineral particles is expected to be different from the bigger ones. On the other hand, the weight percentage of coal A and C is overestimated by CCSEM. The reason is not clear yet, but might be related to mineral composition as suggested by Yu et al. ²⁹ that CCSEM is likely to overestimate the weight percentage of SiO₂.

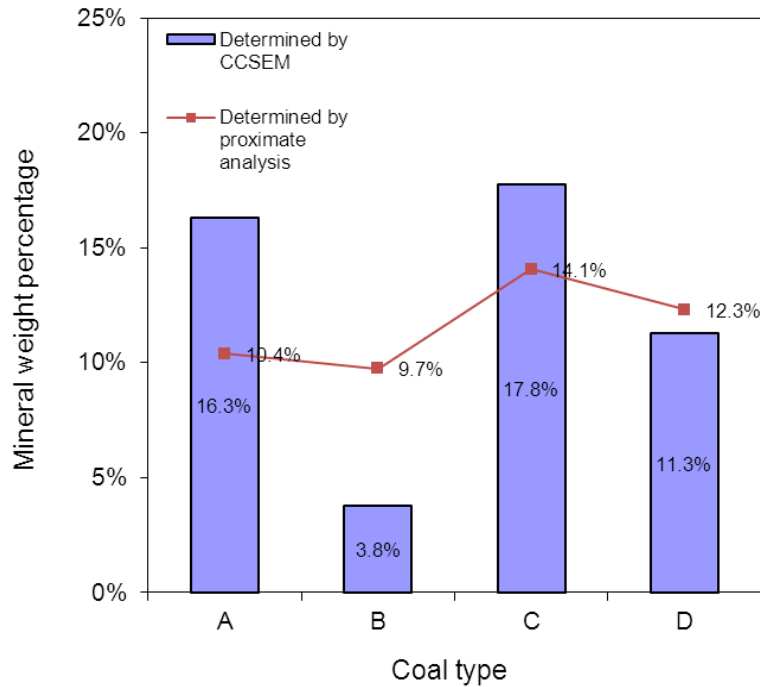


Figure 5-31 Mineral weight percentage of the four coals, determined by CCSEM analysis and proximate analysis.

Besides mineral weight percentage, the size distribution of minerals probably plays a more important role in determining fragmentation behaviour of large coal particles. If the particle is very small, the stress at the interface can be mitigated easily by the coal matrix. Therefore the effect of small particles on the fragmentation of large coal particles can be neglected. In contrast, it is hypothesized that large mineral particles have a greater impact on the fragmentation because of the weak interface areas. Figure 5-32 shows the mineral

particle size distribution obtained from CCSEM data. CCSEM analysis gives mineral weight percentage in six size categories, as seen in Appendix II. It is clear that coal D has the highest mineral mass fraction between the categories of 46-400 μm , followed by coal A, and then coal C, while coal B has merely 2% minerals in this category. This trend is valid as far as particles with a lower limit of 10 μm are concerned. In sharp contrast is the mineral size distribution of coal B, which has over 95% of minerals below 22 μm , and 73% of minerals below 10 μm . As a result, mineral particles in coal D have the most significant influence on fragmentation behaviour, leading to the highest level of fragmentation. Moreover, although the proximate analysis indicates that coal B has the same level of ash content with the other three coals, most of the mineral particles do not affect the fragmentation of large coal particles because of their small sizes.

Except for the size distribution, particle number in each category is also available from CCSEM analysis, and is plotted against mean particle size in Figure 5-33. The total number of mineral particles is also provided in the legend. The trend that coal D has more mineral particles within the categories of 46-400 μm , as well as 22-46 μm than coal A and B is confirmed. The observation that most of the mineral particles in coal B are below 10 μm is also verified. However, coal C has the highest total mineral particles, as well as large amount of particles within the coarser categories. Since the drop test result suggests lower fragmentation of coal C, some other factors are more important to determine the fragmentation behaviour of coal C.

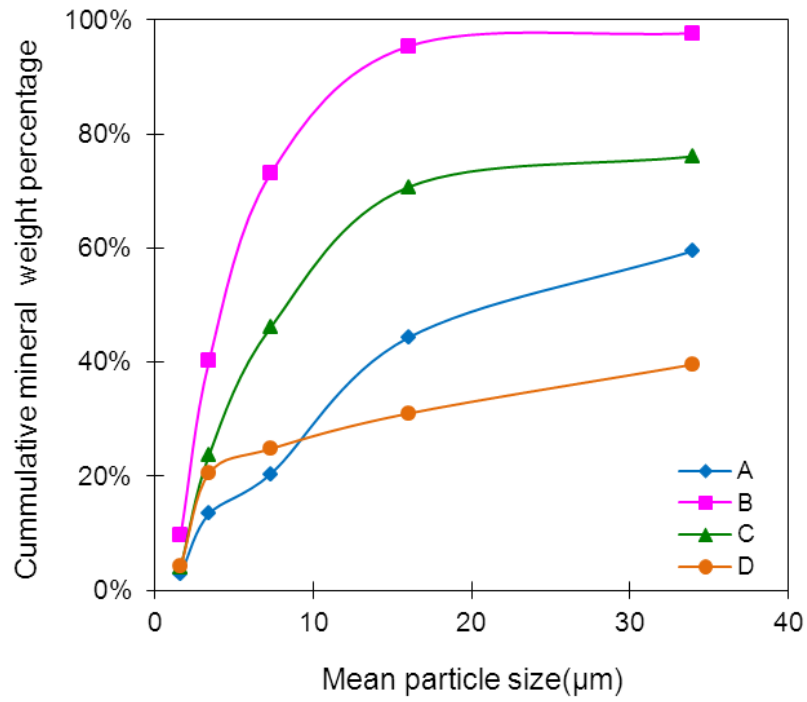


Figure 5-32 Mineral particle size distribution of coal A, B, C, and D.

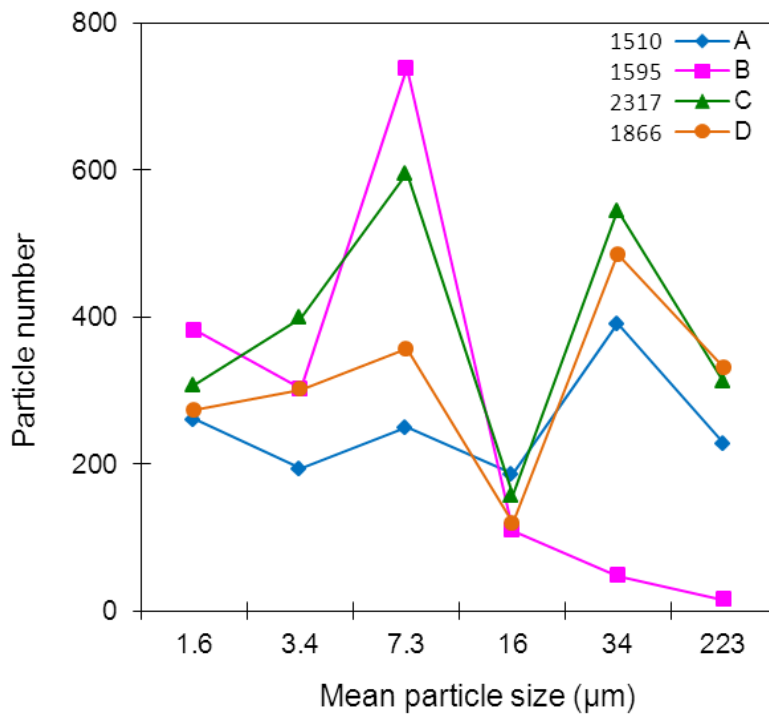


Figure 5-33 Particle number distribution of coal A, B, C, and D.

5.6.1.2 Interface calculation

As stated in the previous section, large particles embedded within carbonaceous matrix might cause fragmentation of coal particles under thermal and mechanical impact. To be specific, the interface between mineral particles and carbonaceous matrix is where weakness of the structure exists, and is likely to be the place where fragmentation happens. Therefore, the interface area between mineral particles and carbonaceous matrix is calculated.

The assumptions based on statistical calculation are as follows:

1. Each mineral particle is a sphere, with a diameter of the arithmetic mean value of each size range.
2. Only particle with a larger size is able to cause fragmentation.

Regarding the second assumption, based on the observation of mineral size distribution discussed in the previous section, particles bigger than 10 μm are included in the interface calculation.

To calculate the interface area, the volume percentage of particles within each size range is first obtained. Then the particle number is estimated by dividing the total volume of the minerals in each size range by individual particle's volume. The interface area is assumed to equal the surface area of all the mineral particles, therefore can be calculated by adding all the surface area of all the mineral particles.

The volume percentage of mineral particles of each phase within each size range equals the corresponding area percentage based on statistics. Then the number of particles within each size range in 1 cm^3 coal:

$$N = \frac{1 \times V\%}{\frac{\pi}{6} \times D^3} \quad (4)$$

where, D is the arithmetic mean diameter of each size range.

Surface area of the particles of each phase within each size range is calculated by Equation (5):

$$A = N \times (\pi D^2) \quad (5)$$

Substituting N with Equation (4), the interface area, A in 1 cm³ of coal is:

$$A = \frac{6 \times V\%}{D} \quad (6)$$

Surface areas of minerals in three size ranges are calculated. In addition, based on the assumption that larger particles are more likely to cause fragmentation, surface areas of minerals larger than a certain size are also determined by adding all the surface areas within the related size ranges. The comparison of the interface area of coal A, B, C, and D is shown in Table 5-4.

Table 5-4 Interface area of minerals within various size ranges in 1 cm³ coal of coal A, B, C, and D

| Sample | Interface area (cm ²) in 1 cm ³ coal | | | | |
|--------|-------------------------------------------------------------|---------------|----------------|----------------|----------------|
| | 10 ~22 μm | 22 ~ 46 μm | 46 ~ 400 μm | 22 ~ 400 μm | 10 ~ 400 μm |
| A | 56.3 | 18.2 | 8.8 | 27.0 | 83.3 |
| B | 16.2 | 0.8 | 0.1 | 0.9 | 17.1 |
| C | 90.3 | 9.3 | 6.3 | 15.6 | 105.9 |
| D | 14.6 | 9.6 | 10.2 | 19.8 | 34.4 |

Table 5-4 suggests quantitatively the effect of minerals of the four coals. Firstly, coal B has the least interface area, with the values of all size ranges much lower than the other three. In this case, there are much less weak areas within the

coal particle, thus reduce the chance of fragmentation. Secondly, comparing coal A and D, it is found that coal A has more interface within 10 ~ 22 μm , and 22 ~ 46 μm , but coal D has more interface within 46 ~ 400 μm . Considering the fact that coal D has a higher level of fragmentation during the drop test at high temperature, it is convinced that larger particles play a more important part in determining the fragmentation behaviour. Moreover, coal C has less interface than coal A and D both within 22 ~ 46 μm , and 46 ~ 400 μm , but it has much more interface than coal B. Nevertheless, the fragmentation level of coal B and C is close to each other. This suggests that some other factor is important in determining the fragmentation of coal C.

To summarize, although proximate analysis suggests limited difference of ash content of the four coals, CCSEM makes it possible to discuss the effect of minerals in depth. One conclusion is that large particles have impact on the fragmentation behaviour while the effect of small particles can be neglected. Moreover, interface area quantifies the effect of mineral. As interface increases, the fragmentation increases as well. The prediction based on interface calculation agrees well with the drop test results. In addition, the mineral interface comparison cannot fully illustrate the fragmentation behaviour of coal C, thus other factors such as organic components should be studied.

5.6.2 The effect of macerals based on petrographic analysis

It has already been suggested that coal C has a higher rank (MVR) than the other three coals. As a matter of fact, coal C is used as a coking coal while the other three are all thermal coals. Therefore, coal C has a good thermal stability at high temperature and a strong char structure after devolatilization. The benefit of higher rank overtakes the disadvantage of high mineral content, thus the fragmentation of coal C at high temperature is much less than that of coal A and D

which also have a high mineral interface. This also explains that thermal treatment has less impact on the fragmentation behaviour of coal C.

Besides the effect of MVR, maceral composition also affects the fragmentation. As mentioned previously, agglomeration of small particles is observed for coal B and C. The agglomeration is largely determined by maceral composition. Vitrinite and liptinite is the reactive maceral, which means that they soften at high temperature to form plastic mass; during solidification process, they bond the inert macerals that do not soften at high temperature to form char, or in the case of a coking plant, to form coke. Inert materials include inertinite and minerals. The bonding of inert materials is verified by Arina et al.⁸, that after a test at 850 °C, the sand particles forming the fluidized bed material were visible in the char particles. Therefore, the reactive macerals are likely to reduce fragmentation. According to Table 5-2, coal A has lower percentage of vitrinite and liptinite, and higher percentage of inertinite and minerals compared to coal B and C, which makes it more vulnerable to breakage. On the other hand, although coal D has a higher percentage of reactive macerals, its MVR is much lower. Therefore, the quality of the macerals is not as good, and the bonding effect is less important. As a result, the fragmentation of coal D is high. This suggests that coal rank (MVR) is more important than that of maceral composition, such as vitrinite percentage.

Although the coke strength is not directly related to fragmentation result in the present study, it is reasonable to assume that a coal with higher coke strength will possibly have less fragmentation because of a stronger char structure. Coke strength prediction based on petrographic data is well established.^{33, 39} An example of the predicted coke strength graph is shown in Figure 5-34. Several observations can be drawn from the Figure. First of all, if the MVR is below 0.8,

the ASTM Stability Index is less than 30, which means that the coke strength is so weak that it cannot be used for coke making. Secondly, when MVR is below 1.5, for the same reactive/inert ratio, as MVR increases, coke strength increases as well. When MVR is very high, the macerals become less reactive, thus not favourable to coke strength. Thirdly, at the same level of MVR, there is an optimum ratio of inert materials, and the value is around 15-20%. Above 20%, increase of inert ratio results in decrease of coke strength. It is obvious that the inert ratio of all the four coals in the present study exceeds 20%, therefore any further increase of inert materials will result in lower coke strength, thus higher fragmentation.

Based on the coke strength prediction graph, coal C is predicted to have a good coking strength, and thus has low fragmentation in the drop test. On the contrary, the MVR of coal A, B, and D is low so they are not coking coal; therefore they are predicted to have a weak char structure and high fragmentation. However, the heterogeneity in coal B is low, which reduces the imperfection and weak areas within the coal particles. As a result, coal B also has low fragmentation.

In summary, coal rank affects the fragmentation behaviour. For the bituminous coals that are tested in the present study, as the rank (MVR) increases, less fragmentation is produced. Maceral composition also affects the fragmentation but not as significantly as coal rank.

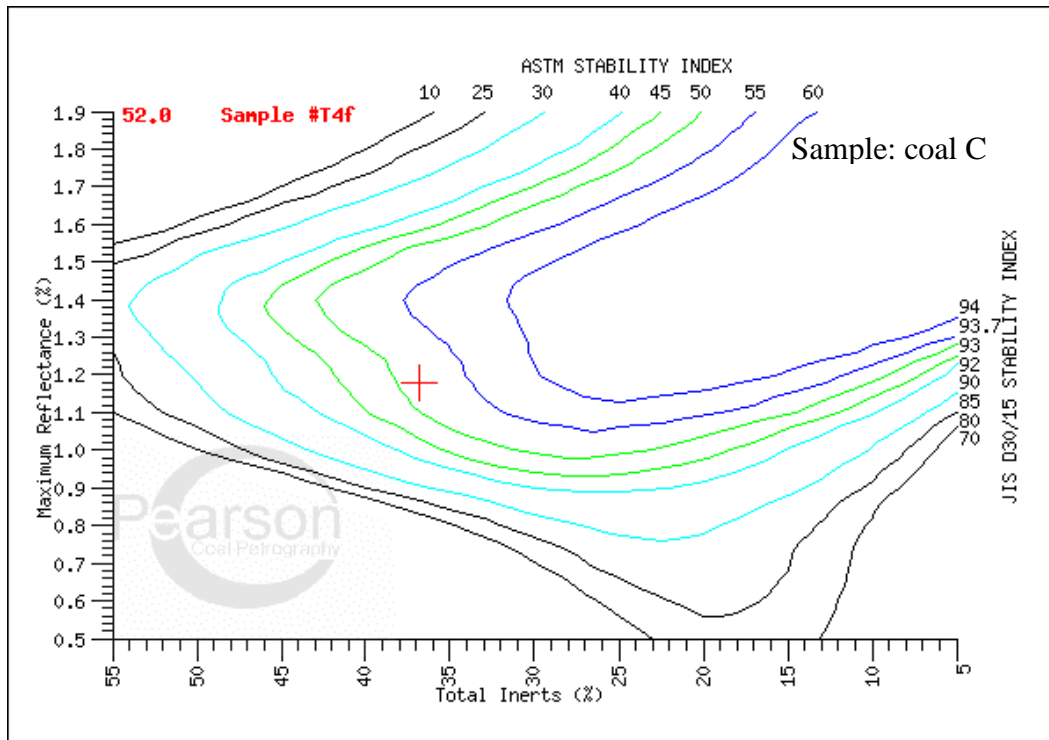


Figure 5-34 Coke strength prediction based on petrographic data of coal C.

6 CONCLUSIONS AND FUTURE DIRECTIONS

In order to study the fragmentation of large coal particles at high temperature, a drop tube furnace was custom designed to simulate the condition in the melter gasifier of the Corex plant. Drop tests of four coals under various conditions were conducted in the drop tube furnace. This method is proved to be efficient in assessing the fragmentation behaviour of different coals, and the effect of feed size, temperature, and residence time, etc.

The four coals were analysed by conventional and advanced characterisation techniques to provide explanation of the drop test results. While ash content in proximate analysis fails to illustrate the effect of minerals, CCSEM provides an explanation based on mineral interface comparison. It is therefore suggested that larger mineral particles are likely to facilitate fragmentation while small particles have insignificant effect. Furthermore, as mineral interface within coal particle increases, fragmentation increases as well, confirming the hypothesis that mineral interface is the weak areas where fragmentation is likely to occur. On the other hand, automated reflectogram is used to understand the effect of organic components. It is found that the fragmentation is less for coal C, because coal C has a higher value of MVR than the other three coals. Therefore, coal C has more mature macerals that bond inert materials at high temperature and cause

agglomeration of small particles.

The drop test results suggest that as feed size increases, more fragmentation occurs. This agrees well with the available literature. However, the effect of temperature is found to be less important, which might be a result of the slow heating condition in the present study.

The drop test results further suggest that as residence time increases, more fragmentation occurs within the first few minutes of residence time, after which its effect is not important. In addition, finer particles diminish as residence time increases, and the reason might be that more tars are released that trap the fines.

The present study provides an efficient method to assess the fragmentation behaviour of large coal particles at high temperature under the condition similar to that in Corex process. Nevertheless, some future work can be considered.

- The product char particles of the drop test can be further analysed. For example, SEM analysis can be used to observe the bonding of small particles.
- The effect of coal blending on fragmentation can be studied using the drop tube furnace, as coal blending is common and necessary in practical Corex operation. The falling time of the particles is limited, so most of the devolatilization occurs after the coal particles rest on the impact plate. Therefore, there are interactions between different coal particles through the release of volatile matter, such as gas and tar. For example, it is possible that the released tar of one coal traps the fines produced from the fragmentation of another coal. In this case, the effect of blending is not linear.
- Moreover, as stated in the literature review section, direct observation of the physical configuration change of the coal particles at high

temperature can be done in a horizontal transparent tube with a camera installed at one side.¹⁷ Similar experiment setup can be used to directly observe the swelling, shrinking, agglomeration and fragmentation of different coal particles. Therefore, the relationship between coal properties and the fragmentation behaviour at high temperature can be further investigated.

Bibliography

1. http://www.steelonthenet.com/files/metallurgical_coal.html (Last accessed in September, 2011).
2. <http://www.steelonthenet.com/files/blast-furnace-coke.html> (Last accessed in September, 2011).
3. EPA, U. S., Carcinogen Assessment of Coke Oven Emissions. *U.S. Environmental Protection Agency, Washington, D.C.* EPA/600/6-82/003F (NTIS PB84170182).
4. Nan, W.; Xuemei, X.; Zongshu, Z.; Li, G.; Wanren, X.; Yusheng, Z., Analysis of Material and Energy Consumption of Corex C3000. *steel research international* **2008**, 79, (7), 547-552.
5. Sahoo, R.; Roach, D., Degradation behaviour of weathered coal during handling for the COREX process of iron making. *Powder Technology* **2005**, 152, (1-3), 1-8.
6. <http://www.industry.siemens.com/metals-mining/en/Ironmaking/corex.htm> (Last accessed in September, 2011).
7. Kumar, P. P.; Rao, Y. S.; Chidambaran, K.; Ranjan, M., Influence of Coal Size on the Performance of Corex Process. *steel research international* **2009**, 80, (3), 179-184.
8. Arena, U.; Cammarota, A.; Chirone, R., Primary and secondary fragmentation of coals in a circulating fluidized bed combustor. *Symposium (International) on Combustion* **1994**, 25, (1), 219-226.
9. Kosowska-Galacbowska, M.; Luckos, A., An Experimental Investigation into the Fragmentation of Coal Particles in a Fluidized-Bed Combustor. In *Proceedings of the 20th International Conference on Fluidized Bed Combustion*, Yue, G.; Zhang, H.; Zhao, C.; Luo, Z., Eds. Springer Berlin Heidelberg: 2010; pp 330-334.
10. Chirone, R.; Salatino, P.; Massimilla, L., Secondary fragmentation of char particles during combustion in a fluidized bed. *Combustion and Flame* **1989**, 77, (1), 79-90.
11. Zhang, H.; Cen, K.; Yan, J.; Ni, M., The fragmentation of coal particles during the coal combustion in a fluidized bed. *Fuel* **2002**, 81, (14), 1835-1840.
12. Chirone, R.; Massimilla, L., The application of Weibull theory to primary fragmentation of a coal during devolatilization. *Powder Technology* **1989**, 57, (3), 197-212.
13. Dakic, D.; van der Honing, G.; Valk, M., Fragmentation and swelling of various coals during devolatilization in a fluidized bed. *Fuel* **1989**, 68, (7), 911-916.
14. Stanmore, B. R.; Brillard, A.; Gilot, P.; Delfosse, L., Fragmentation of small

- coal particles under fluidized-bed combustor conditions. *Symposium (International) on Combustion* **1996**, 26, (2), 3269-3275.
15. Dacombe, P.; Pourkashanian, M.; Williams, A.; Yap, L., Combustion-induced fragmentation behavior of isolated coal particles. *Fuel* **1999**, 78, (15), 1847-1857.
 16. Paprika, M. J.; Komatina, M. M.; Winter, F.; Dakic, D. V., Factors Affecting Primary Fragmentation During Combustion of Serbian Coals. *ASME Conference Proceedings* **2005**, 2005, (41839), 505-511.
 17. Kim, B.-c.; Gupta, S.; Lee, S.-h.; Kim, S.-m.; Sahajwalla, V., Devolatilization and Cracking Characteristics of Australian Lumpy Coals. *Energy & Fuels* **2008**, 22, (1), 514-522.
 18. Borah, R. C.; Ghosh, P.; Rao, P. G., A review on devolatilization of coal in fluidized bed. *International Journal of Energy Research* **2011**, 35, (11), 929-963.
 19. Paul, J.; Peeler, K.; Poynton, H. J., Devolatilization of large coal particles under fluidized bed conditions. *Fuel* **1992**, 71, (4), 425-430.
 20. Stubington, J. F.; Huang, G.; Scaroni, A. W., Devolatilization times of mm-size coal particles. *Fuel* **1991**, 70, (9), 1105-1108.
 21. Stubington, J. F.; Sumaryono, Release of Volatiles from Large Coal Particles in a Hot Fluidized-Bed. *Fuel* **1984**, 63, (7), 1013-1019.
 22. Stubington, J. F.; Linjewile, T. M., The effects of fragmentation on devolatilization of large coal particles. *Fuel* **1989**, 68, (2), 155-160.
 23. Dacombe, P. J.; Hampartsoumian, E.; Pourkashanian, M., Fragmentation of large coal particles in a drop-tube furnace. *Fuel* **1994**, 73, (8), 1365-1367.
 24. No S. Y., Syred N., Thermal stress and pressure effects on coal-particle fragmentation and burning behaviour in a cyclone combustor. *Journal of the Institute of Energy* **1990**, 63, 195-202.
 25. Borah, R. C.; Rao, P. G.; Ghosh, P., Devolatilization of coals of northeastern India in inert atmosphere and in air under fluidized bed conditions. *Fuel Processing Technology* **2010**, 91, (1), 9-16.
 26. Kumar, P. P.; Gupta, D.; Naha, T. K.; Gupta, S. S., Factors affecting fuel rate in Corex process. *Ironmaking & Steelmaking* **2006**, 33, (4), 293-298.
 27. Gupta, R., Advanced Coal Characterization: A Review†. *Energy & Fuels* **2007**, 21, (2), 451-460.
 28. Teo, C. S.; Waters, A. G.; Nicol, S. K., Quantification of the breakage of lump materials during handling operations. *International Journal of Mineral Processing* **1990**, 30, (3-4), 159-184.
 29. Yu, D.; Xu, M.; Zhang, L.; Yao, H.; Wang, Q.; Ninomiya, Y., Computer-Controlled Scanning Electron Microscopy (CCSEM) Investigation on the Heterogeneous Nature of Mineral Matter in Six Typical Chinese Coals†. *Energy & Fuels* **2006**, 21, (2), 468-476.

30. Zhang, L.; Sato, A.; Ninomiya, Y., CCSEM analysis of ash from combustion of coal added with limestone. *Fuel* **2002**, 81, (11-12), 1499-1508.
31. Gupta, R. P.; Wall, T. F.; Kajigaya, I.; Miyamae, S.; Tsumita, Y., Computer-controlled scanning electron microscopy of minerals in coal--Implications for ash deposition. *Progress in Energy and Combustion Science* **1998**, 24, (6), 523-543.
32. O'Brien, G.; Jenkins, B.; Esterle, J.; Beath, H., Coal characterisation by automated coal petrography[small star, filled]. *Fuel* **2003**, 82, (9), 1067-1073.
33. Sutcu, H.; Toroglu, I.; Piskin, S., Prediction of Metallurgical Coke Strength from the Petrographic Composition of Coal Blends. *Energy Sources, Part A: Recovery, Utilization, and Environmental Effects* **2009**, 31, (12), 1047-1055.
34. Gray, R. J., Some petrographic applications to coal, coke and carbons. *Organic Geochemistry* **1991**, 17, (4), 535-555.
35. Gransden, J. F.; Jorgensen, J. G.; Manery, N.; Price, J. T.; Ramey, N. J., Applications of microscopy to coke making. *International Journal of Coal Geology* **1991**, 19, (1-4), 77-107.
36. Pareek, H. S., The application of coal petrography to coking property of Indian coals. *Economic Geology* **1969**, 64, (7), 809-821.
37. Tang, L.; Gupta, R.; Sheng, C.; Wall, T., The char structure characterization from the coal reflectogram. *Fuel* **2005**, 84, (10), 1268-1276.
38. Chao, E. C. T.; Minkin, J. A.; Thompson, C. L., Application of automated image analysis to coal petrography. *International Journal of Coal Geology* **1982**, 2, (2), 113-150.
39. Schapiro N., Gray R. J., The use of coal petrography in coke making. *Journal of the Institute of Fuel* **1964**, 11, (30), 234-242.
40. Pearson, D. E., Probability analysis of blended coking coals. *International Journal of Coal Geology* **1991**, 19, (1-4), 109-119.

Appendix I

Heating Time Calculation

For heating time calculation, required heating time t is defined as the time when the temperature of the particle centre reaches to 95% of the target temperature.

Convection and radiation is responsible to transfer heat to the surface of the particles, while conduction heats the inside. For simplicity, the coal particle is considered to be a sphere with uniform and unchangeable properties. N_2 is purged into the tube, and supposed to reach the target temperature when it passes through the tube down.

The convection coefficient, h can be calculated according to the following equation:

$$h = Nu_D \frac{k}{D} \quad (i)$$

where, k is the thermal conductivity of nitrogen at target temperature, D is the particle diameter. The Nusselt Number, Nu_D is estimated according to the Equation (ii) proposed by Whitaker. ¹

$$Nu_D = 2 + (0.4 Re_D^{1/2} + 0.06 Re_D^{2/3}) Pr^{0.4} \left(\frac{\mu}{\mu_s} \right)^{1/4} \quad (ii)$$

All properties except μ_s should be taken at T_∞ . In this case, T_∞ is the target temperature. Re_D is particle Reynolds number. Pr is Prandtl number of nitrogen. μ is the viscosity of nitrogen at T_∞ ; μ_s is the viscosity of N_2 at $(T_i + 0.95 * T_\infty) / 2$, while T_i is the initial temperature of the particle.

Table 1 shows the h values under various conditions. For particles with sizes ranging from 1 mm to 25 mm, h decreases rapidly with increasing particle size at

the same temperature. With the same size, however, h does not vary much with temperatures. Only a minor increase of h is associated with temperature rise.

Table 1 Convection coefficient, h at various target temperatures for various feed sizes

| Size (mm) \ Target T(°C) | 1 | 2 | 5 | 10 | 20 | 25 |
|---------------------------|-------|------|------|------|------|-----|
| 600 | 134.8 | 71.3 | 31.7 | 17.7 | 10.2 | 8.6 |
| 700 | 145.6 | 76.9 | 34.1 | 19.0 | 10.9 | 9.2 |
| 800 | 157.0 | 82.8 | 36.6 | 20.3 | 11.6 | 9.8 |

Biot number, Bi for different particles under different temperatures is estimated by Equation (iii).

$$Bi = \frac{hL_c}{k_c} \quad (iii)$$

where L_c is the characteristic length, and for a sphere, $L_c = r_0 / 3$. k_c is the thermal conductivity of the particle; for the bituminous coal, it is approximated as 0.26 W/mK

It was found that $0.086 < Bi < 0.171$ under all the conditions. For estimation purpose, it was reasonable to apply lumped capacitance method to calculate the centre temperature of the particles. Therefore, for a sphere, the required heating time can be calculated according to Equation (iv) as follows:

$$t = \frac{\rho D c}{6h} \ln \frac{T_i - T_\infty}{T - T_\infty} \quad (iv)$$

As stated previously, T is considered as $95\%T_\infty$. ρ is the coal density; for a bituminous coal, ρ is assumed to equal 1350 kg/m^3 . c is the heat capacity of coal; for a bituminous coal, c is assumed to be 1260 J/kg K .

The required heating time for particles with different sizes to reach 95% of various target temperatures is given in Table 2.

Table 2 Required heating time, t (in s) under different conditions

| Size(mm) \ Gas T (°C) | 1 | 2 | 5 | 10 | 20 | 25 |
|------------------------|-----|------|-------|-------|--------|--------|
| 600 | 6.2 | 23.5 | 132.1 | 473.6 | 1646.9 | 2442.5 |
| 700 | 5.8 | 21.8 | 123.1 | 442.5 | 1543.7 | 2292.1 |
| 800 | 5.4 | 20.3 | 114.7 | 413.2 | 1445.0 | 2147.2 |

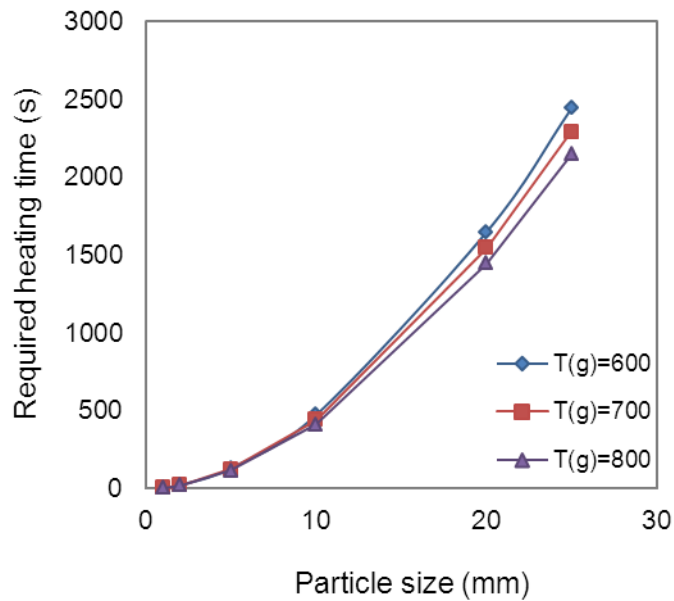


Figure 1 Required heating time, t in variance with particle size.

As indicated by Table 2 and Figure 1, particle size plays an important part in determining the required time of adequate heating. Small particles get heated rapidly, while large particles take much longer time to get heated. The time increases exponentially with increasing particle size. The reason might be that on one hand, large particles have much smaller convection coefficient, implying

lower efficiency of heat transfer from ambient gas to coal particles; on the other hand, much more heat is demanded to heat large particles. Another observation is that as target temperature increases, the required heating time decreases, but only to a limited extent. This indicates that the effect of temperature on the heating process is less important.

Radiation also contributes to the heating of particles. A single particle gets heated in a drop tube furnace, so that a two surface enclosure model is considered reasonable for rough estimation. The heat exchanged between these two surfaces is calculated using Equation (v):

$$q_{12} = \sigma A_1 \varepsilon_1 (T_1^4 - T_2^4) \quad (v)$$

where, σ is the Stefan-Boltzmann constant, and has a number of $5.670 \times 10^{-8} \text{ W/m}^2 \text{ K}^4$. ε is the emissivity of coal; for estimation purpose, it is assumed that $\varepsilon = 1$. T_1 and T_2 are the temperature of the coal, and that of the tube wall, respectively.

The temperature rise because of radiation is then calculated according to the lumped capacity method:

$$qt = C_p m \Delta T \quad (vi)$$

For a single particle with 10 mm, when the ambient temperature is 600 °C, the temperature rise in 474 s resulted from radiation is less than 0.01 °C. For this reason, the radiation effect could be neglected for estimation. Consequently, according to Table 2, 40 min, 20 min, and 10 min is specified to heat coal particles within 32 - 22 mm, 22 - 11 mm, 11 - 5 mm, respectively.

1. Whitaker, S., Forced convection heat transfer correlations for flow in pipes, past flat plates, single cylinders, single spheres, and for flow in packed beds and tube bundles. *AIChE Journal* **1972**, 18, (2), 361-371.

Appendix II

CCSEM Analysis

Table I: CCSEM analysis of coal A

| WEIGHT PERCENT ON A MINERAL BASIS | | | | | | | |
|-----------------------------------|-----|------|------|------|------|-------|--------|
| | 1.0 | 2.2 | 4.6 | 10.0 | 22.0 | 46.0 | |
| | TO | TO | TO | TO | TO | TO | TOTALS |
| | 2.2 | 4.6 | 10.0 | 22.0 | 46.0 | 400.0 | |
| QUARTZ | .3 | .7 | .3 | .3 | .2 | 1.9 | 3.6 |
| IRON OXIDE | .0 | .0 | .0 | .0 | .2 | .2 | .3 |
| PERICLASE | .0 | .0 | .0 | .0 | .0 | .0 | .0 |
| RUTILE | .1 | .0 | .0 | .0 | .0 | .0 | .1 |
| ALUMINA | .0 | .0 | .0 | .0 | .0 | .0 | .0 |
| CALCITE | .0 | .0 | .0 | .0 | .2 | .3 | .5 |
| DOLOMITE | .0 | .0 | .0 | .0 | .0 | .0 | .0 |
| ANKERITE | .0 | .0 | .0 | .0 | .0 | .0 | .0 |
| KAOLINITE | 1.0 | 1.8 | .9 | 2.5 | 2.6 | 14.4 | 23.2 |
| MONTMORILLONITE | .0 | .2 | .1 | .8 | .4 | 1.4 | 2.9 |
| K AL-SILICATE | .3 | .9 | .2 | .7 | .8 | 3.7 | 6.4 |
| FE AL-SILICATE | .1 | .0 | .2 | .1 | .0 | .2 | .6 |
| CA AL-SILICATE | .0 | .1 | .0 | .0 | .0 | .2 | .3 |
| NA AL-SILICATE | .0 | .0 | .0 | .0 | .0 | .0 | .0 |
| ALUMINOSILICATE | .1 | .1 | .1 | .5 | .3 | .9 | 2.0 |
| MIXED AL-SILICA | .0 | .1 | .0 | .0 | .1 | .3 | .5 |
| FE SILICATE | .0 | .0 | .0 | .0 | .0 | .0 | .0 |
| CA SILICATE | .0 | .0 | .0 | .0 | .0 | .0 | .0 |
| CA ALUMINATE | .0 | .0 | .0 | .0 | .0 | .0 | .0 |
| PYRITE | .7 | 5.7 | 3.6 | 15.9 | 7.5 | 11.8 | 45.1 |
| PYRRHOTITE | .0 | .2 | .3 | 1.0 | 1.0 | .8 | 3.2 |
| OXIDIZED PYRRHO | .0 | .0 | .5 | .6 | .7 | .5 | 2.3 |
| GYPSUM | .0 | .0 | .0 | .1 | .1 | .1 | .3 |
| BARITE | .0 | .0 | .0 | .0 | .0 | .0 | .0 |
| APATITE | .0 | .2 | .2 | .3 | .1 | .2 | .9 |
| CA AL-P | .0 | .0 | .0 | .0 | .0 | .0 | .0 |
| KCL | .0 | .0 | .0 | .0 | .0 | .0 | .0 |
| GYPSUM/BARITE | .0 | .0 | .0 | .0 | .0 | .0 | .0 |
| GYPSUM/AL-SILIC | .0 | .0 | .0 | .0 | .0 | .0 | .1 |
| SI-RICH | .1 | .0 | .0 | .0 | .1 | 1.5 | 1.6 |
| CA-RICH | .0 | .0 | .0 | .0 | .1 | .0 | .2 |
| CA-SI RICH | .0 | .0 | .0 | .0 | .0 | .0 | .0 |
| UNKNOWN | .3 | .4 | .6 | 1.3 | .8 | 2.3 | 5.8 |
| TOTALS | 2.9 | 10.5 | 7.0 | 23.9 | 15.2 | 40.5 | 100.0 |

MINERAL AREA % COAL BASIS

| | 1.0 | 2.2 | 4.6 | 10.0 | 22.0 | 46.0 | |
|-----------------|------|------|------|-------|-------|-------|--------|
| | TO | TO | TO | TO | TO | TO | TOTALS |
| | 2.2 | 4.6 | 10.0 | 22.0 | 46.0 | 400.0 | |
| QUARTZ | .026 | .070 | .025 | .026 | .016 | .184 | .348 |
| IRON OXIDE | .000 | .000 | .000 | .000 | .007 | .009 | .016 |
| PERICLASE | .000 | .000 | .000 | .000 | .000 | .000 | .000 |
| RUTILE | .004 | .000 | .001 | .000 | .000 | .000 | .005 |
| ALUMINA | .000 | .000 | .000 | .000 | .000 | .000 | .000 |
| CALCITE | .001 | .000 | .001 | .000 | .015 | .029 | .046 |
| DOLOMITE | .000 | .000 | .000 | .000 | .000 | .000 | .000 |
| ANKERITE | .000 | .000 | .000 | .000 | .000 | .000 | .000 |
| KAOLINITE | .092 | .174 | .083 | .238 | .246 | 1.378 | 2.209 |
| MONTMORILLONITE | .003 | .023 | .010 | .081 | .038 | .137 | .292 |
| K AL-SILICATE | .026 | .085 | .015 | .065 | .076 | .359 | .626 |
| FE AL-SILICATE | .010 | .003 | .021 | .005 | .002 | .015 | .056 |
| CA AL-SILICATE | .000 | .006 | .004 | .000 | .002 | .019 | .030 |
| NA AL-SILICATE | .001 | .000 | .000 | .000 | .000 | .000 | .001 |
| ALUMINOSILICATE | .010 | .011 | .007 | .045 | .029 | .089 | .191 |
| MIXED AL-SILICA | .001 | .008 | .002 | .000 | .012 | .025 | .049 |
| FE SILICATE | .000 | .000 | .000 | .000 | .000 | .000 | .000 |
| CA SILICATE | .000 | .000 | .000 | .000 | .000 | .000 | .000 |
| CA ALUMINATE | .000 | .000 | .000 | .000 | .000 | .000 | .000 |
| PYRITE | .036 | .287 | .180 | .805 | .378 | .594 | 2.280 |
| PYRRHOTITE | .000 | .012 | .016 | .053 | .053 | .043 | .177 |
| OXIDIZED PYRRHO | .000 | .000 | .026 | .026 | .034 | .023 | .109 |
| GYPSUM | .000 | .000 | .000 | .008 | .015 | .006 | .029 |
| BARITE | .000 | .000 | .000 | .000 | .000 | .000 | .000 |
| APATITE | .000 | .015 | .013 | .023 | .010 | .013 | .073 |
| CA AL-P | .000 | .000 | .000 | .000 | .000 | .000 | .000 |
| KCL | .000 | .000 | .000 | .000 | .000 | .000 | .000 |
| GYPSUM/BARITE | .000 | .000 | .000 | .000 | .000 | .000 | .000 |
| GYPSUM/AL-SILIC | .000 | .000 | .001 | .000 | .004 | .000 | .005 |
| SI-RICH | .007 | .000 | .003 | .000 | .007 | .139 | .156 |
| CA-RICH | .004 | .002 | .000 | .004 | .008 | .000 | .018 |
| CA-SI RICH | .000 | .000 | .000 | .000 | .000 | .000 | .000 |
| UNKNOWN | .024 | .041 | .054 | .125 | .078 | .217 | .538 |
| TOTALS | .243 | .738 | .463 | 1.502 | 1.029 | 3.279 | 7.254 |

Table II: CCSEM analysis of coal B

| WEIGHT PERCENT ON A MINERAL BASIS | | | | | | | |
|-----------------------------------|-----|------|------|------|------|-------|--------|
| | 1.0 | 2.2 | 4.6 | 10.0 | 22.0 | 46.0 | TOTALS |
| | TO | TO | TO | TO | TO | TO | |
| | 2.2 | 4.6 | 10.0 | 22.0 | 46.0 | 400.0 | |
| QUARTZ | .0 | .2 | .0 | .0 | .0 | .0 | .2 |
| IRON OXIDE | .0 | .2 | .1 | .0 | .0 | .0 | .3 |
| PERICLASE | .0 | .0 | .0 | .0 | .0 | .0 | .0 |
| RUTILE | .1 | .2 | .0 | .0 | .0 | .0 | .2 |
| ALUMINA | .0 | .1 | .0 | .0 | .0 | .0 | .1 |
| CALCITE | .2 | .1 | 1.2 | 1.8 | .0 | .0 | 3.3 |
| DOLOMITE | .0 | .1 | .4 | 1.1 | .0 | .0 | 1.7 |
| ANKERITE | .0 | .0 | .0 | .0 | .0 | .0 | .0 |
| KAOLINITE | 6.0 | 22.8 | 21.0 | 11.3 | .9 | .9 | 62.8 |
| MONTMORILLONITE | .3 | .5 | .2 | .0 | .1 | .3 | 1.4 |
| K AL-SILICATE | .1 | .4 | .2 | .2 | .1 | .5 | 1.4 |
| FE AL-SILICATE | .2 | .6 | .4 | .1 | .0 | .0 | 1.4 |
| CA AL-SILICATE | .1 | .4 | .3 | .0 | .1 | .0 | 1.0 |
| NA AL-SILICATE | .0 | .0 | .0 | .0 | .0 | .0 | .0 |
| ALUMINOSILICATE | .2 | 1.2 | 2.7 | 3.1 | .3 | .5 | 8.0 |
| MIXED AL-SILICA | .1 | .2 | .3 | .0 | .0 | .0 | .5 |
| FE SILICATE | .0 | .0 | .0 | .0 | .0 | .0 | .0 |
| CA SILICATE | .0 | .0 | .0 | .0 | .0 | .0 | .0 |
| CA ALUMINATE | .0 | .0 | .0 | .0 | .0 | .0 | .0 |
| PYRITE | .4 | 1.5 | 1.4 | 1.7 | .1 | .0 | 5.2 |
| PYRRHOTITE | .0 | .0 | .0 | .0 | .0 | .0 | .0 |
| OXIDIZED PYRRHO | .0 | .0 | .0 | .0 | .1 | .0 | .1 |
| GYPSUM | .0 | .1 | .1 | .0 | .0 | .0 | .2 |
| BARITE | .0 | .0 | .0 | .0 | .0 | .0 | .0 |
| APATITE | .0 | .1 | .1 | .0 | .0 | .0 | .2 |
| CA AL-P | .0 | .0 | .0 | .0 | .0 | .0 | .0 |
| KCL | .0 | .0 | .0 | .0 | .0 | .0 | .0 |
| GYPSUM/BARITE | .0 | .0 | .0 | .0 | .0 | .0 | .0 |
| GYPSUM/AL-SILIC | .0 | .3 | .0 | .0 | .0 | .0 | .3 |
| SI-RICH | .0 | .0 | .0 | .0 | .0 | .0 | .0 |
| CA-RICH | .2 | .2 | .5 | .0 | .0 | .0 | 1.0 |
| CA-SI RICH | .0 | .0 | .0 | .0 | .0 | .0 | .0 |
| UNKNOWN | 1.6 | 1.7 | 3.8 | 2.9 | .5 | .0 | 10.5 |
| TOTALS | 9.6 | 30.6 | 32.9 | 22.3 | 2.3 | 2.3 | 100.0 |

MINERAL AREA % COAL BASIS

| | 1.0 | 2.2 | 4.6 | 10.0 | 22.0 | 46.0 | |
|-------------------|------|------|------|------|------|-------|--------|
| | TO | TO | TO | TO | TO | TO | TOTALS |
| | 2.2 | 4.6 | 10.0 | 22.0 | 46.0 | 400.0 | |
| QUARTZ | .000 | .004 | .001 | .000 | .000 | .000 | .005 |
| IRON OXIDE | .000 | .002 | .001 | .000 | .000 | .000 | .003 |
| PERICLASE | .000 | .000 | .000 | .000 | .000 | .000 | .000 |
| RUTILE | .001 | .002 | .000 | .000 | .000 | .000 | .003 |
| ALUMINA | .000 | .001 | .000 | .000 | .000 | .000 | .001 |
| CALCITE | .004 | .001 | .022 | .035 | .000 | .000 | .063 |
| DOLOMITE | .000 | .002 | .008 | .021 | .001 | .000 | .032 |
| ANKERITE | .000 | .000 | .000 | .000 | .000 | .000 | .000 |
| KAOLINITE | .121 | .462 | .425 | .230 | .019 | .017 | 1.275 |
| MONTMORILLONITE | .006 | .011 | .005 | .000 | .002 | .007 | .030 |
| K AL-SILICATE | .001 | .008 | .004 | .003 | .002 | .011 | .029 |
| FE AL-SILICATE | .004 | .012 | .008 | .003 | .000 | .000 | .027 |
| CA AL-SILICATE | .003 | .007 | .007 | .000 | .003 | .000 | .020 |
| NA AL-SILICATE | .000 | .000 | .000 | .000 | .000 | .000 | .000 |
| ALUMINOSILICATE | .004 | .024 | .055 | .062 | .006 | .011 | .162 |
| MIXED AL-SILICA | .001 | .004 | .006 | .000 | .000 | .000 | .011 |
| FE SILICATE | .000 | .000 | .000 | .000 | .000 | .000 | .000 |
| CA SILICATE | .000 | .000 | .000 | .000 | .000 | .000 | .000 |
| CA ALUMINATE | .000 | .000 | .000 | .000 | .000 | .000 | .000 |
| PYRITE | .005 | .016 | .015 | .019 | .001 | .000 | .056 |
| PYRRHOTITE | .000 | .000 | .000 | .000 | .000 | .000 | .000 |
| OXIDIZEDED PYRRHO | .000 | .000 | .000 | .000 | .001 | .000 | .001 |
| GYPSUM | .001 | .002 | .002 | .000 | .000 | .000 | .004 |
| BARITE | .000 | .000 | .000 | .000 | .000 | .000 | .000 |
| APATITE | .000 | .001 | .002 | .000 | .000 | .000 | .004 |
| CA AL-P | .000 | .000 | .000 | .000 | .000 | .000 | .000 |
| KCL | .000 | .000 | .000 | .000 | .000 | .000 | .000 |
| GYPSUM/BARITE | .000 | .000 | .000 | .000 | .000 | .000 | .000 |
| GYPSUM/AL-SILIC | .000 | .006 | .000 | .000 | .000 | .000 | .007 |
| SI-RICH | .000 | .000 | .000 | .000 | .001 | .000 | .001 |
| CA-RICH | .005 | .005 | .011 | .000 | .000 | .000 | .020 |
| CA-SI RICH | .000 | .000 | .000 | .000 | .000 | .000 | .000 |
| UNKNOWN | .032 | .034 | .076 | .058 | .009 | .000 | .210 |
| TOTALS | .189 | .603 | .649 | .431 | .045 | .047 | 1.964 |

Table III: CCSEM analysis of coal C

| WEIGHT PERCENT ON A MINERAL BASIS | | | | | | | |
|-----------------------------------|-----|------|------|------|------|-------|-------|
| | 1.0 | 2.2 | 4.6 | 10.0 | 22.0 | 46.0 | |
| | TO | TO | TO | TO | TO | TO | TOTAL |
| | 2.2 | 4.6 | 10.0 | 22.0 | 46.0 | 400.0 | |
| QUARTZ | .3 | 1.8 | .8 | 1.3 | .4 | 1.3 | 5.8 |
| IRON OXIDE | .0 | .0 | .2 | 1.6 | .4 | 1.7 | 3.9 |
| PERICLASE | .0 | .0 | .0 | .0 | .0 | .0 | .0 |
| RUTILE | .0 | .0 | .1 | .0 | .0 | .0 | .2 |
| ALUMINA | .0 | .1 | .0 | .0 | .0 | .1 | .2 |
| CALCITE | .0 | .1 | .1 | .4 | .0 | .1 | .7 |
| DOLOMITE | .0 | .0 | .0 | .0 | .0 | .1 | .1 |
| ANKERITE | .0 | .0 | .0 | .0 | .0 | .0 | .0 |
| KAOLINITE | 2.1 | 10.6 | 12.2 | 10.1 | 2.6 | 10.5 | 48.0 |
| MONTMORILLONITE | .2 | .7 | .5 | 1.5 | .2 | .6 | 3.7 |
| K AL-SILICATE | .1 | .3 | .5 | .8 | .2 | 1.3 | 3.2 |
| FE AL-SILICATE | .0 | .0 | .0 | .0 | .0 | .1 | .2 |
| CA AL-SILICATE | .0 | .2 | .3 | .2 | .0 | .1 | .9 |
| NA AL-SILICATE | .0 | .0 | .0 | .0 | .0 | .0 | .1 |
| ALUMINOSILICATE | .1 | .1 | .3 | .4 | .4 | .3 | 1.5 |
| MIXED AL-SILICA | .1 | .2 | .4 | .0 | .0 | .0 | .8 |
| FE SILICATE | .0 | .0 | .0 | .0 | .0 | .0 | .0 |
| CA SILICATE | .0 | .1 | .0 | .0 | .0 | .0 | .1 |
| CA ALUMINATE | .0 | .0 | .0 | .0 | .0 | .0 | .0 |
| PYRITE | .0 | .1 | .4 | .0 | .0 | .0 | .5 |
| PYRRHOTITE | .0 | .0 | .0 | .0 | .0 | .0 | .0 |
| OXIDIZED PYRRHO | .0 | .0 | .0 | .0 | .0 | .1 | .1 |
| GYPSUM | .0 | .0 | .0 | .0 | .0 | .0 | .0 |
| BARITE | .0 | .0 | .0 | .0 | .0 | .0 | .0 |
| APATITE | .2 | 1.8 | 1.7 | 2.2 | .1 | .2 | 6.2 |
| CA AL-P | .0 | .0 | .1 | .0 | .0 | .0 | .1 |
| KCL .0 | .0 | .0 | .0 | .0 | .0 | .0 | .0 |
| GYPSUM/BARITE | .0 | .0 | .0 | .0 | .0 | .0 | .0 |
| GYPSUM/AL-SILIC | .0 | .1 | .2 | .0 | .0 | .0 | .2 |
| SI-RICH | .1 | .4 | .3 | 1.3 | .2 | .3 | 2.7 |
| CA-RICH | .0 | .2 | .3 | .4 | .0 | .0 | .9 |
| CA-SI RICH | .0 | .0 | .0 | .0 | .0 | .0 | .0 |
| UNKNOWN | .8 | 3.1 | 3.9 | 4.5 | .7 | 7.0 | 19.9 |
| TOTALS | 4.0 | 19.7 | 22.4 | 24.6 | 5.4 | 23.8 | 100.0 |

MINERAL AREA % COAL BASIS

| | 1.0 TO 2.2 | 2.2 TO 4.6 | 4.6 TO 10.0 | 10.0 TO 22.0 | 22.0 TO 46.0 | 46.0 TO 400.0 | TOTALS |
|-------------------|------------------|------------------|-------------------|--------------------|--------------------|---------------------|--------|
| QUARTZ | .030 | .185 | .081 | .130 | .042 | .133 | .601 |
| IRON OXIDE | .000 | .000 | .012 | .082 | .020 | .087 | .200 |
| PERICLASE | .000 | .000 | .000 | .000 | .000 | .000 | .000 |
| RUTILE | .000 | .000 | .007 | .000 | .002 | .000 | .009 |
| ALUMINA | .000 | .006 | .002 | .000 | .000 | .005 | .013 |
| CALCITE | .000 | .008 | .013 | .038 | .004 | .005 | .069 |
| DOLOMITE | .000 | .000 | .000 | .000 | .000 | .007 | .007 |
| ANKERITE | .000 | .000 | .000 | .000 | .000 | .000 | .000 |
| KAOLINITE | .213 | 1.084 | 1.254 | 1.033 | .269 | 1.077 | 4.929 |
| MONTMORILLONITE | .022 | .072 | .059 | .162 | .025 | .062 | .401 |
| K AL-SILICATE | .012 | .030 | .054 | .084 | .016 | .141 | .337 |
| FE AL-SILICATE | .001 | .000 | .000 | .000 | .003 | .014 | .018 |
| CA AL-SILICATE | .002 | .023 | .029 | .025 | .001 | .014 | .095 |
| NA AL-SILICATE | .002 | .000 | .003 | .000 | .000 | .000 | .005 |
| ALUMINOSILICATE | .011 | .006 | .031 | .041 | .037 | .032 | .159 |
| MIXED AL-SILICA | .010 | .020 | .044 | .000 | .004 | .002 | .080 |
| FE SILICATE | .000 | .000 | .000 | .000 | .000 | .000 | .000 |
| CA SILICATE | .002 | .005 | .000 | .000 | .000 | .000 | .006 |
| CA ALUMINATE | .000 | .000 | .000 | .000 | .000 | .000 | .000 |
| PYRITE | .000 | .008 | .020 | .000 | .001 | .000 | .029 |
| PYRRHOTITE | .000 | .000 | .000 | .000 | .000 | .000 | .000 |
| OXIDIZEDED PYRRHO | .000 | .000 | .000 | .000 | .001 | .004 | .005 |
| GYPSUM | .000 | .000 | .000 | .000 | .000 | .000 | .000 |
| BARITE | .000 | .000 | .000 | .000 | .000 | .000 | .000 |
| APATITE | .015 | .154 | .148 | .188 | .011 | .015 | .531 |
| CA AL-P | .000 | .000 | .005 | .000 | .000 | .000 | .005 |
| KCL | .000 | .000 | .000 | .000 | .000 | .000 | .000 |
| GYPSUM/BARITE | .000 | .000 | .000 | .000 | .000 | .000 | .000 |
| GYPSUM/AL-SILIC | .000 | .007 | .019 | .000 | .000 | .000 | .026 |
| SI-RICH | .009 | .046 | .027 | .136 | .020 | .035 | .274 |
| CA-RICH | .002 | .018 | .033 | .037 | .001 | .003 | .093 |
| CA-SI RICH | .000 | .000 | .000 | .000 | .000 | .000 | .000 |
| UNKNOWN | .081 | .312 | .389 | .450 | .068 | .709 | 2.009 |
| TOTALS | .412 | 1.983 | 2.232 | 2.408 | .524 | 2.343 | 9.900 |

Table IV: CCSEM analysis of coal D

| WEIGHT PERCENT ON A MINERAL BASIS | | | | | | | |
|-----------------------------------|-----|------|------|------|-------|--------|-------|
| 1.0 | 2.2 | 4.6 | 10.0 | 22.0 | 46.0 | | |
| TO | TO | TO | TO | TO | TO | TOTALS | |
| 2.2 | 4.6 | 10.0 | 22.0 | 46.0 | 400.0 | | |
| ----- | | | | | | | |
| ----- QUARTZ | .8 | 2.9 | .7 | .6 | .6 | 3.5 | 9.1 |
| IRON OXIDE | .0 | .0 | .0 | .0 | .0 | .7 | .7 |
| PERICLASE | .0 | .0 | .0 | .0 | .0 | .0 | .0 |
| RUTILE | .0 | .0 | .0 | .0 | .0 | .0 | .0 |
| ALUMINA | .1 | .1 | .0 | .0 | .0 | .0 | .2 |
| CALCITE | .0 | .0 | .0 | .0 | .0 | 1.2 | 1.3 |
| DOLOMITE | .0 | .0 | .0 | .0 | .0 | .0 | .0 |
| ANKERITE | .0 | .0 | .0 | .0 | .0 | .0 | .0 |
| KAOLINITE | .7 | 4.6 | 1.6 | 2.5 | 3.5 | 16.2 | 29.1 |
| MONTMORILLONITE | .3 | 1.7 | .6 | .9 | 1.7 | 10.5 | 15.6 |
| K AL-SILICATE | .1 | .4 | .5 | .2 | .2 | 3.0 | 4.4 |
| FE AL-SILICATE | .1 | .2 | .0 | .1 | .1 | 1.1 | 1.6 |
| CA AL-SILICATE | .4 | 1.1 | .0 | .2 | .3 | .4 | 2.4 |
| NA AL-SILICATE | .2 | .4 | .1 | .1 | .0 | .8 | 1.6 |
| ALUMINOSILICATE | .1 | 1.0 | .2 | .8 | .5 | 6.2 | 8.9 |
| MIXED AL-SILICA | .4 | .7 | .0 | .2 | .3 | .2 | 1.9 |
| FE SILICATE | .0 | .0 | .0 | .0 | .0 | .0 | .0 |
| CA SILICATE | .0 | .0 | .0 | .0 | .0 | .0 | .0 |
| CA ALUMINATE | .0 | .0 | .0 | .0 | .0 | .0 | .0 |
| PYRITE | .0 | .1 | .1 | .1 | .0 | .0 | .3 |
| PYRRHOTITE | .0 | .0 | .0 | .0 | .0 | .0 | .0 |
| OXIDIZED PYRRHO | .0 | .0 | .0 | .0 | .0 | .0 | .0 |
| GYPSUM | .0 | .0 | .0 | .0 | .0 | .0 | .0 |
| BARITE | .0 | .0 | .0 | .0 | .0 | .0 | .0 |
| APATITE | .0 | .0 | .0 | .0 | .0 | .0 | .0 |
| CA AL-P | .0 | .0 | .0 | .0 | .0 | .0 | .0 |
| KCL | .0 | .0 | .0 | .0 | .0 | .0 | .0 |
| GYPSUM/BARITE | .0 | .0 | .0 | .0 | .0 | .0 | .0 |
| GYPSUM/AL-SILIC | .0 | .1 | .0 | .0 | .0 | .1 | .3 |
| SI-RICH | .5 | 1.3 | .2 | .3 | .6 | 8.2 | 11.1 |
| CA-RICH | .0 | .0 | .0 | .0 | .0 | .0 | .0 |
| CA-SI RICH | .0 | .0 | .0 | .0 | .0 | .3 | .3 |
| UNKNOWN | .4 | 1.6 | .3 | .4 | .6 | 7.9 | 11.3 |
| ----- | | | | | | | |
| --- TOTALS | 4.2 | 16.3 | 4.3 | 6.2 | 8.6 | 60.4 | 100.0 |

| MINERAL | AREA % COAL BASIS | | | | | | TOTALS |
|-------------------|-------------------|-------|------|------|------|-------|--------|
| | 1.0 | 2.2 | 4.6 | 10.0 | 22.0 | 46.0 | |
| | TO | TO | TO | TO | TO | TO | |
| | 2.2 | 4.6 | 10.0 | 22.0 | 46.0 | 400.0 | |
| QUARTZ | .052 | .185 | .043 | .035 | .035 | .220 | .569 |
| IRON OXIDE | .000 | .000 | .000 | .000 | .000 | .023 | .023 |
| PERICLASE | .000 | .000 | .000 | .000 | .000 | .000 | .000 |
| RUTILE | .000 | .000 | .000 | .000 | .000 | .000 | .000 |
| ALUMINA | .002 | .006 | .000 | .000 | .000 | .000 | .008 |
| CALCITE | .002 | .000 | .002 | .000 | .001 | .074 | .078 |
| DOLOMITE | .000 | .000 | .000 | .000 | .000 | .000 | .000 |
| ANKERITE | .000 | .000 | .000 | .000 | .000 | .000 | .000 |
| KAOLINITE | .044 | .290 | .102 | .157 | .221 | 1.018 | 1.831 |
| MONTMORILLONITE | .021 | .112 | .037 | .057 | .116 | .699 | 1.041 |
| K AL-SILICATE | .006 | .027 | .029 | .015 | .014 | .190 | .281 |
| FE AL-SILICATE | .004 | .011 | .003 | .005 | .006 | .064 | .093 |
| CA AL-SILICATE | .025 | .071 | .000 | .011 | .019 | .027 | .153 |
| NA AL-SILICATE | .015 | .024 | .004 | .006 | .002 | .049 | .100 |
| ALUMINOSILICATE | .007 | .066 | .013 | .049 | .034 | .389 | .558 |
| MIXED AL-SILICA | .028 | .042 | .002 | .012 | .020 | .014 | .117 |
| FE SILICATE | .000 | .000 | .000 | .000 | .000 | .000 | .000 |
| CA SILICATE | .000 | .000 | .000 | .000 | .000 | .000 | .000 |
| CA ALUMINATE | .000 | .000 | .000 | .000 | .000 | .000 | .000 |
| PYRITE | .000 | .003 | .003 | .002 | .001 | .000 | .008 |
| PYRRHOTITE | .000 | .000 | .000 | .000 | .000 | .000 | .000 |
| OXIDIZEDED PYRRHO | .000 | .000 | .000 | .000 | .000 | .000 | .000 |
| GYPSUM | .000 | .000 | .000 | .000 | .000 | .000 | .000 |
| BARITE | .000 | .000 | .000 | .000 | .000 | .000 | .000 |
| APATITE | .000 | .000 | .000 | .000 | .000 | .000 | .000 |
| CA AL-P | .000 | .000 | .000 | .000 | .000 | .000 | .000 |
| KCL | .000 | .000 | .000 | .000 | .000 | .000 | .000 |
| GYPSUM/BARITE | .000 | .000 | .000 | .000 | .000 | .000 | .000 |
| GYPSUM/AL-SILIC | .002 | .008 | .000 | .000 | .002 | .007 | .020 |
| SI-RICH | .033 | .080 | .012 | .016 | .037 | .517 | .695 |
| CA-RICH | .000 | .000 | .000 | .000 | .000 | .000 | .000 |
| CA-SI RICH | .000 | .000 | .000 | .000 | .000 | .022 | .022 |
| UNKNOWN | .027 | .101 | .021 | .024 | .037 | .484 | .694 |
| TOTALS | .266 | 1.024 | .273 | .389 | .544 | 3.796 | 6.291 |

Appendix III

Automated Reflectogram

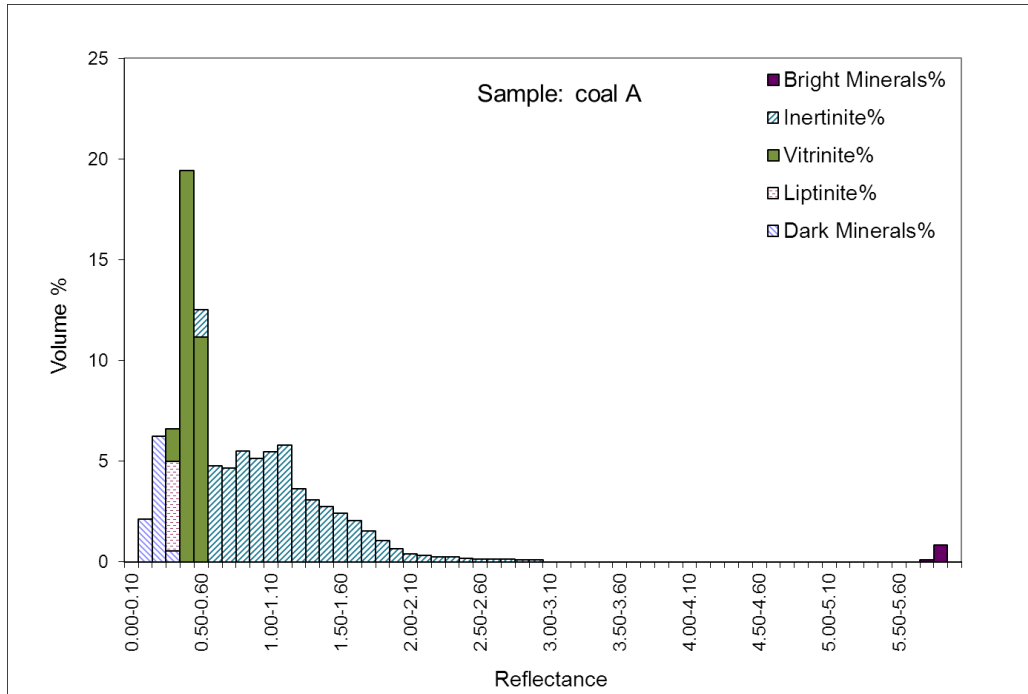


Figure I. Automated reflectogram of coal A

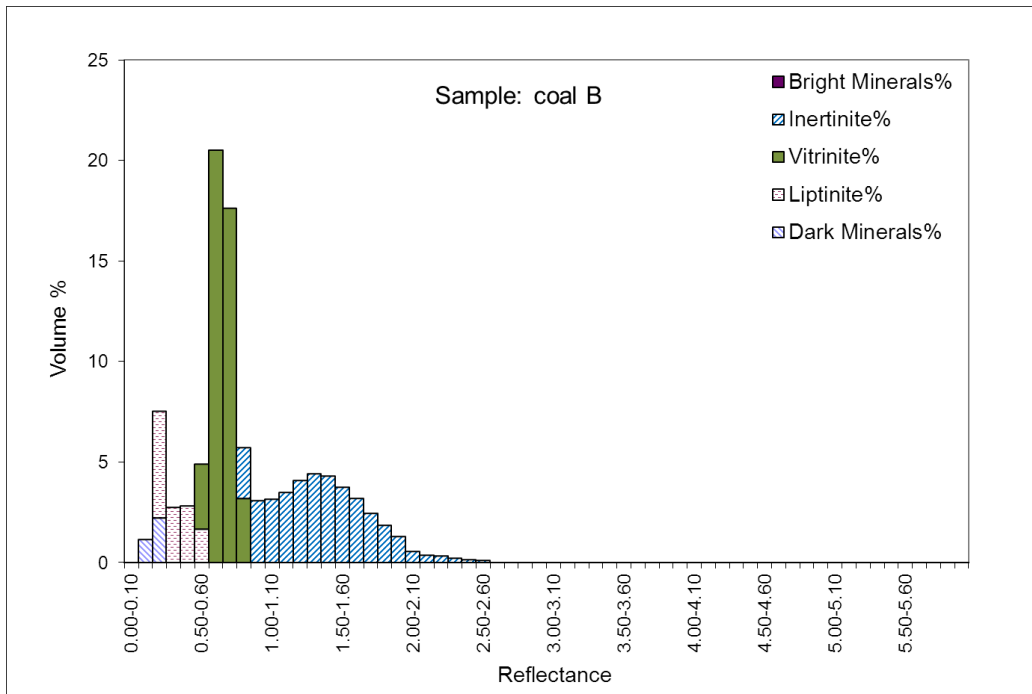


Figure II. Automated reflectogram of coal B

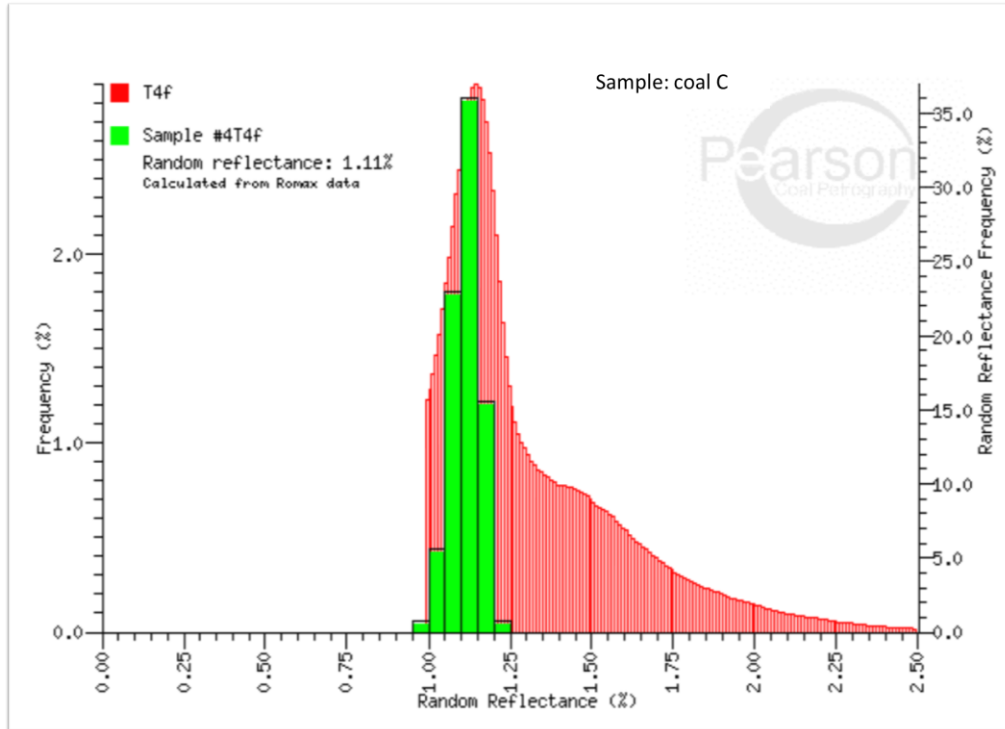


Figure III. Automated reflectogram of coal C

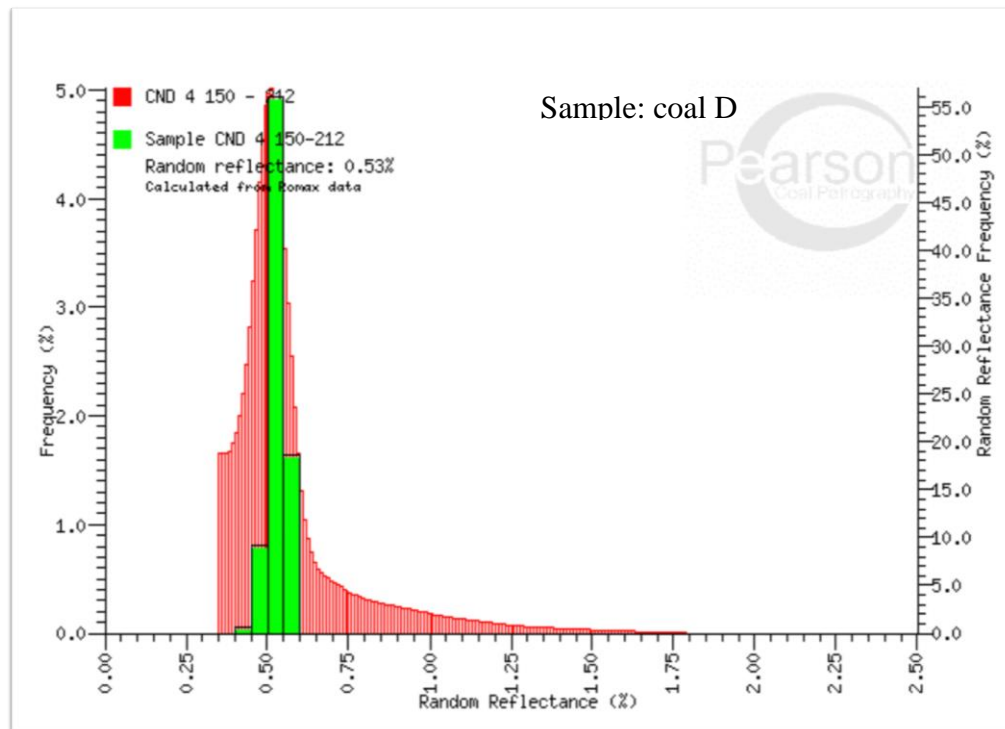


Figure IV. Automated reflectogram of coal D